Modulation of NF-κB Activity with Synthetic Inhibitors of NEMO

by

Jorge Becerra

A dissertation submitted in partial fulfillment
of the requirements for the degree of
Doctor of Philosophy
(Chemical Biology)
In the University of Michigan
2023

Doctoral Committee:

Professor Anna K. Mapp, Chair
Assistant Professor Michael Cianfrocco
Associate Professor Amanda L. Garner
Associate Professor Allison Narayan

Jorge Becerra

jbecerra@umich.edu

ORCID iD 0000-0003-2746-2814

TABLE OF CONTENTS

Chapter One: Targeting Cytosolic Protein-Protein Interactions for NF-κB Inhibition

Chapter Two: Strategies for the Discovery of Synthetic Inhibitors for NEMO

Chapter 3 Transformation of a NEMO Inhibitor into a NEMO Degrader

List of Figures

List of Tables

List of Abbreviations

ATP	Adenosine triphosphate
BCA	Bicinchoninic acid
BME	2-Mercaptoethanol
BSA	Bovine serum albumin
CDK	Cyclin dependent kinases
CPP	Cell-penetrating peptide
CRISPR	Clustered Regularly Interspaced Short Palindromic Repeats
DCM	Dichloromethane
DIPEA	Diisopropylethylamine
DMEM	Dulbecco's Modified Eagle Medium
DMF	N, N-Dimethylformamide
DMSO	Dimethyl sulfoxide
DNA	Deoxyribonucleic acid
DTT	Dithiothreitol
FBS	Fetal Bovine Serum
FITC	Fluorescein isothiocyanate
FMOC	Fluorenylmethyloxycarbonyl
FPLC	Fast protein Liquid Chromatography
GPCR	G Protein Coupled Receptor
HCl	Hydrochloric acid
HDAC	Histone deacetylase
HEK	Human embryonic kidney
HOBT	1-Hydroxybenzotriazole
HP	High-pressure
HPLC	High-pressure liquid chromatography
HRP	Horseradish peroxidase
HTS	High-throughput screening
IC	Inhibitory concentration
IKK	IkappaB kinase
IL	Interleukin
IPTG	Isopropyl ß-D-1-thiogalactopyranoside
KD	Dissociation constant
KO	Knock out
LDS	Lithium dodecyl sulphate
MG	Molecular glue
mut	Mutant
NaCl	Sodium chloride

NBD	NEMO binding domain
NEMO	NF-κB essential modulator
NF-κB	Nuclear Factor Kappa B
NP	NEMO PROTAC
OD	Optical density
PAMPAS	Pathogen-associated molecular patterns
PBS	Phosphate-buffered saline
PDVF	Polyvinylidene fluoride
PEG	Polyethylene glycol
POI	Protein of interest
PPIs	Protein-protein interactions
PROTAC	Proteolysis-targeting chimera
RHD	Rel homology domain
RNAi	Double-stranded RNA-mediated interference
rpm	Rotations per minute
SAR	Structure activity relationship
SDOM	Standard deviation of mean
SDS-PAGE	Sodium dodecyl-sulfate polyacrylamide gel Electrophoresis
SLRP	Synthetic loop replacement peptide
TAD	Topologically Associated Domain
TAT	Transactivation domain
TCEP	Tris(2-carboxyethyl) phosphine
TF	Transcription factor
TLR	Toll-like receptor
TNFα	Tumor necrosis factor-alpha
TNFR	Tumor necrosis factor receptor
UAA	Unnatural amino acids
UV	Ultraviolet
VHL	Von Hippel-Lindau
WT	Wild type

Abstract

The NF-κB pathway becomes constituently active in cancer, autoimmune disorders, and in infectious diseases such as COVID-19 and has thus been the focus of much drug-discovery research. Targeting NF-κB activity is challenging due to the complexity of the different activation pathways and apparent crosstalk between the pathways themselves. Additionally, many of the constituent pathway proteins and protein complexes are classed as 'undruggable' due to their intrinsically disordered regions and the well-folded domains lacking discrete binding sites. Selectivity for particular arms in the pathway has been problematic as well since many of the kinases play multiple roles.

This dissertation focused primarily on regulating NF-κB transcriptional activity through modulation of the IKK pathway by targeting NEMO. NEMO was chosen as a target because of the critical role it plays as a scaffold protein that functions to recruit both IKKα and IKKβ for phosphorylation in addition to its exclusivity with the canonical pathway. The main goal of this thesis focused on mimicking key features from NEMO binding partners in order to block NEMO's function in the NF-κB pathway. By applying targeted NEMO binding domain peptides derived from native binding partner IKKβ, we expanded past the native functionality of previously characterized molecules. Disrupting PPIs is challenging, however they provide distinct interaction motifs that rational peptide drug design can utilize for increasing efficacy. The NEMO-IKK interaction is largely dependent on hydrophobic interactions between aromatic residues present on both

proteins that present a pharmacophore for targeting. Through this rational we designed a series of unnatural amino acid NEMO binding domain peptides with varying tryptophan substituents at key residues 739 and 741. We found that by altering the electron density at these positions through chlorine atom additions, we were able to increase the binding affinity substantially and produce a 13-mer NEMO binding domain construct with relative high affinity.

Inhibitor through degradation can be an effective strategy for modulating the activity of hard-to-target PPIs as well. Our attempt to apply this strategy onto KKβ-derived peptides to achieve an alternative mode of modulation of NEMO and NF-κB activity led us to a functional study using both large (45-mer) and small (11-mer) IKKβ derived peptides. We explored and dissected the different components that make peptide based PROTACs effective for targeting NEMO. This resulted in the identification of a molecule (NP-8) that showed retained binding affinity to NEMO and modestly decreased the activity of NF-κB in HEK-293T cells. The overarching results from this dissertation showcase how utilization of peptide designed mimics can be an effective and promising avenue for targeting protein-protein interactions and inhibition of NF-κB.

Chapter One

Targeting Cytosolic Protein-Protein Interactions for NF-κB Inhibition

A. Abstract

Transcription is an essential process required for the regulation of the genome. Transcriptional hub proteins like NF-κB regulate various diseases like cancer that is fueled by overexpression of NF-κB controlled cell proliferation genes. NF-κB has therefore been the study of various modes of inhibition, but intricate pathway complexities has led to little targeted selectivity between the canonical and noncanonical pathway.

This introductory chapter will introduce NF-κB pathways and players involved with pathway activation and their role in targeted approaches. The difficulties associated with targeting different NF-κB targets is discussed with an emphasis on targeting PPIs. Finally, a strategy is proposed that relies on targeting cytosolic PPIs with rational peptide-based drug design to inhibit NF-κB activity

B. NF-κB transcriptional activation is dependent upon up-stream signaling interactions

NF-κB: A master transcriptional regulator

The main subject of study in this thesis is the transcription factor NF-κB and the complex protein assemblies required for its activation. NF-κB was initially discovered in Beta immune cells as a subunit that bound to specific κB enhancer regions in DNA.[1] Subsequent studies revealed that NF-κB plays a key role in immune responses, including inducing the production of chemokines and cytokines, and it is also essential in production of cell cycle regulators and adhesion molecules.[2]

In the nucleus, NF-κB consists of homo- and heterodimeric complexes that interact with DNA sequence-specifically and also form protein-protein interactions (PPIs) with components in the transcriptional machinery.[3] All NF-κB transcription factors possess a Rel homology domain (RHD) in the N-terminus that is necessary for DNA binding activity but differ in domain composition at the C-terminus. Rel-family proteins contain TAD sequences that are essential for promotion of gene expression while NF-κB-family proteins contain inhibitory ankyrin-repeat domains. Ankyrin-repeat domains have the ability to bind DNA but not to activate it for transcription, enabling a homodimer NF-κB-family pair to silence transcription. Among the many combinations of NF-κB

monomers, the p50/RelA heterodimer is the most abundant type involved in the

canonical pathway (Figure 1.1).[4]
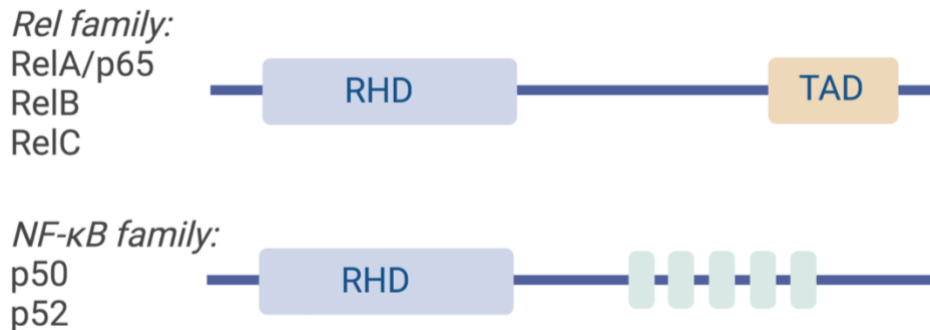
Figure 1.1 NF-κB monomer families. The two sub families of NF-κB transcription factors and their domains involved in DNA transcription. The blue bar represents the Rel homology domain present in both families. The orange bar in C-terminus of the Rel family represent the transactivation domain and the cyan rectangles represent the ankyrin repeats in the NF-κB family.

When not needed, NF-κB transcription factors reside in cytoplasmic complexes;

specific extracellular signals lead to their release, translocation to the nucleus, and

upregulation of needed gene circuits. There are two primary paths by which the NF-κB

transcription factors are activated. One is the so-called canonical pathway which

terminates in transiently activation of p50/p65/c-Rel-containing NF-κB transcription

factors.[5] This pathway initiates with stimulation of immune receptors, leading to

phosphorylation of the IKK complex and activation of its kinase activity.[6] Subsequent

phosphorylation of the NF-κB transcription factor inhibitor IκB marks it for degradation

and the transcription factors are then transported to the nucleus to upregulate immune

response genes, including proinflammatory cytokines such as IL-6 and IL-12. The

reliance of NF-κB on specific extracellular signals such as pathogen-associated

molecular patterns (PAMPs) provides tight control of this important pathway.[7] However,

mutations of the constituent proteins can lead to aberrant activation of NF-κB. One

example is in colorectal cancer, in which constitutive activation of the NF-κB RelA-p50

dimer leads to further invasion and migration of cancer cells.[8] As discussed in more detail later in the chapter, it is for this reason that there continues to be much interest in strategies to inhibit the canonical NF-κB pathway.

The noncanonical NF-κB pathway is similarly initiated by extracellular signals, but in this case modulated by members of the TNFR superfamily.[9] This pathway activates distinct NF-κB transcription factors, p52 and RelB, that are held in an inactive form through complexation with p100 in the cytoplasm. Initiation of the noncanonical pathway does not proceed through the IKK complex, but rather via IKKα; once IKKα is activated through phosphorylation it marks p100 for further processing. This processing leads to production of p52 and the release of RelB, which are then translocated to the nucleus as active transcription factors (Figure 1.2). In contrast to the canonical pathway, this pathway has a slow induction and is relatively persistent. It plays an essential role in development, innate immunity, and the function of specific immune cell subtypes.[9] Aberrant activation is associated with autoimmune diseases and autoinflammatory disorders.
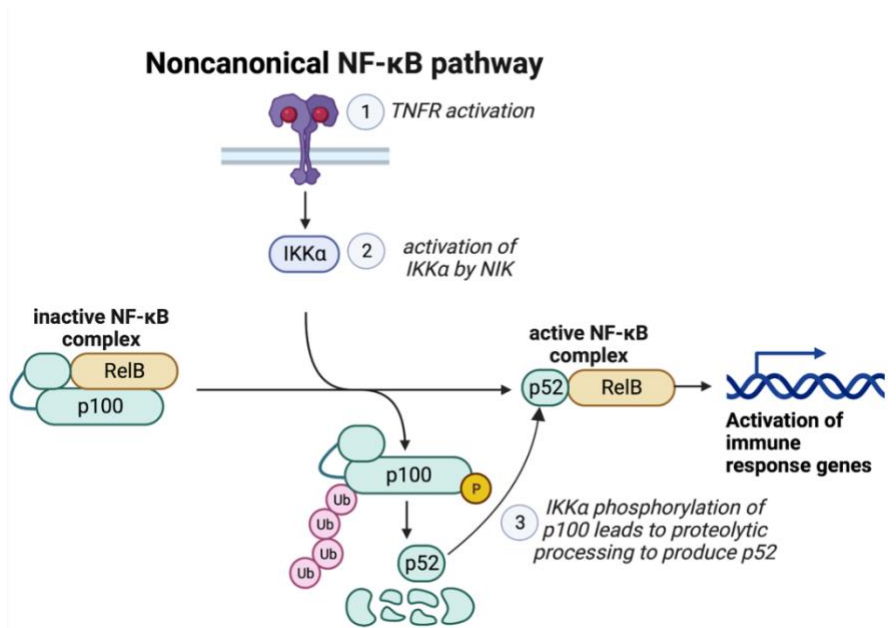
Figure 1.2 The noncanonical NF-κB activation pathway. The noncanonical pathway relies on kinase NIK to phosphorylate IKKα which then marks p100 and RelB for further processing to activate transcription

Both pathways are susceptible to mutations among key players that can lead to improper function of NF-κB activity. One example of this stems from colorectal cancer cells that exhibit constitutive activation of the NF-κB RelA-p50 dimer that leads to further invasion and migration of cancer cells.[8] For this reason, it is important to find mitigation strategies to curb aberrant NF-κB activity.

The IKK complex

The main target associated with the studies of this dissertation is the IKK complex, and more specifically, the IKKγ or Nuclear factor κB essential modulator (NEMO) component. The IKK complex is composed of 4 subunits and includes a NEMO dimer interacting with an IKKα/β dimer. Although several combinations of IKKα/β have been found to associate with NEMO, the most common complex associated with canonical NF-κB activation consists of the IKKα/β pair. Non-canonical NF-κB pathway

activation is dependent only on IKKα dimerized kinase despite having a 50% sequence identity and 70% protein similarity to IKKβ and NEMO is not involved.[10]

The IKK complex serves as a critical point in NF-κB activation due to a signal relay funneling into this key junction which leads to the phosphorylation of Ser 32 and 36 of IκBα. In the canonical pathway, NEMO functions as a scaffolding protein that allows the IKK kinase to coordinate this phosphorylation event with IκBα. By doing so, IκBα is signaled for processing and degradation by the 26S proteosome which allows the TFs to shuttle into the nucleus (Figure 1.3). Mutational genetic studies in mice where NEMO was KO have shown that without NEMO, the canonical pathway cannot proceed in activating the NF-κB transcription factors. In addition, male mice with NEMO KO were prone to death due to key cell survival NF-κB regulation that was lost.[11,12] The lost NF-κB activity can be attributed to the required ubiquitination event on NEMO by upstream regulator RIP1 that allows for IKK complex association.[13] The interaction between NEMO and the IKK kinases are critical for further pathway relay as it allows for processing of IKKα/β by phosphorylating Ser 176/180 and Ser 177/181 respectively by upstream kinases such as TAK1 and MEKK3.[14]

Canonical NF-κB pathway
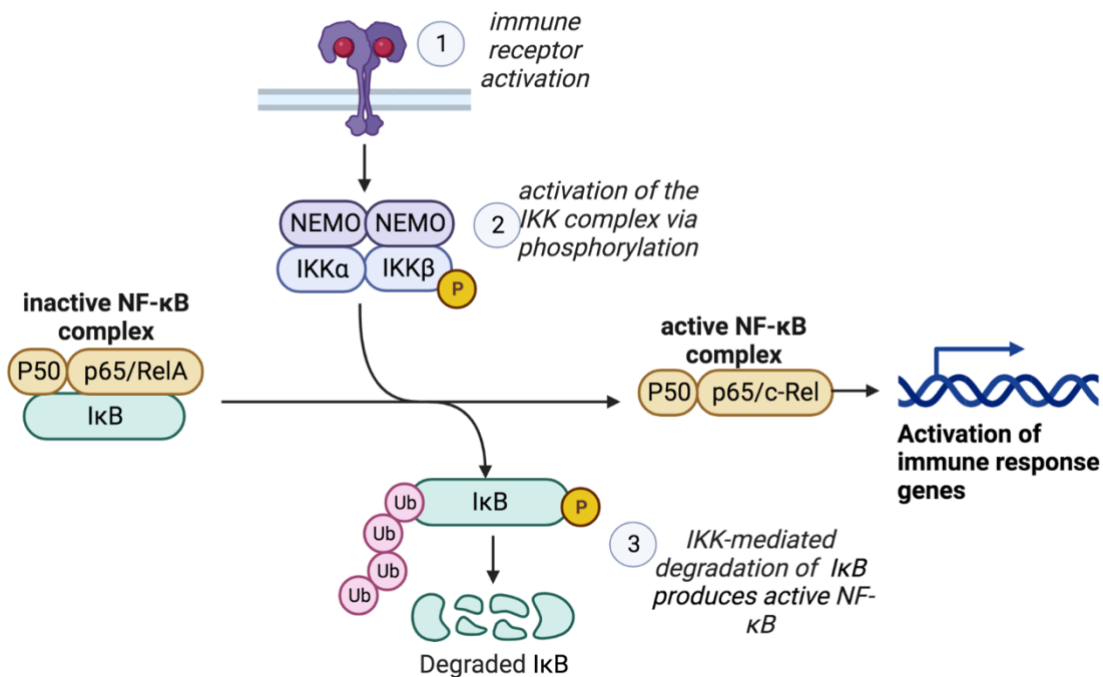
Figure 1.3. The canonical NF-κB activation pathway. The activation of NF-κB is primarily dependent on the schemes depicted above. The canonical pathway relies in the IKK complex associated by two heterodimer protein complexes and processes repressed transcription factors like p50 and Rel A. The non-canonical pathway is dependent solely on IKKα which processes other NF-κB family members like p100 and Rel B into active forms.

IKKα has been shown to have other activity associated with NF-κB processing like playing a direct role in the phosphorylation of RelA/P65 in the nucleus. Because NEMO is only involved in the canonical pathway, primarily binds to the IKKs, and does not possess additional phosphorylating activity like IKKα, it serves as a good target to selectively inhibit the canonical pathway. The interaction between NEMO and IKK is characterized by two coiled-coiled PPIs with each other. More specifically, the C-terminus of the IKK kinases and the N-terminus of NEMO between the first alpha helical region and coiled-coil domain is the location of this interaction (Figure 1.4).

NEMO Domains
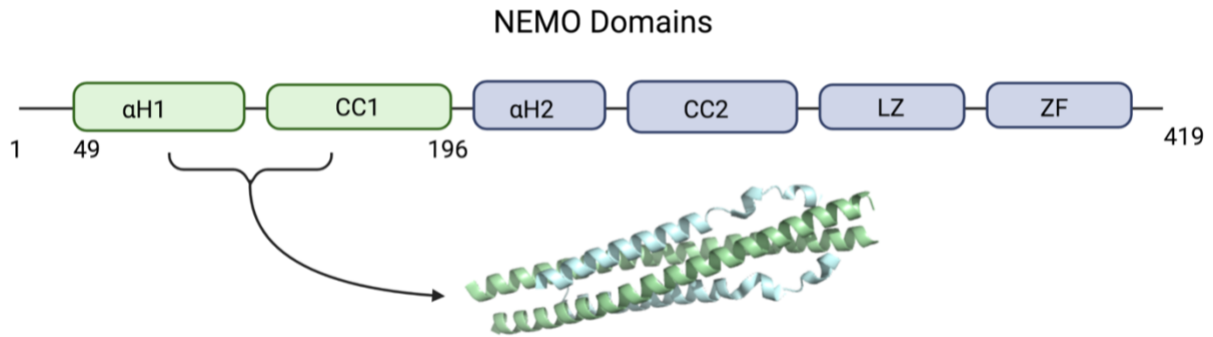
Figure 1.4. Association between NEMO and IKKβ. The association between NEMO and IKK is dependent on two dimer associations between the N-terminus of NEMO (green) and the C-terminal domain of IKKβ (shown in cyan) (PDB 3BRV).

The C-terminus of the IKK kinases contains what has been denoted as the NEMO binding domain (NBD), minimally residues 735-745, and interacts primarily with the N-terminus of NEMO's residues 92-101. A crystallographic study of the NEMO (44-111) and IKKβ (701-745) interaction through X-ray crystallography identified Trp 739, Trp 741 and Phe 734 as three key residues from the NBD that reside in the hydrophobic cleft of NEMO. Additional hydrogen bond interactions between NEMO's Glu89 side chain and the backbone carbonyl of Phe734 occur between the two proteins (Figure 1.5).[15] Further studies have demonstrated through mutational analysis of those specific residues that the interaction between NEMO and IKK cannot continue if they are not present.[16] The IKK complex certainly plays a prominent role in NF-κB activation and is an area of intensive research. However, while this suggests that the IKK complex and more specifically NEMO are potentially important targets for drug discovery, they are challenging proteins for screening or design given the large surface areas used for complex formation.
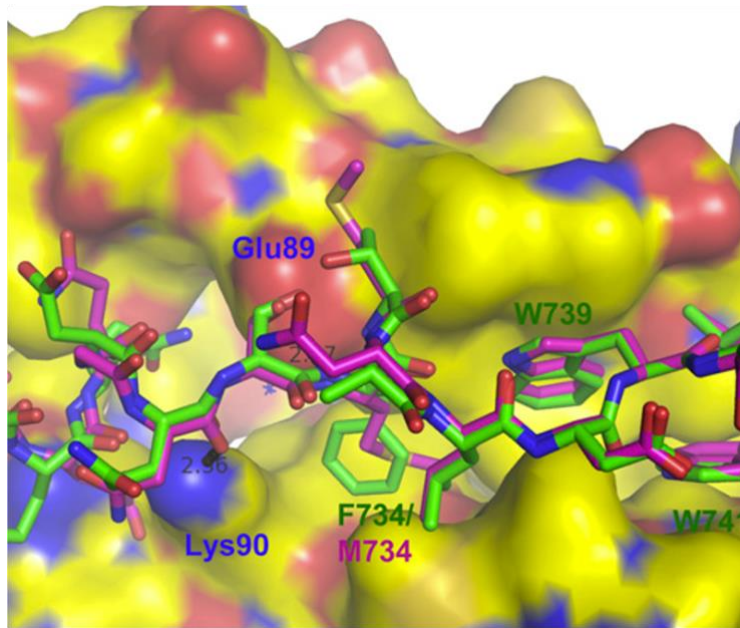
Figure 1.5. Interaction of key NBD residues with NEMO's binding surface. The image above depicts the binding cleft of NEMO with hydrophobic hotspots outlined in yellow, positively charged areas in blue, and negative areas in red. The ball and stick peptide demonstrates a superimposed NBD sequence between IKKα/β. All three aromatic residues form the NBD localize into the hydrophobic areas of NEMO (PDB 3BRV). Image used with permission from Rushe et al., 2008, Structure 16,5, 798-808.

C. The landscape of NF-κB pathway inhibitors

Targeting of major NF-κB players for inhibition

Given the complexity of the NF-κB pathway, it is no surprise that there are myriad targets for inhibitor discovery (Figure 1.6). One of the most significant challenges is selectivity for NF-κB and selectivity for the canonical or noncanonical pathway. The targets most examined are cell-surface receptors. TNF-R, for example, has been targeted though antibody therapy to block its activation and aid in inflammatory diseases like irritable bowel syndrome.[17,18] Other receptors like TLR7/8/9 have been extensively studied and as a result many drug candidates have entered clinical trials like MN-166.[19] Additionally, adaptor proteins to these receptors have been targeted as well such as IRAK, that is inhibited by small molecule inhibitor Pacritinib.[20] The issue with these target approaches, however, is that they are usually not selective. Even though MN-166 was found to have some neuroprotective benefits, it was classified as a nonselective phosphodiesterase inhibitor. Pacritnib too, was found to inhibit additional adaptor proteins JAK2 and FLT3. Targeting receptor and adaptor proteins are relatively easy targets to engage, but they lack specificity in their inhibition of NF-kB due to crosstalk between various signal relay messengers.
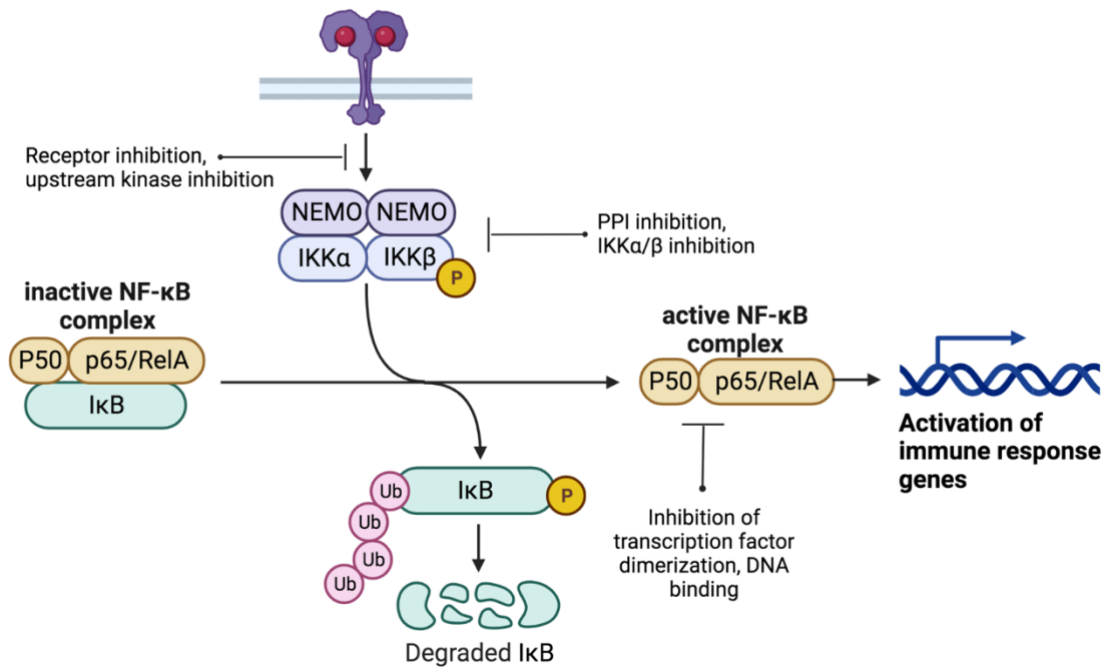
Figure 1.6. Inhibitory checkpoints of the canonical NF-κB pathway. The figure above depicts different intervention points associated with canonical NF-κB pathway blocking.

NF-κB transcription factor inhibition

Targeting the canonical NF-κB transcription factors p50 and Rel A for inhibition has been historically challenging as they exist in an inactive mode in the cytoplasm. Additionally, in their active state inside the nuclease, they act as hub proteins that upregulate transcriptional activity of various important factors for cell regulation like those of cyclin dependent kinases (CDKs)[21–24], histone deacetylases (HDACs 1 and 2)[25,26], GPCRs[27–29], Toll-like Receptors (TLRs)[30,31], and important BCL2 death regulators.[25,32–34] Over recent years, various molecules have been synthesized to target the Rel A NF-κB that contains the TAD domain. However, most of those molecules have had poor ligand characteristics. Small molecules 5259, 338120, and 1680942 for

example, have shown inhibition capabilities of Rel A but are marred by toxicity, selectivity issues, and poor potency. In addition, all of the compounds fail to differentiate between NF-κB family members and other transcription factors like Jun.[35]

IKK inhibition

Other methods of intervention have been to target the IKK complex composed of three subunits as discussed earlier. Much effort has been devoted into targeting the IKK kinases involved in pathway activation. One issue with using a kinase-targeting approach, however, is that it can be difficult to target selectively when closely related kinases have similar motifs designated for ATP binding.[36] The NF-κB pathway notably is dependent upon additional kinase activity from MEKK3, NIK, TAK-1, TBK1 and IKKε in addition to the IKK complex, and analyzing pathway inhibition through a single kinase can be complex.[37]

Selectivity can be a challenging hurdle to overcome, especially when trying to differentially target IKKα and IKKβ. Even though they are very similar kinases, they still have very different functions in their activation of NF-κB. Targeting either kinase at the ATP binding site has proved to be difficult in many cases. For example, kinases inhibitor SU1266 meant to target IKKα was not able to differentiate against IKKβ and other compounds like staurosporine and quercetin effectively inhibit the activity of both kinases.[38,39] Dual IKK kinase targeted approaches have also been attempted with thienopyridine analogues 22 and 23 that showed promising NF-κB inhibition; however, off target effects against FTL3 was observed.[40]

The kinases' involvement in separate canonical and non-canonical NF-κB activity leads to the regulation of different genes. Ideally, avoiding inhibition of IKKα when

targeting the IKK complex is central due to its dominant role in the non-canonical pathway.

A third point of intervention to modulate NF-κB activity has been to target non-enzymatic proteins like NEMO. Disrupting the interaction between NEMO and the IKK kinases has been extensively studied with varied attempts at making NEMO inhibitors. The main issue with this targeted approach has been that it relies on disrupting buried PPIs between proteins which have been classified as undruggable targets. PPIs vary in surface areas and affinities between protein pairs (Figure 1.7), and depending on these variables, will affect the efficacy of targeted molecules. The interaction link between NEMO and IKK is characterized by a volume of 800 cubic angstroms with an affinity in the low nanomolar range, making it a difficult association to disrupt.[41]

An important study by May *et al* however proposed utilizing a small peptide sequence derived from the C-terminal region of IKK discussed earlier called the NBD.[42] This small 10-mer peptide was found to have modest activity in cells (>100 μM) as an inhibitor of the PPI between NEMO and IKK. One advantage of utilizing a peptide-based inhibitor is that they are generally less promiscuous due to their topological complexity and allow for peptidomimetic modifications at certain residues. However, there are challenges associated with proteolytic stability affecting inhibitor lifetime and the need for additional moieties to improve cell penetration.

An additional issue with using NEMO as a point of intervention is that it is a particularly difficult protein to purify for biochemical studies. In nature, NEMO associates as a dimer and contains 11 cysteine residues that tend to cause aggregation of isolated protein which has even prompted researchers to make structural mutations of these

residues to facilitate its purification.[43] We suspect this issue alone prevents further research development in finding small molecules through high-throughput screening (HTS) methodologies. In addition, these PPIs are difficult to disrupt, and targeting with small molecule scaffolds have led to little success with the exception of some molecules with modest activity.[44,45] Other attempts however have been made at elucidating potential ways to disrupt the NEMO and IKK binding interface. PPIs by computationally mapping energy hot spots to produce potential fragment scaffolds.[46]
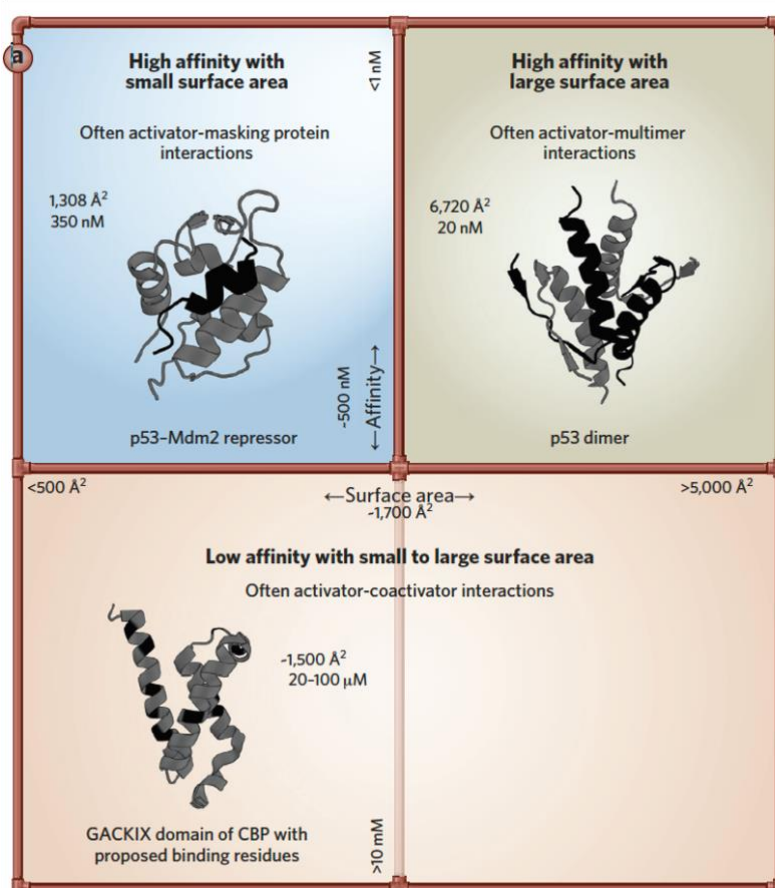
Figure 1.7. Characterization of PPIs. The image above depicts the characterization of known PPIs of transcription factors like p53 and KIX by surface area (X-axis) and affinity (Y-axis). Each quadrant represents unique PPI classes. The association between NEMO and IKK likely falls under the top 2 quadrants depending on motif size studied. Image used with permission from Mapp et al., 2015, Nature Chemical Biology 11, 891-894.

Despite all these caveats, NEMO is still an attractive avenue for NF-κB inhibition due to its sole involvement in the canonical pathway and the added benefit of not being a kinase. Other novel approaches have been more successful at utilizing the NBD peptide and turning it into a more biologically active compound. Peptidomimetics are a class of peptides that make modifications on amino acids by implementing structural changes that allow peptides to keep respective inhibitory activity towards targets.[47] Types of peptidomimetics include utilizing techniques like stapling of side chains that add covalent bond character, macrocyclization that facilitate transport across membranes, implementing D-amino acid characters that are less susceptible to protease degradation, and changing the backbone character entirely.[48–50] An example of a peptidomimetic molecule utilized to successfully target NEMO comes from the Pei lab that employed a macrocyclic peptide with NEMO binding motifs and cell penetrating motifs and resulted in an IC_{50} value of 1 μM in ovarian cancer cells (Figure 1.8).[51] Applying these peptide scaffolds together resulted in a synergistic molecule with increased pharmacophore activity.

NEMO Binding (IC_{50} = 1.0 μM)
Cell-permeable; Proteolytically stable
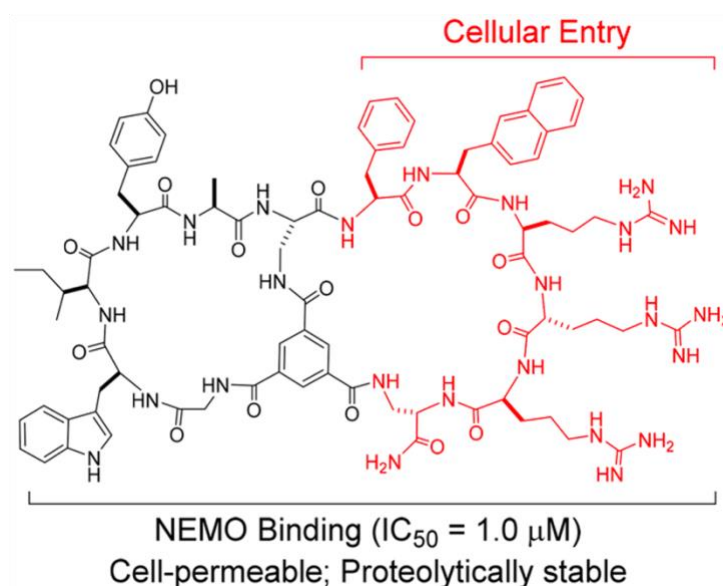
Figure 1.8. Peptide 7 NEMO binder. The macrocyclic binder above contained ring A (black) composed of a peptide scaffold used to target NEMO and ring B (red) that contained charged residues for cell entry and was found to have a low µM inhibitory activity. Image used with permission from Rhodes et al., 2018, J. Am. Chem. Soc. 140, 38, 12102-12110.

Exploring the NBD sequence potential

The original NBD 11-mer peptide provided an avenue for intervention at disrupting

the NEMO's PPI. However, it possessed subpar activity, with an IC_{50} of approximately

100 µM. Our lab previously applied peptidomimetic techniques to the 11-mer NBD

sequence to stabilize the interaction of the peptide with NEMO. Modifications on the

adjoining residues next to Trp 739 through a ring closing metathesis reacting using

Grubbs' catalyst allowed for the addition of a synthetic brace (Figure 1.9). This

modification was done to stabilize the small loop region critical for interaction with

NEMO and was found through Ramachandran computational analysis to provide a

more favorable structure for binding potential. Further studies in cells showed that this

compound was 10-fold more biologically active at inhibiting NF-κB activity. The

importance of this experiment demonstrates the possibility to make synthetic

modifications on peptide sequences that can be utilized to increase their activity in cells.
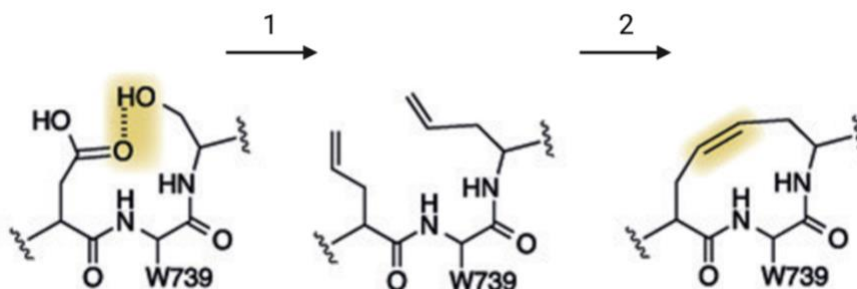
Figure 1.9. Peptidomimetic transformation of key NBD residues. The 11-mer NBD WT peptide was turned into a peptide mimetic by substituting the adjacent Asp and Ser residues of Trp739 for Allyl-L-Glycine residues (1) and then subjecting to ring closing metathesis using Grubbs' catalyst (2). Image adapted with permission from Bruno et al., 2016, Angewandte Chemie. 128, 48, 15221-15225.

This thesis focuses primarily on expanding the hypothesis that peptide molecules can be modified at critical residues to produce molecules with greater efficacy without compromising on selectivity. The NBD sequence has very specific residue interactions that position the peptide in a favorable position to interact with NEMO. We aim to exploit these critical interactions and apply different methodologies to increase the activity of the peptide and subsequently inhibit NF-κB activity.

D. Dissertation Summary

Transcription factors are important in various disease states due to their regulation of genes that can aberrate conditions further. The regulation of transcriptional activity is therefore critical and prompts the need for producing innovating modulators to curb activity. NF-κB activity is a well-documented transcriptional regulator involved in cancer and overactive immune responses and is regulated by several upstream PPIs. These interactions present challenges for targeting but have high impact potential if successfully inhibited. The interaction between NEMO and the IKK kinases is an ideal PPI to disrupt to prevent NF-κB activity and a small peptide derived from this interaction was identified as an inhibitor which has since been modified in an attempt to increase its activity. The subsequent chapters of this dissertation describe various assay development techniques to test the activity of NBD peptide-derived molecules targeted at NEMO.

In chapter two of this dissertation, an NBD peptidomimetic molecule, NBD_2, was tested for relative binding affinity against NEMO relative to the WT sequence by developing a fluorescence polarization assay. The synthetic brace was found to have no effect on binding which led to a search of NBD peptide derivatives that did. A further

exploration of the NEMO-NBD chemical space through SAR analysis of Trp-NBD derivatives was studied to find an optimal peptide binder. These derivatives were characterized to have better binding activity to NEMO and increased the affinity significantly. The results of this chapter highlight the ability to increase activity of peptide binders through small modifications that impact PPIs.

In chapter three, optimization of the NBD peptide was explored by utilizing a PROTAC-peptide technique. This led to the synthesis of NBD-PROTACs (NPs) between 2 phases of development. By testing and modifying the 3-part components of the NPs, we were able to optimize each part to produce the most effective molecule NP-8. Although NP-8 was found to have the best characteristic to inhibit NF-κB activity, its functionality as a degrader to NEMO requires further study. Additionally, the cellular environment such as the cancer type in which NPs are most functional may vary depending on the tumor type. Together, these chapters outline different mitigation strategies by which simple peptide inhibitors may be enhanced to produce competent inhibitors to the NF-κB pathway.

E. References

1.   Sen, R. & Baltimore, D. Multiple nuclear factors interact with the immunoglobulin enhancer sequences. *Cell* **46**, 705–716 (1986).

2.   Liu, T., Zhang, L., Joo, D. & Sun, S.-C. NF-κB signaling in inflammation. (2017). doi:10.1038/sigtrans.2017.23

3.   Albensi, B. C. What is nuclear factor kappa B (NF-κB) doing in and to the mitochondrion? *Front. Cell Dev. Biol.* **7**, (2019).

4.   Gilmore, T. D. Introduction to NF-κB: players, pathways, perspectives. *Oncogene 2006 2551* **25**, 6680–6684 (2006).

5.   Oeckinghaus, A. & Ghosh, S. The NF-kB Family of Transcription Factors and Its Regulation. doi:10.1101/cshperspect.a000034

6.   Huang, X. & Yang, Y. Innate immune recognition of viruses and viral vectors. *Hum. Gene Ther.* **20**, 293–302 (2009).

7.   Sode, J. *et al.* Genetically determined high activities of the TNF-alpha, IL23/IL17, and NFkB pathways were associated with increased risk of ankylosing spondylitis. *BMC Med. Genet.* **19**, 1–16 (2018).

8.   Jana, A. *et al.* NFkB is essential for activin-induced colorectal cancer migration via upregulation of PI3K-MDM2 pathway. (2017).

9.   Sun, S. C. The non-canonical NF-κB pathway in immunity and inflammation. *Nat. Rev. Immunol. 2017 179* **17**, 545–558 (2017).

10.   Häcker, H. & Karin, M. Regulation and function of IKK and IKK-related kinases. *Sci. STKE* **2006**, 2023 (2006).

11.   Schmidt-Supprian, M. *et al.* NEMO/IKKγ-Deficient Mice Model Incontinentia

Pigmenti. *Mol. Cell* **5**, 981–992 (2000).

12. Tarassishin, L. & Horwitz, M. S. Sites on FIP-3 (NEMO/IKKγ) Essential for Its Phosphorylation and NF-κB Modulating Activity. *Biochem. Biophys. Res. Commun.* **285**, 555–560 (2001).

13. Zhang, J. *et al.* RIP1-mediated regulation of lymphocyte survival and death responses. *Immunol. Res.* **51**, 227 (2011).

14. Israë, A. The IKK Complex, a Central Regulator of NF-kB Activation. doi:10.1101/cshperspect.a000158

15. Rushe, M. *et al.* Structure of a NEMO/IKK-Associating Domain Reveals Architecture of the Interaction Site. *Structure* **16**, 798–808 (2008).

16. May, M. J., Marienfeld, R. B. & Ghosh, S. Characterization of the IκB-kinase NEMO binding domain. *J. Biol. Chem.* **277**, 45992–46000 (2002).

17. Gilmore, T. D. & Herscovitch, M. Inhibitors of NF-κB signaling: 785 and counting. *Oncogene 2006 2551* **25**, 6887–6899 (2006).

18. Song, X. yu R., Torphy, T. J., Griswold, D. E. & Shealy, D. Coming of Age:Anti–Cytokine Therapies. *Mol. Interv.* **2**, 36 (2002).

19. Ramadass, V., Vaiyapuri, T. & Tergaonkar, V. Molecular Sciences Small Molecule NF-κB Pathway Inhibitors in Clinic. doi:10.3390/ijms21145164

20. Singer, J. W. *et al.* Inhibition of interleukin-1 receptor-associated kinase 1 (IRAK1) as a therapeutic strategy. *Oncotarget* **9**, 33416 (2018).

21. Sethi, G., Ahn, K. S., Sung, B. & Aggarwal, B. B. Pinitol targets nuclear factor-kappaB activation pathway leading to inhibition of gene products associated with proliferation, apoptosis, invasion, and angiogenesis. *Mol. Cancer Ther.* **7**, 1604–

1614 (2008).

22. Guttridge, D. C., Albanese, C., Reuther, J. Y., Pestell, R. G. & Baldwin, A. S. NF-kappaB controls cell growth and differentiation through transcriptional regulation of cyclin D1. *Mol. Cell. Biol.* **19**, 5785–5799 (1999).

23. Iwanaga, R. *et al.* Activation of the cyclin D2 and cdk6 genes through NF-kappaB is critical for cell-cycle progression induced by HTLV-I Tax. *Oncogene* **27**, 5635–5642 (2008).

24. Li, F. *et al.* Ganoderic acids suppress growth and angiogenesis by modulating the NF-κB signaling pathway in breast cancer cells. *Int. J. Clin. Pharmacol. Ther.* **50**, 712–721 (2012).

25. Essaghir, A. & Demoulin, J. B. A minimal connected network of transcription factors regulated in human tumors and its application to the quest for universal cancer biomarkers. *PLoS One* **7**, (2012).

26. Kuo, P. L., Shen, K. H., Hung, S. H. & Hsu, Y. L. CXCL1/GROα increases cell migration and invasion of prostate cancer by decreasing fibulin-1 expression through NF-κB/HDAC1 epigenetic regulation. *Carcinogenesis* **33**, 2477–2487 (2012).

27. Helbig, G. *et al.* NF-kappaB promotes breast cancer cell migration and metastasis by inducing the expression of the chemokine receptor CXCR4. *J. Biol. Chem.* **278**, 21631–21638 (2003).

28. Kukreja, P., Abdel-Mageed, A. B., Mondal, D., Liu, K. & Agrawal, K. C. Up-regulation of CXCR4 expression in PC-3 cells by stromal-derived factor-1alpha (CXCL12) increases endothelial adhesion and transendothelial migration: role of

MEK/ERK signaling pathway-dependent NF-kappaB activation. *Cancer Res.* **65**, 9891–9898 (2005).

29.   Tarnowski, M. *et al.* Regulation of expression of stromal-derived factor-1 receptors: CXCR4 and CXCR7 in human rhabdomyosarcomas. *Mol. Cancer Res.* **8**, 1–14 (2010).

30.   Li, H. *et al.* Herpes simplex virus 1 infection induces the expression of proinflammatory cytokines, interferons and TLR7 in human corneal epithelial cells. *Immunology* **117**, 167–176 (2006).

31.   Stärkel, P., De Saeger, C., Strain, A. J., Leclercq, I. & Horsmans, Y. NFkappaB, cytokines, TLR 3 and 7 expression in human end-stage HCV and alcoholic liver disease. *Eur. J. Clin. Invest.* **40**, 575–584 (2010).

32.   Yang, X. & Chan, C. Repression of PKR mediates palmitate-induced apoptosis in HepG2 cells through regulation of Bcl-2. *Cell Res.* **19**, 469–486 (2009).

33.   He, B. *et al.* Lymphoma B cells evade apoptosis through the TNF family members BAFF/BLyS and APRIL. *J. Immunol.* **172**, 3268–3279 (2004).

34.   Vajpayee, N., Hussain, J., Tolocica, I., Hutchison, R. E. & Gajra, A. Expression of signal transducer and activator of transcription 3 (STAT3) in primary central nervous system diffuse large B-cell lymphoma: a retrospective analysis of 17 cases. *J. Neurooncol.* **100**, 249–253 (2010).

35.   Mitsopoulos, C. *et al.* CanSAR: Update to the cancer translational research and drug discovery knowledgebase. *Nucleic Acids Res.* **49**, D1074–D1082 (2021).

36.   Hanson, S. M. *et al.* What Makes a Kinase Promiscuous for Inhibitors? *Cell Chem. Biol.* **26**, 390-399.e5 (2019).

37. YOUNG, E. R. R. *CHAPTER 9 - IKKβ as a Therapeutic Intervention Point for Diseases Related to Inflammation*. (2012). doi:10.1039/9781849735346-00255

38. Ho, H. K., Plevin, R., Mackay, S. & Paul, A. 193 A Novel First in Class IKK Alpha Inhibitor Abrogates Endothelial Cell Nuclear Factor Kappa B Signalling and Inflammatory Protein Expression. *Heart* **100**, A107–A107 (2014).

39. Peet, G. W. & Li, J. IκB Kinases α and β Show a Random Sequential Kinetic Mechanism and Are Inhibited by Staurosporine and Quercetin. *J. Biol. Chem.* **274**, 32655–32661 (1999).

40. Huber, M. A. *et al.* BI 5700, a selective chemical inhibitor of IκB Kinase 2, specifically suppresses epithelial-mesenchymal transition and metastasis in mouse models of tumor progression. *Genes and Cancer* **1**, 101–114 (2010).

41. Rushe, M. *et al.* Structure of a NEMO/IKK-Associating Domain Reveals Architecture of the Interaction Site. *Structure* **16**, 798–808 (2008).

42. May, M. J. *et al.* Selective Inhibition of NF-κB Activation by a Peptide That Blocks the Interaction of NEMO with the IκB Kinase Complex. *Science (80-.).* **289**, 1550 LP – 1554 (2000).

43. Cote, S. M. *et al.* Mutation of nonessential cysteines shows that the NF-κB essential modulator forms a constitutive noncovalent dimer that binds IκB kinase-β with high affinity. *Biochemistry* **52**, 9141–9154 (2013).

44. Gotoh, Y., Nagata, H., Kase, H., Shimonishi, M. & Ido, M. A homogeneous time-resolved fluorescence-based high-throughput screening system for discovery of inhibitors of IKKβ-NEMO interaction. *Anal. Biochem.* **405**, 19–27 (2010).

45. Chao, W. C. *et al.* The azatryptophan-based fluorescent platform for in vitro rapid

screening of inhibitors disrupting IKKβ-NEMO interaction. *Bioorg. Chem.* **81**, 504–511 (2018).

46.   Golden, M. S. *et al.* Comprehensive Experimental and Computational Analysis of Binding Energy Hot Spots at the NF-κB Essential Modulator/IKKβ Protein−Protein Interface. *J. Am. Chem. Soc* **135**, (2013).

47.   Grauer, A. & König, B. Peptidomimetics - A versatile route to biologically active compounds. *European J. Org. Chem.* 5099–5111 (2009). doi:10.1002/EJOC.200900599

48.   Molchanova, N., Hansen, P. R. & Franzyk, H. molecules Advances in Development of Antimicrobial Peptidomimetics as Potential Drugs. (2017). doi:10.3390/molecules22091430

49.   Perez, J. J. Designing Peptidomimetics. *Curr. Top. Med. Chem.* **18**, 566–590 (2018).

50.   Ahn, J.-M., Boyle, N., MacDonald, M. & Janda, K. Peptidomimetics and peptide backbone modifications. *Mini Rev. Med. Chem.* **2**, 463–473 (2002).

51.   Rhodes, C. A. *et al.* Cell-Permeable Bicyclic Peptidyl Inhibitors against NEMO-IκB Kinase Interaction Directly from a Combinatorial Library. *J. Am. Chem. Soc.* **140**, 12102–12110 (2018).

Chapter 2

Strategies for the Discovery of Synthetic Inhibitors for NEMO

A. Abstract

The activity of the canonical NF-κB pathway is directly dependent on the interaction between the IKK complex composed of NEMO and IKKα, β. Targeting of this specific pathway complex is alluring due to the selectivity it provides when targeting cancer associated genes. However, this interaction has been denoted as an "undruggable" target due to the large surface area that small molecules have minimal affinity for. A peptide sequence derived from IKKβ (NBD) has been previously shown to modestly inhibit the interaction between NEMO and KKβ. Recently Bruno and coworkers reported peptide NBD$_2$, a modified peptidomimetic of NBD, to have 10-fold increased inhibition of NF-κB in HeL cells (10μM) yet no binding affinity data was procured due to the complexities involved with purifying NEMO for biochemical assays. In this Chapter, I examine the relation between NBD$_2$ and NEMO through the development of a fluorescence polarization assay that led to the discovery of further NBD analogues. In particular, we found substituting aromatic residues 739 and 741 for unnatural amino acid Cl-Trp derivates to yield substantially better binders to NEMO and led to peptide "6Cl-739, 6Cl-741 NBD" having 100-fold greater affinity ($K_D = 4 \pm 1$) over the WT NBD peptide.

B. Introduction

As discussed in Chapter 1, there are many avenues to disrupt the pathways that regulate NF-κB transcriptional activity. Between the transcription factors themselves, kinases involved in signal transduction, and non-enzymatic proteins involved in pathway regulation, a complex network of potential targets modulate NF-κB activity.[1] However, the IKK complex is a unique checkpoint in the canonical pathway activity due to its phosphorylation activity directly affecting the activation of repressed NF-κB transcription factors.[2] For this reason, blocking the IKK complex has been of great interest to a number of researchers.

The IKK complex is composed of two kinases ($IKK\alpha, \beta$) and a regulatory dimer unit $IKK\gamma$, also known as NEMO.[3] The PPIs formed between $IKK\beta$ and NEMO are particularly attractive as therapeutic targets for NF-κB downregulation. However, despite extensive efforts, there has been limited success in identifying NEMO-IKK PPI inhibitors. This PPI falls within a specific category of challenging motifs to target due to a large surface area of interaction (~800 A^3) and relatively low nM affinity between binding partners.[4,5]

The interaction between NEMO and IKK has previously been modulated in our lab by taking advantage of the minimal sequence of interaction needed from IKK. IKK's C-terminal region between residues 701 and 747 interacts with NEMO's N-terminal alpha helix/coiled-coil 1 domain between residues 44-111.[6] More specifically, a sequence termed the NEMO-binding domain (NBD) composed of residues [735]TALDWSWLQTE[745] has been linked as the minimal NEMO interaction sequence of IKK.[7] The most critical residues of the NBD are the tryptophans at positions 739 and

741 that form critical contacts with additional residues of NEMO's hydrophobic cleft. The

Asp738 and Ser740 residues form key intramolecular H-bonds, presumably to stabilize

the loop conformation that the sequence assumes upon binding to NEMO.[8] Additionally,

the backbone N-H of each residue is engaged in hydrogen bonds. Despite its short

length, NBD alone does function as an inhibitor of NEMO-IKK interactions, although the

modest affinity translates to >100 μM IC$_{50}$ values.[9] Nonetheless, NBD functionalized

with a cell-penetrating peptide (CPP) motif has been an important tool for the field.[10]

Our lab previously sought to explore this loop interaction further and replace the

H-bond with a carbon-carbon bond that would provide additional stability to the NBD

peptide and was termed a synthetic loop replacement peptide (SLRP).[11] This was

achieved by replacing the Asp and Ser residues with allyl-glycine residues that were

subjected to olefin ring closing metathesis to form a new alkene functional group that

would replace the H-bond in the native structure. We termed this new NBD peptide

variant NBD$_2$. Additional computational analysis also demonstrated that these

modifications to the NBD sequence would position the Trp residues in a more favorable

confirmation for binding to NEMO against the WT peptide.

A small peptide library was made to test NF-κB inhibition in mammalian HeLa

cells transfected with a luciferase gene. The results from these studies showed that

NBD$_2$, which had the synthetic brace, was a 10-fold better inhibitor than the WT NBD

peptide (Figure 2.1). Despite NBD$_2$ having good biological activity and showing target

engagement with NEMO through a pulldown assay, no direct binding data was procured

due to the significant challenge of expressing and handling full-length NEMO. Thus, it

was not clear if the activity observed in cells was due to the conformational locking, the

increased resistance to proteolysis, or some combination of the two. As with the NBD peptide itself, NBD_2 required a poly-lysine tag on its N-terminus separated from the main sequence by a glycine spacer linker for cell entry. These additional modifications to the peptide presented the following questions related to its activity: what effect does the synthetic brace and the poly-lysine tag have on NDB_2's binding affinity relative to NEMO? And additionally, could the affinity of NBD peptides and derivatives be significantly improved through sequence modification? With regard to the latter goal, a ligand with single digit micromolar (or better) affinity for NEMO would be most useful. Here I describe in detail the biochemical characterization between NBD_2 and the poly-lysine tag through the development of a fluorescence polarization assay made possible by the success of purifying NEMO. This guided further development of NBD peptide derivates that increased binding activity >100-fold without the need for a synthetic brace.
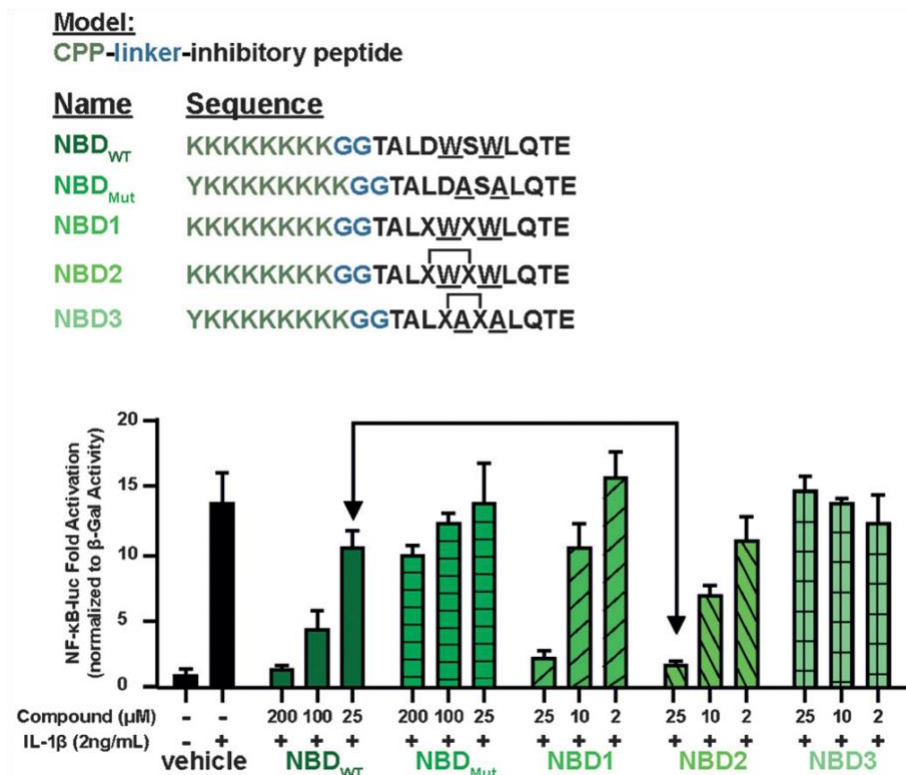
Figure 2.1 Inhibition of NF-κB with NBD peptidomimetic. The figure above shows the effects of NF-κB inhibition with the small NBD peptide library. NBD$_2$, which contains the synthetic brace, inhibited the transcriptional activity of NF-κB 10-fold more potently than the WT sequence. The Mut peptides that contained Ala substitutions failed to show significant activity, showcasing the importance of the Trp residues. Image used with permission from Bruno et al., 2016, Angewandte Chemie. 128, 48, 15221-15225.

C. Results and discussion

Development of an in vitro binding assay for full-length NEMO

To answer the questions posed at the beginning of this chapter, a fluorescence polarization assay was developed to test the affinity of various NBD peptides relative to NEMO. To do this, full-length NEMO protein was required. However, there have been a number of reports of the challenges of expressing and handling the isolated protein. Indeed, previous co-workers in our laboratory had been unsuccessful in isolating sufficient folded protein for biophysical studies. A substantial obstacle is the multiple cysteine residues present throughout various domains, leading to misfolding and aggregation. NEMO exists as a dimer through 2 coiled-coil motifs and a leucine zipper. These traits mean that isolation of the protein in non-optimal buffering conditions can results in aggregation and non-specific associations with other cysteine-rich proteins.[12] Other researchers have designed mutated Cys NEMO constructs to ease the purification process, although in our hands significant aggregation was still observed.[13] Lastly, various reports of bacterial chaperone protein DnaK co-eluting with NEMO have been reported that present an additional hurdle during purification.[14,15,16]

Due to the issues outlined above, my goal was to learn from the previously reported expression and purification protocols to optimize production of full-length, native NEMO. Towards this end, I tested variables such as induction times, temperature, and IPTG concentrations in order to identify conditions that did not lead to

overproduction/aggregation of NEMO. For example, as shown in Figure 2.2, after 3

hours of induction, soluble protein yields were significantly reduced. Ultimately I found

that allowing the cultures to grow under 1mM IPTG for 3 hours was ideal for soluble

protein production (Figure 2.2).

| Time	-	30 min	1H	2H	3H	24H
IPTG	-	+	+	+	+	+
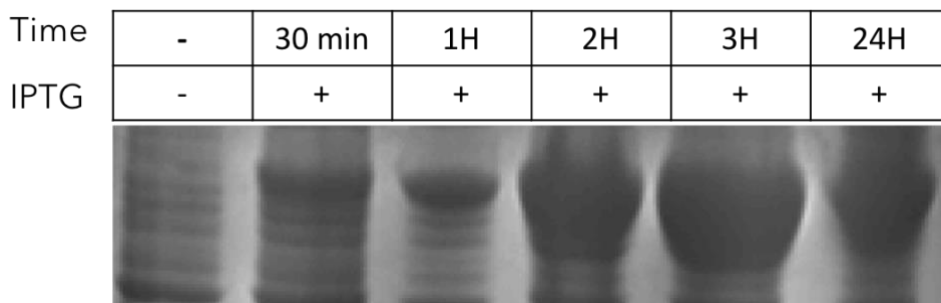
Figure 2.2 Induction test of NEMO production. The figure above depicts the optimization of NEMO protein production in E. Coli cells culture at 37°C with 1mM IPTG. Production maximized noticeably after 3 hours post induction. Samples collected after overnight incubation show IPTG toxicity effects as expected with such high concentration. Cells were lysed using buffered conditions in the Material and methods section. Lysate was loaded onto an SDS-page gel and visualized with Coomassie stain.

After the induction test successfully demonstrated high NEMO protein levels, we

proceeded with full scale purification of the protein by loading treated lysate onto an

AKTA Pure FPLC (GE Healthcare) equipped with a 5 mL Ni HisTrap HP column

(Cytivia). The loaded protein was allowed to equilibrate on the column and then

subjected to a step gradient with elution buffer (50 mM NaCl, 50 mM Tris, 5 mM TCEP,

500 mM imidazole pH 7.4) (further details in Material and Methods section). The identity

of the purified protein was verified through Western blot and mass spectrometry

analysis (Figure 2.3).
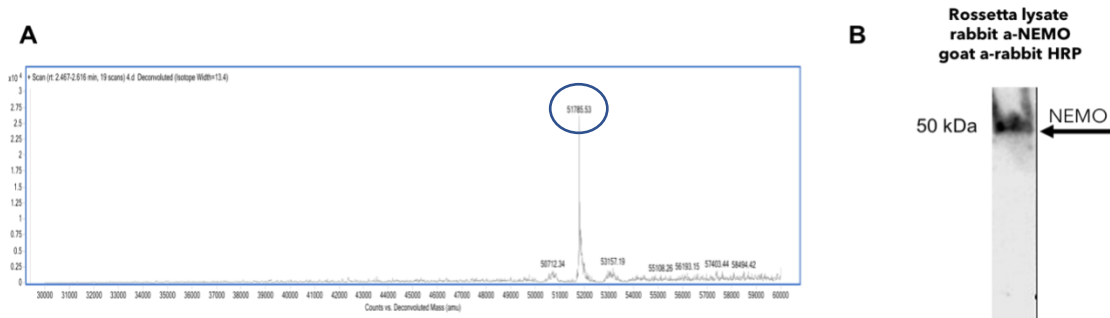
Figure 2.3 Panel of NEMO purification progression and validation. The panel above depicts the following: **A)** LC-MS qTOF analysis of purified protein taken in negative ionization mode. Molecular weight of protein construct is 51785.50 Da and the reported spectral value is 51785.53 Da. **B)** Western blot analysis of purified protein using antibodies specific to NEMO further validating its purity and identification.

In preparation for binding studies with the full-length NEMO protein, I synthesized fluorescein-tagged NBD, NBD derivatives, and a larger sequence derived from the NEMO binding region of IKKα/β ('IKKwt'). For comparison purposes I also prepared NBD$_2$ as well as two sequences in which Trp739 and Trp741 were mutated to alanine, leading to significantly attenuated affinity for NEMO (Figure 2.4). All of the peptides showing in Figure 2.4 were then tested for binding to NEMO using a standard fluorescence polarization assay.
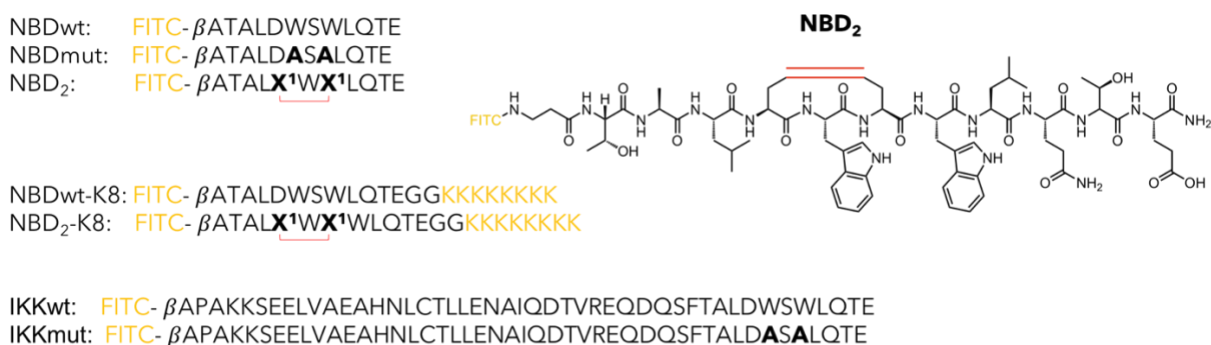

X1 = Allylglycine

Figure 2.4 NBD peptide library 1. The library above consists of NBD derivatives from the 11-mer WT peptide including the peptidomimetic NBD$_2$. Fluoresceine tags (FITC) are labelled in yellow, charged CPP

31

sequences are labeled in purple, and substitutions are in bold. X_1 denotes allylglycine residues that form the synthetic brace (red) post metathesis.

The results of the fluorescence polarization binding experiments are shown in Figure 2.5 and highlight the modest binding affinity of the minimal NBDwt peptide (K_D>100 μM), particularly in comparison with the longer IKKwt sequence (K_D 0.6 μM). An important finding was that the synthetic brace in NBD_2 did not measurably increase binding. Thus, we assume that the increase in potency in cells is largely due to an increased resistance to proteolytic degradation, although there may be other factors. The comparison of IKKwt and IKKmut, as well as NBDwt and NBDmut provides further support for the important role that the tryptophan residues at positions 739 and 741 play in binding, as even in the context of the longer IKK sequence, affinity was decreased >100-fold. Finally, the polyK tag did not increase affinity of the peptides for NEMO, in contrast to other NEMO ligands; indeed, the results suggest that it slightly decreased affinity.
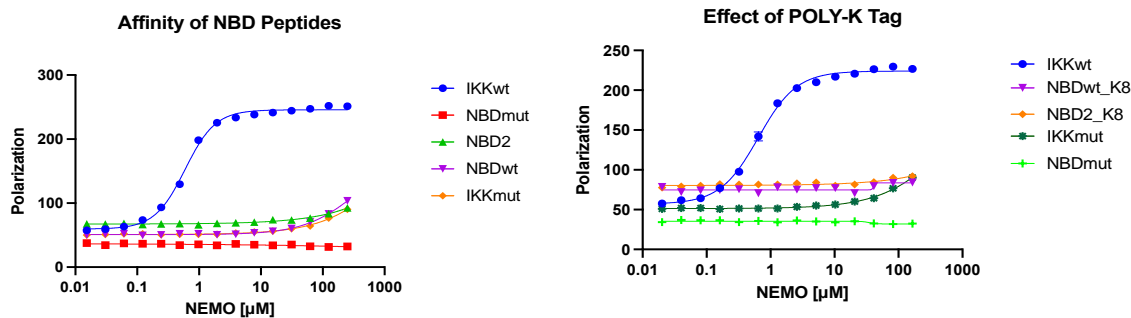
Figure 2.5 Affinity of NBD peptide library 1. The binding affinities of **A)** small NBD peptides without CPP attachments and **B)** NBD peptides with CPP attachments. IKK$_{wt}$ and IKK$_{mut}$ are utilized as standard controls in both experiments. The polarization levels are similar when comparing NBD$_{wt}$ and NBD$_2$ however they reach a saturated binding state classifying them as weak binders. The addition of the CPP to the peptides essentially flattens out the binding curve and shows that it negatively affects binding. Mutational constructs where the Trp residues are replaced lose binding ability. Experiments were performed in triplicate with the indicated standard error (SDOM).

Increasing the binding affinity of weak NBD peptide binders

After testing the effect of the synthetic brace, the contribution of the charged CPP

tag, and realizing they had no measurable effect on binding, we explored further

derivatives of the NBD peptide in search of better binders. A re-examination of the

NEMO-IKK complex crystal structure revealed critical contacts were missing from the

original design of the synthetic loop replacement peptides such as NBD$_2$. By extending

the NBD sequence to include 2 additional residues on the N-terminus, we were able to

increase the affinity of the NBDwt peptide substantially (termed NBD$_4$). The

intermolecular interactions that occur with the addition of S733 and F734 provide

33

additional aromatic pi-pi interactions with the indole ring of the W739 and binding into

NEMO's 3rd hydrophobic pocket. They also provide an additional intermolecular

hydrogen bond interaction between the backbone amide and the side chain of E89 on

NEMO's N-terminus. While the NBD$_{wt}$ peptide struggled to demonstrate high affinity

association with NEMO, the small modifications on NBD$_4$ increased its K$_D$ minimally 2-

fold with a value of 54 μM (Figure 2.6).
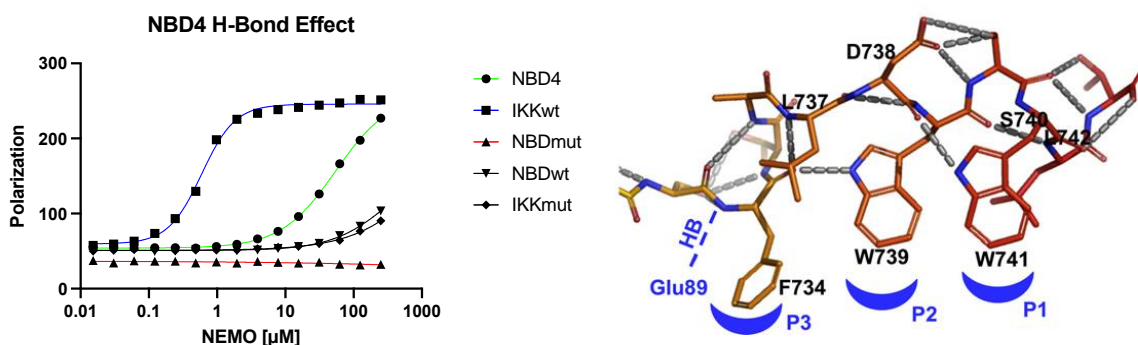
Peptide	K$_D$ (μM)
NBD WT	> 100
NBD 4	**54± 3**
IKK WT	0.60 ± 0.02
W739A, W741A NBD Mut	NA
W739A, W741A IKK Mut	NA

Figure 2.6 Increasing NBD$_{wt}$ peptide affinity. The binding affinity of NBD$_4$ increased 2-fold by extending the NBD$_{wt}$ sequence to include 2 additional amino acids Ser733 and Phe734. The modifications on peptide NBD$_4$ allows for both inter and intramolecular interactions to occur. Experiments were performed in triplicate with the indicated standard error (SDOM). Image used with permission from Rushe et al., 2008, Structure 16,5, 798-808

Analysis of tryptophan 739 and 741 residue interactions within the NEMO hydrophobic

binding surface

The results of the NBD peptide library demonstrated that with minor

modifications, the short sequences could bind effectively with the inclusion of 2

additional aa at the N-terminus. The data also demonstrated the importance of the W

residues in both the small and large constructs- without these residues, nearly all affinity

is lost. Because of this, we hypothesized that expanding the interactions of the Trp

residues through the incorporation of substituents could increase affinity for NEMO. By

analyzing the crystal structure of the NEMO-IKK complex, it became apparent that the

aromatic residues of the NBD are forming various hydrophobic interactions like

L93:F734, M94:F734, F97:W739, and A100:W741 (NEMO to IKKβ).[4] Interestingly, key

residue W739 from the NBD is also being intermolecularly coordinated by NEMO chain

A residues K96, F92 and F97 From NEMO chain B (Figure 2.7). The other critical NBD

residue W741, seems to not be as extensively coordinated, however it has been

reported to interact with R101. Since both of these highly important aromatic residues

are interacting with charged residues in the NEMO specificity pocket, we hypothesized

that we could take advantage of these cation-pi interactions by potentially altering the

pi-electronic system of the Trp side chains.
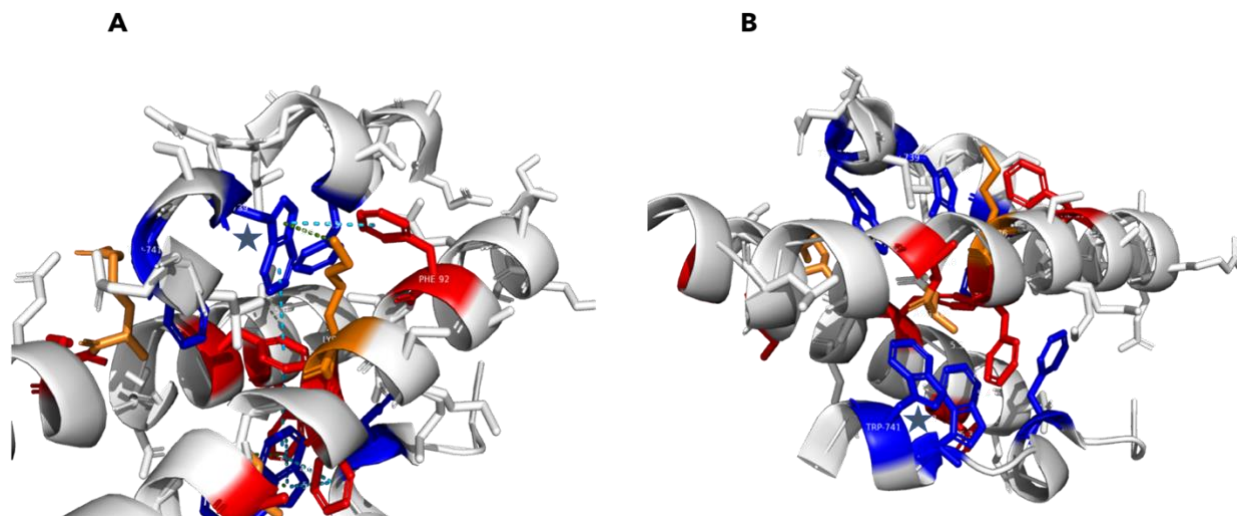
Figure 2.7 Key NEMO-IKKβ associating domains. The crystal structure above depicts the 4-helix associating bundle between NEMO and KKβ. The critical aromatic residues pertaining to the NBD are outlined in blue and NEMO aromatic residues are shown in red. Corresponding NEMO charged residues are shown in orange. **A)** Trp739 interaction with K96/ F92 from NEMO chain A and F97 from chain B. **B)** Trp741 in close proximity to R101 (PDB 3BRV).

Beyond the role of the tryptophan residues, additional literature supports the theory that charged-charged interactions can be beneficial in targeting the NEMO-IKKβ PPI interphase. Pei *et. al*. synthesized a macrocyclic peptide inhibitor, peptide 7, composed of two structural ring motifs: a scaffold with aromatic amino acids that binds NEMO and a second ring motif with charged amino acids utilized for cell entry (Figure 2.8).[17] Interestingly, it was discovered that the charged ring section interacted favorably with NEMO acidic residues next to the NBD binding groove. Peptide 7 inhibited NEMO with low μM activity and further guided our hypothesis that charged structural residues in the NEMO binding pocket could play a significant role in the efficacy of an inhibitor.
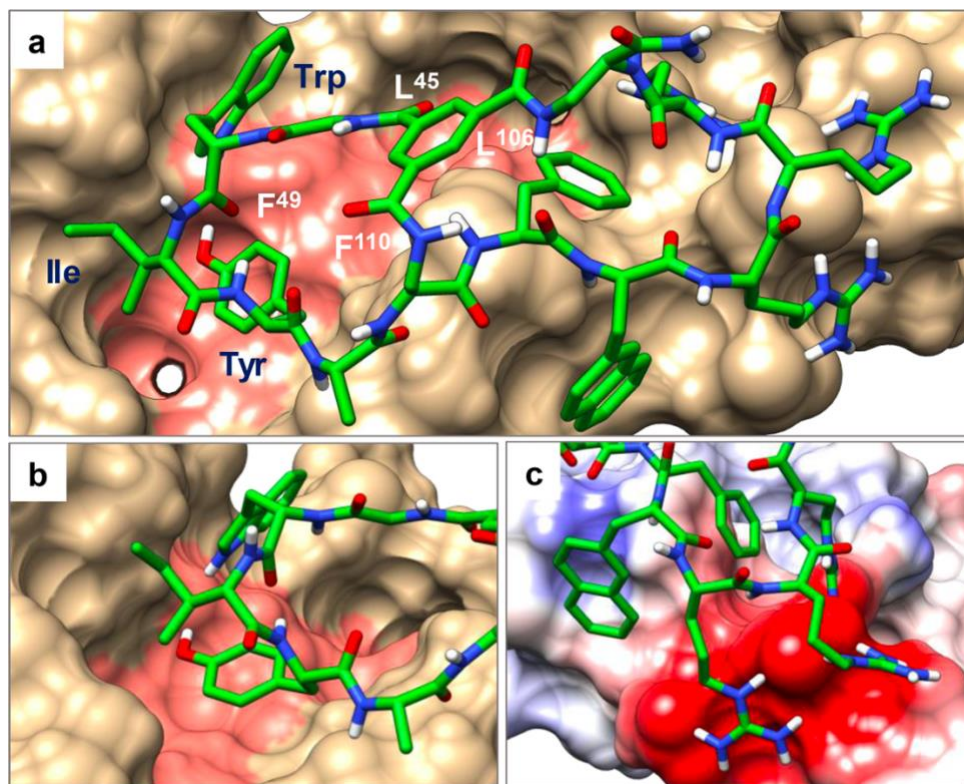
Figure 2.8 Binding interactions of peptide 7. Complex between NEMO and peptide 7 **A)** The binding interactions of peptide 7 and NEMO. Key NEMO binding residues are shown in pink. **B)** Interaction between key aromatic residues of peptide 7 and the hydrophobic binding pocket of NEMO. **C)** The charge-charge interactions between the Arg residues of peptide 7 and NEMO's acidic residues (red). Image used with permission from Rhodes et al., 2018, J. Am. Chem. Soc. 140, 38, 12102-12110.

We proposed to study altering charged interactions from the perspective of the Trp residues due to their interactions and proximity to cationic residues on NEMO. Cation-pi interactions have been well documented to play a significant role in protein interactions through positively charged aa side chains and the pi-electron cloud in aromatic residues.[18,19] They have also been successfully manipulated to produce higher affinity (nM) PPIs by altering electron density in unnatural Trp residues.[20] We hypothesized that by utilizing 3 commercially available unnatural amino acids Trp derivatives with chloro, fluoro, and methoxy substituents on the indole ring we could probe the chemical space around NEMO and develop binders with increased affinity.

We therefore designed a series of NBD peptides containing electron donating and withdrawing substituents on the indole ring at positions 5 and 6 (Figure 2.9).
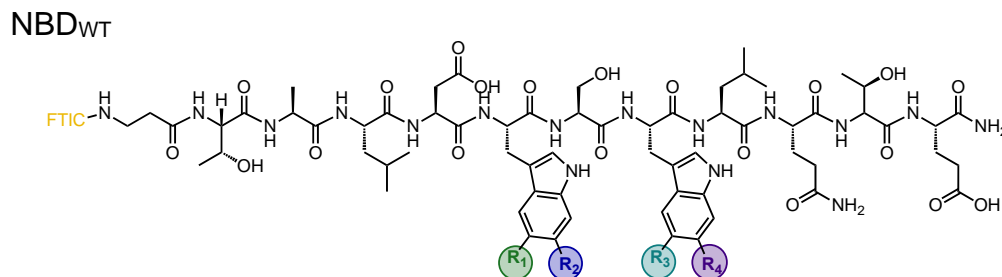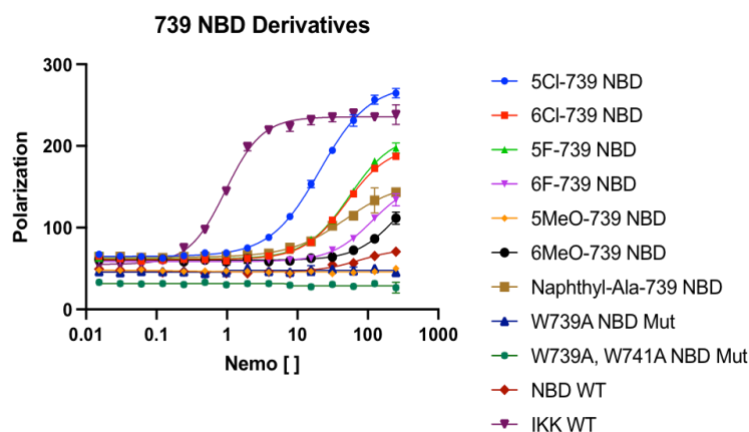
NBD$_{WT}$

Peptide	R1	R2	R3	R4
NBD WT	-H	-H	-H	-H
5Cl-739 NBD	-Cl	-H	-H	-H
5F-739 NBD	-F	-H	-H	-H
5MeO-739 NBD	-OCH$_3$	-H	-H	-H
6Cl-739 NBD	-H	-Cl	-H	-H
6F-739 NBD	-H	-F	-H	-H
6MeO-739 NBD	-H	-OCH$_3$	-H	-H
5Cl-741 NBD	-H	-H	-Cl	-H
5F-741 NBD	-H	-H	-F	-H
5MeO-741 NBD	-H	-H	-OCH$_3$	-H
6Cl-741 NBD	-H	-H	-H	-Cl
6F-741 NBD	-H	-H	-H	-F
6MeO-741 NBD	-H	-H	-H	-OCH$_3$

Figure 2.9 Charged NBD peptide library 1. The table depicts the different charged atom substitutions at positions 5 and 6 of the indole rings in Trp 739 and 741. Each peptide was connected to FITC by a β-Ala linker.

Analysis of electron donating and withdrawing substituents on tryptophan 739

Substituting W739 with groups such as fluorine, chlorine, and methoxy that vary in electronic properties at indole positions 5 and 6 had varying effects on binding. The incorporation of F or Cl at the 5 position notably increased affinity; substitution at the 6 position had a smaller effect (Figure 2.10). In contrast, methoxy group substitution at the 5-position abrogated binding, likely due to steric clashes. Substitution at the 6 position modestly increased affinity. Overall, the 5Cl-739 NBD peptide represented a >5-fold improvement over the parent NBD WT with just a single atom change.

To further assess modifications at residue 739, Trp739 was replaced with either an Ala residue or a naphthyl-Ala residue. The naphthyl-Ala substitution served to test the effect of larger aromatic residues with a more hydrophobic core relative the indole ring of tryptophan. Unsurprisingly, the peptide with the Ala mut was not able to retain its binding association with NEMO and acted equally to the double Ala mutant at positions 739 and 741(W739A, W741A NBD Mut). The naphthyl-Ala mutant did show improved binding relative to NBD WT but was not comparable to the halogen-substituted Trp analogs.
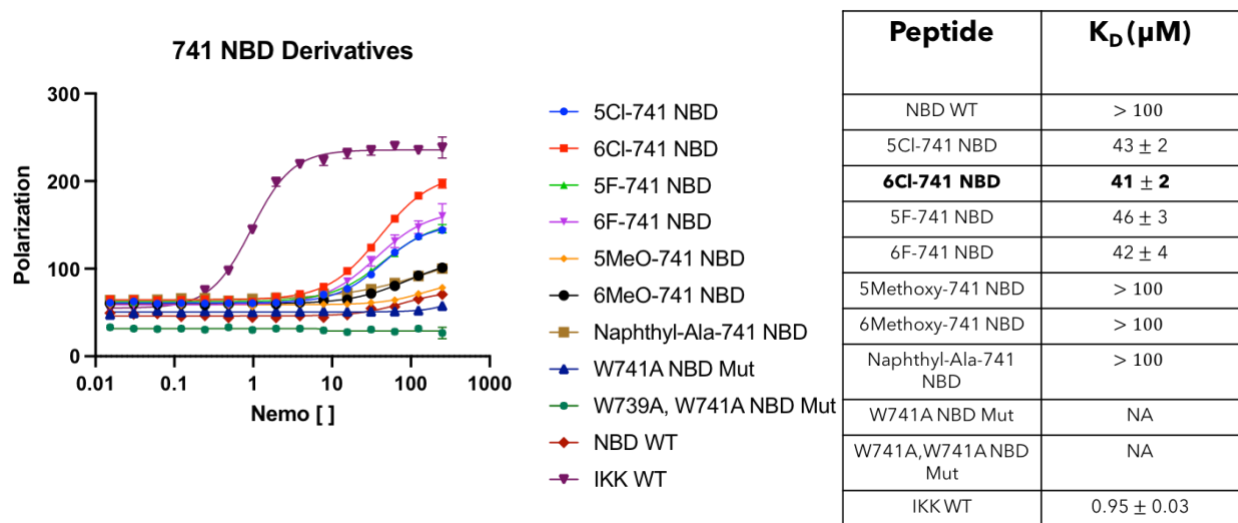
739 NBD Derivatives

Legend:
- 5Cl-739 NBD
- 6Cl-739 NBD
- 5F-739 NBD
- 6F-739 NBD
- 5MeO-739 NBD
- 6MeO-739 NBD
- Naphthyl-Ala-739 NBD
- W739A NBD Mut
- W739A, W741A NBD Mut
- NBD WT
- IKK WT

Peptide	K_D (µM)
NBD WT	> 100
5Cl-739 NBD	**20.8 ± 0.7**
6Cl-739 NBD	50 ± 2
5F-739 NBD	54 ± 3
6F-739 NBD	> 100
5Methoxy-739 NBD	> 100
6Methoxy-739 NBD	> 100
Naphthyl-Ala-739 NBD	> 100
W739A NBD Mut	NA
W739A, W741A NBD Mut	NA
IKK WT	0.95 ± 0.03

Figure 2.10 Affinity of charged NBD peptide library 1 (739 NBD peptides). The data above represents the relative binding affinities between the single residue substitutions at W739 from the small 11-mer NBD peptide. Elongated NBD sequence (IKK WT) was utilized as positive control and W739A NBD Mut and W739A, W741A NBD Mut as respective negative controls missing either 1 or both Trp residues. The electronegative fluoro and chloro atom substitutions had the largest increased affinity relative to the NBD WT peptide, with a chloro substitution at position 5 having the largest impact. Experiments were performed in triplicate with the indicated standard error (SDOM).

Analysis of electron donating and withdrawing substituents on tryptophan 741

The substitution of Trp residue 741 also prompted further investigation due to its equally important role in binding and slightly different micro-environment relative to position 739. An analogous series of NBD WT derivatives were synthesized and analyzed (Figure 2.11). As with the Trp739 series, the halogen substitutions favorably affected affinity for NEMO, with all analogs displaying essentially identical K_Ds (40-45 µM). The methoxy substitution only slightly increase affinity. Ala mutation at this residue also showed no binding activity and the naphthyl-Ala substitution bound similarly to the NBD WT. Taken together, the data suggest that the binding pocket for Trp741 is more flexible.

40

741 NBD Derivatives

Peptide	K_D (µM)
NBD WT	> 100
5Cl-741 NBD	43 ± 2
6Cl-741 NBD	**41 ± 2**
5F-741 NBD	46 ± 3
6F-741 NBD	42 ± 4
5Methoxy-741 NBD	> 100
6Methoxy-741 NBD	> 100
Naphthyl-Ala-741 NBD	> 100
W741A NBD Mut	NA
W741A,W741A NBD Mut	NA
IKK WT	0.95 ± 0.03

Figure 2.11 Affinity of charged NBD peptide library 1 (741 NBD peptides). The data above represents the relative binding affinities between the single residue substitutions at W741 from the small 11-mer NBD peptide. Elongated NBD sequence (IKK WT) was utilized as positive control and W739A NBD Mut and W739A, W741A NBD Mut as respective negative controls missing either 1 or both Trp residues. The electronegative fluoro and chloro atom substitutions again had the largest increased affinity, with a chloro substitution at position 6 having the largest impact relative to the WT NBD peptide. Experiments were performed in triplicate with the indicated standard error (SDOM).

Impact of substitutions at both Trp739 and Trp741

After exploring the chemical space concerning each individual Trp residue, we questioned how those results would translate to a double substituted electronegative Trp NBD WT peptide. In addition, we also wondered if including Ser733 and Phe734 residues at the N-terminus (NBD₄), shown in previous experiments to boost affinity significantly, would complement the findings. A second library of NBD peptides was thus synthesized to test these added variables (Figure 2.12).

The new library yielded differed results than our expected hypothesis driven by the initial SAR studies. We expected residue W739 to favor a chloro substitution at indole position 5 and residue W741 at position 6. However, this was not the case (Figure
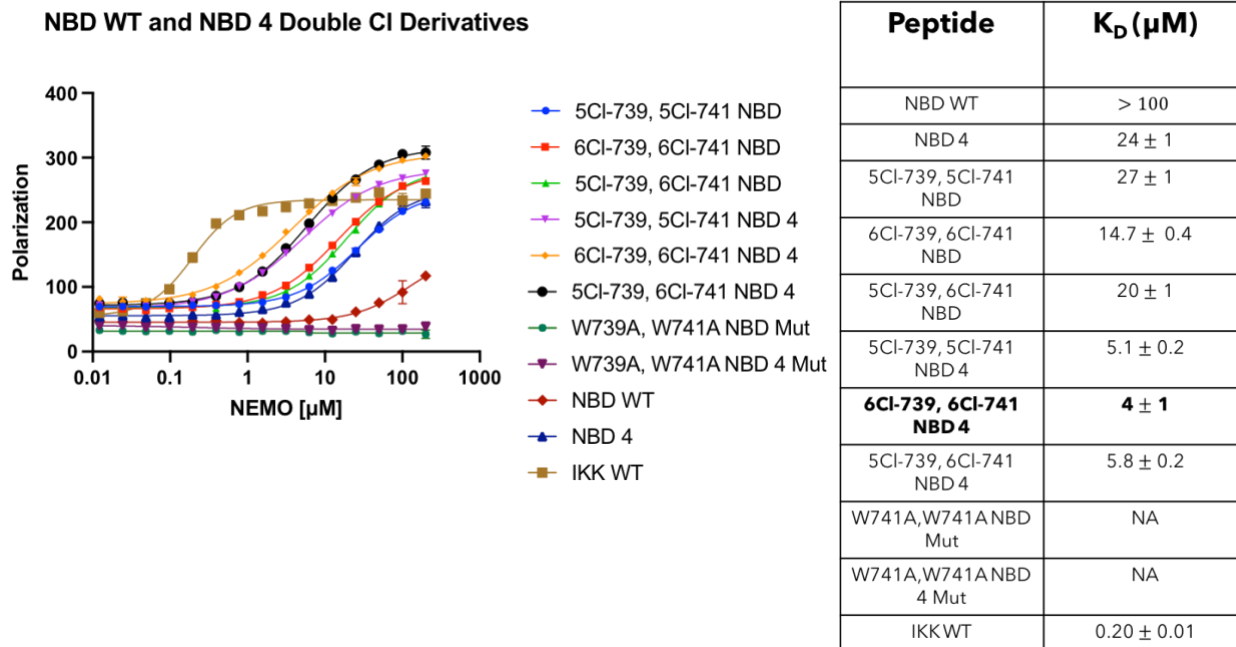
41

2.13). All double chloro substituted NBD WT peptides increased affinity with a small preference for position 6. We suspect that addition of electron withdrawing groups on both Trp residues changes the pi-pi interactions that occur between both aromatic residues and affects other aromatic interactions within the NEMO binding cage as well. NBD$_4$ peptide variants that contained the same substitutional derivatives had similar trends. All double chloro substituted NBD$_4$ peptides increased affinity further with a small preference for position 6 as well. The results from these modifications highlight how the growing peptide chain provides additional interactions; the addition of Phe734 interacts with NEMO residues Met94 and Lue93 and likely affects the intra and intermolecular interactions of the electron deficient indole ring substitutions of the aromatic cage. I did note that over time the concentration of active protein decreased, perhaps due to aggregation. For this reason, in each binding experiment positive (IKK) and negative (mutant peptides) were included as benchmarks.
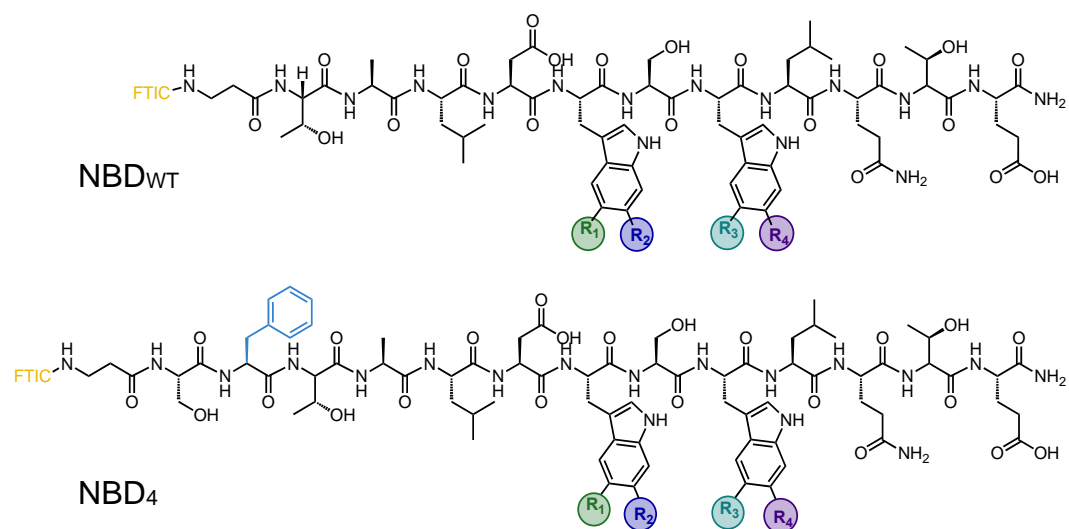
Peptide	R1	R2	R3	R4
NBD WT	-H	-H	-H	-H
5Cl-739, 5Cl-741 NBD	-Cl	-H	-Cl	-H
6Cl-739, 6Cl-741 NBD	-H	-Cl	-H	-Cl
5Cl-739, 6Cl-741 NBD	-Cl	-H	-H	-Cl
5Cl-739, 5Cl-741 NBD 4	-Cl	-H	-Cl	-H
6Cl-739, 6Cl-741 NBD 4	-H	-Cl	-H	-Cl
5Cl-739, 6Cl-741 NBD 4	-Cl	-H	-H	-Cl

Figure 2.12 Charged NBD peptide library 2. The table depicts different electronegative atom substitutions at positions 5 and 6 of the indole rings of both Trp 739 and 741. An additional construct (NBD4) was subjected to the same substitutions to probe how additional residues Ser733 and Phe734 previously demonstrated to add additional key interactions would be affected by the atom changes. Each peptide was connected to FITC by a beta-Ala linker.

Figure 2.13 graph "NBD WT and NBD 4 Double Cl Derivatives" with legend:
- 5Cl-739, 5Cl-741 NBD
- 6Cl-739, 6Cl-741 NBD
- 5Cl-739, 6Cl-741 NBD
- 5Cl-739, 5Cl-741 NBD 4
- 6Cl-739, 6Cl-741 NBD 4
- 5Cl-739, 6Cl-741 NBD 4
- W739A, W741A NBD Mut
- W739A, W741A NBD 4 Mut
- NBD WT
- NBD 4
- IKK WT

Peptide	K_D (µM)
NBD WT	> 100
NBD 4	24 ± 1
5Cl-739, 5Cl-741 NBD	27 ± 1
6Cl-739, 6Cl-741 NBD	14.7 ± 0.4
5Cl-739, 6Cl-741 NBD	20 ± 1
5Cl-739, 5Cl-741 NBD 4	5.1 ± 0.2
6Cl-739, 6Cl-741 NBD 4	**4 ± 1**
5Cl-739, 6Cl-741 NBD 4	5.8 ± 0.2
W741A,W741A NBD Mut	NA
W741A,W741A NBD 4 Mut	NA
IKK WT	0.20 ± 0.01

Figure 2.13 Affinity of charged NBD peptide library 2. The data above represents the relative binding affinities between double residue substitutions at W741 and W739 for the 11-mer NBD peptide (NBD WT) and 13-mer (NBD 4). Both NBD derivatives experienced an increase in affinity with all the electronegative substituted variants, especially at position 6. The best derivative binder was NBD$_4$ with chloro substitutions at positions 6 that showed synergy with the added resides. Experiments were performed in triplicate with the indicated standard error (SDOM).

D. Assessments and Future Directions

The principal goal of this chapter was to connect the bio activity of the SLRPs to binding activity with NEMO through a fluorescence polarization assay, and in effect, develop better binders. The result of the direct binding activity of the SLRP, NBD$_2$, demonstrated to not affect the binding activity relative to the WT NBD-peptide, however it did not give any additive effects in terms of binding. This leads us to theorize that the increased biological activity observed is due to the structural stability of the peptide that is also less prone to degradation by proteases. The poly-lysine tag seems to detract the small NBD-peptides from binding. The WT NBD peptide that consists of residues 735 to

745 binds minimally to NEMO with very low affinity although inclusion of 2 additional residues to the N-terminus spikes the affinity substantially (NBD$_4$). The removal of either tryptophan residue from position 739 or 741 demonstrate how critical these residues are towards binding activity for any NBD-derived peptides.

Additional studies to test the functional changes of the tryptophan residues when substituents that add or remove electron density demonstrated the preferential modification for a tighter binding event. The NBD peptide relies heavily on binding through its hydrophobic interactions in NEMO's binding pocket and aromatic residues compliment that binding interface. By testing the modified Trp residues against NEMO binding interactions we were able to find a double chloro substituent at position 6 to bind most effectively with a K$_D$ of 3.8 μM. To our knowledge, this molecule is the best short NBD-peptide-based derivative binder found in the literature. We also noticed the affinity of the mono chloro substitutions differed from each other at each Trp, showcasing the different microenvironments between residues. Those mutants also interacted differently when double substitutions were made and when the peptide chain grew longer. To us, these results demonstrate the inter and intramolecular NBD-NEMO interactions that occur between residues and crosstalk between the 3 aromatic residues that stabilize the complex for efficient binding.

Future directions for this work involve further investigation of the NBD peptide at the Phe734 residue due to its aromatic character that interacts with other aromatics in the NEMO binding pocket. The SAR studies involving Phe734 (NBD$_4$) and a modified Trp739 resulted in a low μM binder and we are curious to test the effects of additional modifiers on Phe734. By adding either electron donating or withdrawing substituents on

the Phe residue's aromatic sidechain, we believe the affinity of the peptide molecule can reach a high nM K_D binding activity.

Additional studies will involve the use of synthetic braces to make additional synthetic loop replacement peptides. Since we tested and found the brace to have minimal effect on binding activity, we can still implement that tool to a modified NBD-peptide with high affinity for NEMO and make it more proteolytically stable. Finding the optimal sequence of the NBD peptide will be followed by the exploration of its use as a bifunctional molecule. That includes experiments to explore additive CPP sequences such as Clip6, TAT, penetrin, antennapeda, poly-R, and poly-K. Since the WT peptide sequence will be modified extensively, it may be worthwhile to find a CPP that affects its binding capabilities the least. The CPP additive will greatly influence how effective the peptide behaves in a more biological environment and how the peptide acts as an inhibitor. Further studies into the peptide should be done if it does not bode well as an inhibitor to NF-κB. Tactics such as implementation of a peptide-PROTAC approach can be utilized to further its biological activity.

Lastly, our data support the hypothesis that aromatic side chains are critical to the interaction between NEMO and IKK. Because of this, we propose additional high-throughput screening to be done with libraries that include diverse macrocyclic molecules. Our hypothesis is that a rich aromatic system with varying charge distribution would perform well to disrupt the binding interface between these two proteins, gain cell permeability, and act as an efficient inhibitor towards NF-κB.

E. Materials and Methods

Reagents and Instrumentation

Chemical and biological reagents were obtained from commercial sources and were utilized without additional modifications (unless otherwise specified). DNA, protein, peptide, and O.D. concentrations were determined using a Thermo Scientific NanoDrop One Spectrophotometer.

Plasmids for protein expression

The plasmid utilized for NEMO purification was commercially purchased from Addgene (Plasmid # 11966). Plasmid pET-NEMO's sequence identity was confirmed through Sangar sequencing on an Aplied Biosystems 3730xl DNA Analyzer at the University of Michigan DNA Sequencing Core and analyzed using SeqMan Pro from the Lasergene DNASTAR software suite.

Protein Expression of NEMO

All procedures were performed under standard sterile conditions and recommended antibiotic concentrations from Addgene. Transformation of the plasmid was introduced to chemically competent Rosetta 2 (DE3) pLysS competent cells and plated in agar containing Kanamycin/Chloramphenicol and incubated at 37ºC overnight. The next day a single colony was chosen and inoculated into 50 mL of LB media containing 50 µg/mL and 25 µg/mL of respective antibiotic and incubated overnight at 37ºC at 250 rpm. The following day, 5 mL of the stater culture was removed and added to a 1L LB culture containing the same antibiotic concentrations and grown to an OD_{600} of 0.4- 0.6 at 37ºC at 250 rpm. Once the desired OD_{600} was reached, induction of the

47

culture proceeded by adding 1mM of IPTG and shaken at 37ºC and 250 rpm for 3 hours as done in other published protocols.[13] After the 3 hours, the bacteria cultures were spun down at 10,000 x G for 30 minutes at 4ºC. The pellets were stored at -80ºC until use.

Protein Purification of NEMO

To purify NEMO, affinity chromatography was utilized. Prepping for the protein purification involved resuspending the bacterial pellet in 50 mL of lysis buffer (50mM NaCl, 50mM Tris, 5mM TCEP, pH 7.4) which was supplemented with streptomycin sulfate (10mg/mL), ATP, and 1 Roche complete mini protease tablet. The pellet slurry was then lysed through sonication for 5 total minutes with a frequency of 5 seconds on and a 10 second cool down. The lysate was then centrifuged at 20,000 rpm for a total of 30 minutes. To remove any remaining bound nucleic acid impurities or chaperons, an additional sonication step was implemented as described previously to the supernatant which was then subjugated to an additional centrifuging step.

The supernatant was then pushed through a 0.45 syringe filter (CellTreat) and loaded onto an AKTA Pure FPLC (GE Healthcare) equipped with a 5 mL Ni HisTrap HP column (Cytivia). The column was pre-equilibrated with the same lysis buffer as described above and NEMO was sequentially purified utilizing a step gradient with elution buffer (50mM NaCl, 50mM Tris, 5mM TCEP, 500 mM Immidazole pH 7.4). The pooled fractions were collected and concentrated to a volume of 2.5 mL using an EMD Amicron Ultra Centrifugal Filter Units with a MWCO of 30kDa (MilliporeSigma). The concentrated protein was then subjected to a buffer exchange (200 mM NaCl, 50mM Tris, 0.01% Triton X-100 (V/V), 1mM DTT) using a PD-10 desalting column (GE

Healthcare). The concentration of the protein was determined using UV/Vis

spectroscopy on a NanonDrop instrument at 280 nm using an extinction coefficient of

14,440 $M^{-1}cm^{-1}$. Aliquots were flash frozen and stored at -80ºC until further use. Protein

identity was confirmed through mass spectrometry (Agilent Q-TOF) and through

Western Blot analysis by incubating nitrocellulose membrane with NEMO primary

antibody (Santa Cruz 166398) and then secondary antibody (Santa Cruz 525408).

Purity was monitored throughout purification process by SDS-PAGE on 4-12% bis-tris

gel stained with Quick Coomassie (Anatrace).

Solid-Phase Peptide Synthesis and HPLC Purification of NBD Peptides

Table 2.1. Sequences of peptides used in chapter 2

Peptide	Sequence (N'-C')
NBDwt (735-745)	FITC-βAla-TALDWSWLQTE
NBDWT-PolyK	FITC-βAla-TALDWSWLQTEGGKKKKKKK
NBDmut	FITC-βAla-TALDASALQTE
NBDmut_W739A	FITC-βAla-TALDASWLQTE
NBDmut_W741A	FITC-βAla-TALDWSALQTE
IKKwt	FITC-βAla-PAKKSEELVAEHNLCTLLENAIQDTVREQDQSFTALDWSWLQTE
IKKmut	FITC-βAla-PAKKSEELVAEHNLCTLLENAIQDTVREQDQSFTALDASALQTE

NBD4	FITC-βAla-SFTALDWSWLQTE	
NBD4mut	FITC-βAla-SFTALDASALQTE	
Naphthyl-Ala -739 NBD	FITC-βAla-TALDX$_1$SWLQTE	X$_1$ =Naphthyl-Ala
5MeO-739 NBD	FITC-βAla-TALDX$_2$SWLQTE	X$_2$ =5-Methoxy-Trp
6MeO-739 NBD	FITC-βAla-TALDX$_3$SWLQTE	X$_3$=6-Methoxy-Trp
5Cl-739 NBD	FITC-βAla-TALDX$_4$SWLQTE	X$_4$ =5-Chloro-Trp
6Cl-739 NBD	FITC-βAla-TALDX$_5$SWLQTE	X$_5$ =6-Chloro-Trp
5F-739 NBD	FITC-βAla-TALDX$_6$SWLQTE	X$_6$ =5-Fluoro-Trp
6F-739NBD	FITC-βAla-TALDX$_7$SWLQTE	X$_6$ =6-Fluoro-Trp
Naphthyl-Ala -741 NBD	FITC-βAla-TALDWSX$_1$LQTE	X$_1$ =Naphthyl-Ala
5MeO-741 NBD	FITC-βAla-TALDWSX$_2$LQTE	X$_2$ =5-Methoxy-Trp
6MeO-741 NBD	FITC-βAla-TALDWSX$_3$LQTE	X$_3$=6-Methoxy-Trp
5Cl-741 NBD	FITC-βAla-TALDWSX$_4$LQTE	X$_4$ =5-Chloro-Trp
6Cl-741 NBD	FITC-βAla-TALDWSX$_5$LQTE	X$_5$ =6-Chloro-Trp
5F-741 NBD	FITC-βAla-TALDWSX$_6$LQTE	X$_6$ =5-Fluoro-Trp
6F-741NBD	FITC-βAla-TALDWSX$_7$LQTE	X$_6$ =6-Fluoro-Trp
5Cl-739, 5Cl-741 NBD	FITC-βAla-TALDX$_4$SX$_4$LQTE	X$_4$ =5-Chloro-Trp
6Cl-739, 6Cl-741 NBD	FITC-βAla-TALDX$_5$SX$_5$LQTE	X$_5$ =6-Chloro-Trp
5Cl-739, 6Cl-741 NBD	FITC-βAla-TALDX$_4$SX$_5$LQTE	X$_4$ =5-Chloro-Trp X$_5$ =6-Chloro-Trp
5Cl-739, 5Cl-741 NBD 4	FITC-βAla- SFTALDX$_4$SX$_4$LQTE	X$_4$ =5-Chloro-Trp

6Cl-739, 6Cl-741 NBD 4	FITC-βAla- SFTALDX$_5$SX$_5$LQTE	X$_5$ =6-Chloro-Trp
5Cl-739, 6Cl-741 NBD 4	FITC-βAla- SFTALDX$_4$SX$_5$LQTE	X$_4$ =5-Chloro-Trp X$_5$ =6-Chloro-Trp

The peptides in Table 2.4 were synthesized under standard FMOC solid-phase conditions on a Liberty Blue Microwave Synthesizer (CEM) using Rink Amide resin (CEM). Deprotection of FMOC groups was done in 20% piperidine (ChemImpex) in DMF that was supplemented with 0.2M Oxyma Pure (CEM) and irridated under variable power to maintain a temperature of 90ºC for 1 minute. Coupling of each amino acid was done at 5 eq relative to resin with diisopropylcarbodiimide (7 eq, ChemImpex) and Oxyma (5 eq) in DMF and irradiated at variable power to maintain a temperature of 90ºC for 4 minutes. All coupling and deprotection steps were rinsed 4 times with excess DMF. All peptides were subjected to a final coupling step to add β-Ala on the N-terminus and deprotected in a final solution of 20% piperidine in DMF.

All peptides were treated with a 5% N,N diisopropylethylamine solution in DMF containing 2 eq of fluorescein isothiocyanate (FITC, ThermoFisher) and allowed to incubate overnight. Final cleavage from the resin was completed by subjecting the peptide to a cleavage cocktail composed of 95% TFA, 2.5% H$_2$O, and 2.5% triisopropylsilane for 4 hours. The solution was then filtered to separate resin and precipitated with chilled diethyl ether. The precipitated peptide was centrifuged down and dissolved in 70/30 0.1% TFA in water and acetonitrile, syringe filtered using a 0.45 µn, and purified by reversed phase HPLC purification on an Agilent 1260 Series

instrument with a 250 X 10 mm Luna Omega 5 µm PS C18 column. Each peptide was purified using 10-50 elution gradient of acetonitrile in 0.1% TFA in water over 50 minutes. Fractions were collected from peaks visible using the 495nm fluoresce signal in addition to 280nm when Trp was present.

Each purified peptide was identified using mass spectrometry in negative ion mode (Agilent qTOF). Further purity assessment was done utilizing analytical HPLC. Post-analysis each peptide was dissolved in DMSO and quantified through UV/VIS spectroscopy using FITC absorbance at 495 nm (ε495= 73,500 M^{-1}cm^{-1}).

Solid-Phase Peptide Synthesis and HPLC Purification of SLRPs

Table 2.5. Structure of SLRPs used in chapter 2

Peptide	Structure
NBD2	
NBD2-PolyK	

The peptides in Table 2.5 were synthesized under the same conditions as the peptides in Table 2.4. To synthesize the synthetic loop, the Asp and Ser residues from the NBDwt peptide were substituted for FMOC-Allyl-L-Glycine residues and the peptide on resin was transferred to a 10 mL microwave reaction vessel. The peptide-resin (eq) was prepped in 2 mL of dry DMF containing 0.4 M LiCl and allowed to charge under N$_2$

for 1 hour, after which Grubs Gen II catalyst (20 mol% in dry DCM) was added to the mixture. The vessel was then inserted in the microwave reactor attachment (CEM) and radiated at varying power for 15 minutes at a temperature of 100ºC. Following exposure to the microwave reactor, the resin was washed 3X with DCM, DMF and MeOH, and was worked up as described in the previous section.

Direct Binding Assay

Direct binding assays between the fluorescently labeled peptides and NEMO were done in a 384-well black plate (Corning) with a final volume of 20 µL and performed in triplicate. NEMO protein stocks were allowed to thaw and a 2x serial dilution for 15 different concentration points was prepared. Each lane was filled with 16 µL of corresponding dilution point with the highest concentration in Row A being 250 µM. The peptides, previously dissolved in DMSO, were diluted down in the assay buffer (200 mM NaCl, 50mM Tris, 0.01% Triton X-100 (V/V), 1mM DTT) to a concentration of 150 nM which were then mixed with equal volume of a reducing agent solution (DTT 100 mM) in a black Eppendorf tube. To the wells with previously loaded protein, 4 µL of the tracer peptide/reducing agent mixture was added for a final concentration of 15 nM for each peptide. Row P was treated as a control containing only buffer and tracer peptide. The plate was allowed to incubate for 30 minutes at room temperature and after was read on a PHERAStar multi-mode plate reader using polarized excitation at 485 nm with emission intensity measured through a parallel and 72 perpendicularly polarized 535 nm filter. Polarization values were plotted against log [NEMO] and fit into a non-linear regression curve utilizing Prism's built-in equation "log(agonist) vs response-variable slope (four parameters)". The K_D values were calculated using the

EC$_{50}$ values from Prism and using the equations from cited papers.[21,22] Each data point is an average 3 technical replicates with the error representing the standard deviation between them.

F. References

1.   Gilmore, T. D. Introduction to NF-κB: players, pathways, perspectives. *Oncogene 2006 2551* **25**, 6680–6684 (2006).

2.   Tarassishin, L. & Horwitz, M. S. Sites on FIP-3 (NEMO/IKKγ) Essential for Its Phosphorylation and NF-κB Modulating Activity. *Biochem. Biophys. Res. Commun.* **285**, 555–560 (2001).

3.   Häcker, H. & Karin, M. Regulation and function of IKK and IKK-related kinases. *Sci. STKE* **2006**, 2023 (2006).

4.   Rushe, M. *et al.* Structure of a NEMO/IKK-Associating Domain Reveals Architecture of the Interaction Site. *Structure* **16**, 798–808 (2008).

5.   Mapp, A. K., Pricer, R. & Sturlis, S. Targeting transcription is no longer a quixotic quest. *Nat. Chem. Biol.* **11**, 891 (2015).

6.   Guo, B., Audu, C. O., Cochran, J. C., Mierke, D. F. & Pellegrini, M. Protein engineering of the n-terminus of NEMO: Structure stabilization and rescue of ikkβ binding. *Biochemistry* **53**, 6776–6785 (2014).

7.   May, M. J., Marienfeld, R. B. & Ghosh, S. Characterization of the IκB-kinase NEMO binding domain. *J. Biol. Chem.* **277**, 45992–46000 (2002).

8.   Golden, M. S. *et al.* Comprehensive Experimental and Computational Analysis of Binding Energy Hot Spots at the NF-κB Essential Modulator/IKKβ Protein−Protein Interface. *J. Am. Chem. Soc* **135**, (2013).

9.   May, M. J. *et al.* Selective Inhibition of NF-κB Activation by a Peptide That Blocks the Interaction of NEMO with the IκB Kinase Complex. *Science (80-.).* **289**, 1550 LP – 1554 (2000).

10. Jones, S. W. *et al.* Characterisation of cell-penetrating peptide-mediated peptide delivery. *Br. J. Pharmacol.* **145**, 1093 (2005).

11. Bruno, P. A., Morriss-Andrews, A., Henderson, A. R., Brooks, C. L. & Mapp, A. K. A Synthetic Loop Replacement Peptide That Blocks Canonical NF-κB Signaling. *Angew. Chemie Int. Ed.* **55**, 14997–15001 (2016).

12. Ivins, F. J. *et al.* NEMO oligomerization and its ubiquitin-binding properties. *Biochem. J.* **421**, 243–251 (2009).

13. Cote, S. M. *et al.* Mutation of nonessential cysteines shows that the NF-κB essential modulator forms a constitutive noncovalent dimer that binds IκB kinase-β with high affinity. *Biochemistry* **52**, 9141–9154 (2013).

14. Ratelade, J. *et al.* Production of recombinant proteins in the lon-deficient BL21(DE3) strain of Escherichia coli in the absence of the DnaK chaperone. *Appl. Environ. Microbiol.* **75**, 3803–3807 (2009).

15. Agou, F. *et al.* NEMO trimerizes through its coiled-coil C-terminal domain. *J. Biol. Chem.* **277**, 17464–17475 (2002).

16. Fontan, E. *et al.* NEMO oligomerization in the dynamic assembly of the IκB kinase core complex. *FEBS J.* **274**, 2540–2551 (2007).

17. Rhodes, C. A. *et al.* Cell-Permeable Bicyclic Peptidyl Inhibitors against NEMO-IκB Kinase Interaction Directly from a Combinatorial Library. *J. Am. Chem. Soc.* **140**, 12102–12110 (2018).

18. Ma, J. C. & Dougherty, D. A. The cation-π interaction. *Chem. Rev.* **97**, 1303–1324 (1997).

19. Infield, D. T. *et al.* Cation-π interactions and their functional roles in membrane

proteins. *J. Mol. Biol.* **433**, 167035 (2021).

20.	Zhao, H. *et al.* Manipulating Cation-πInteractions with Genetically Encoded

	Tryptophan Derivatives. *J. Am. Chem. Soc.* **144**, 6742–6748 (2022).

21.	Hall, M. D. *et al.* Fluorescence polarization assays in high-throughput screening

	and drug discovery: a review. *Methods Appl. Fluoresc.* **4**, (2016).

22.	Roehrl, M. H. A., Wang, J. Y. & Wagner, G. A general framework for development

	and data analysis of competitive high-throughput screens for small-molecule

	inhibitors of protein-protein interactions by fluorescence polarization. *Biochemistry*

	43, 16056–16066 (2004).

Chapter 3

Transformation of a NEMO Inhibitor into a NEMO Degrader

A. Abstract

The protein-protein interactions (PPIs) within the IKK complex are a gateway for NF-κB activation which regulates gene expression of cell cycle actors in cancer. The interaction between NEMO and IKKβ is largely dependent on key hydrophobic interactions over a large surface area that has made it difficult for small molecule drug discovery to alter activity. The regulation of this complex has previously been successful by utilizing short peptide sequences derived from IKKβ. However the peptide character of these inhibitors decreases their activity and functionality in cell studies. Recently, advancement in PROTAC technology has demonstrated that inhibition through degradation can be an effective strategy for modulating the activity of hard-to-target PPIs. PROTACs functionality as degraders has been shown to also be an effective tool for peptide ligand motifs and increase their bioactivity. In this Chapter, I examine the functionality of turning both large (45-mer) and small (11-mer) IKKβ derived peptides into PROATCs through utilization of different E3 recruiter and linker motifs. In addition to correlating the various structural motif additivities to their effect on binding to NEMO. This resulted in the identification of a molecule (NP-8) that retained binding affinity to NEMO and modestly decreased the activity of NF-κB in HEK-293T cells relative to other PROTAC derivative synthesized.

B. Introduction

As is true of many events in the cell, the signal that a particular protein is no longer useful or needed is a post-translational modification.[1] In this case, the post-translational modification is the covalent linkage to the protein ubiquitin or smaller ubiquitin-like proteins. Ubiquitination of proteins is functionally critical because it consequently leads to degradation by the proteasome. A protein can become ubuiquinated when an E3 ligase covalently links poly-ubiquitin chains on a protein's Cys, Ser, Thr, Lys, or N-terminus. As a ubiquitin chain is formed, monomer units of ubiquitin are linked to the building chain at residues Lys 29 or Lys 48 of the previous ubiquitin protein. Only those chains that build on residues 29 and 48 lead to proteasomal degradation of the target protein by the E3 ligase though.[2] Other ubiquitination events are possible at residues Met 1, Lys 6, Lys 11, and Lys 63 of ubiquitin which leads to other housekeeping events like autophagy.[3]

In a landmark study of 2001, Craig Crews and colleagues revealed that the endogenous ubiquitination and degradation machinery could be hijacked to degrade proteins.[4] By re-directing how the E3 ligase interacts with a protein of interest (POI), it is now possible to degrade proteins with aberrant activity, leading to functional inhibition. Researchers first engaged in 'inhibition-through-degradation' through the use of so-called molecular glues, molecules that facilitate the recognition of proteins that would not otherwise interact.[5] Molecular glues (MG), however, do have a history marred with terrible consequences. Thalidomide is a MG that was discovered in the 1950's and utilized in pregnant women to help ease their morning sickness. It was later discovered that thalidomide was a teratogen with horrible side effects; its use resulted in infants

with undeveloped limbs and body parts. The reason for these effects has been attributed to thalidomide's mode of action as a MG.[6] Thalidomide binds strongly to an E3 ligase substrate called cereblon while simultaneously binding to transcription factors, resulting in aberrant degradation of the transcription factors.[7] Thalidomide's use in pregnant women was discontinued due to this side effect; however, it has found many uses in the degradation field.

The utilization of MGs sparked a different targeted approach to inhibit target activity and led to the development proteolysis targeting chimeras (PROTACs). PROTACs are bi-funcitonal molecules that target E3 ligases to degrade POIs, similar to MGs.[8] A PROTAC has three components: a moiety that binds to an E3 ligase, another that binds to a POI, and lastly, a linker that binds the units together (Figure 3.1). PROTACs offer a significant advantage relative to MGs, in that they can be easily constructed from a pre-existing ligand for a POI.[9]
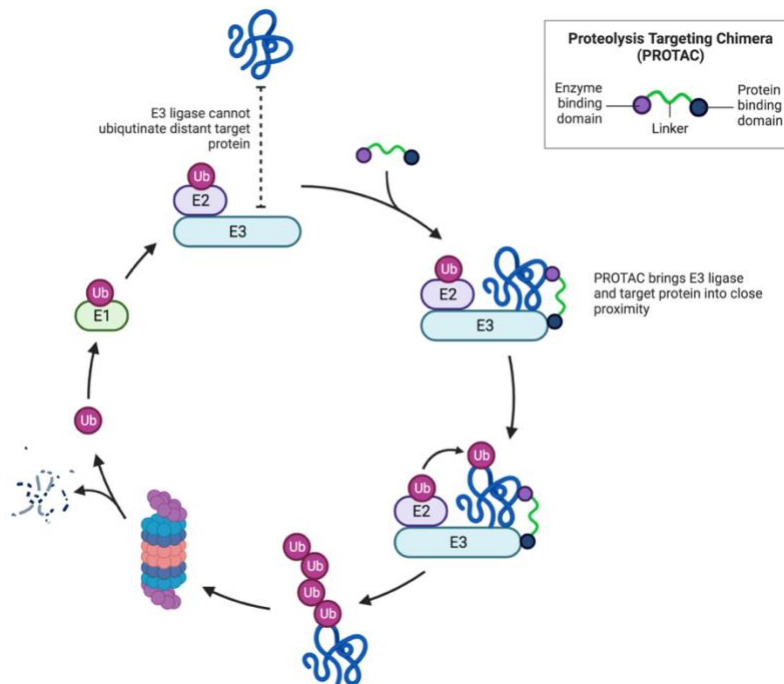
Figure 3.1 PROTAC degradation cycle. The 3 functional PROTAC components are shown in the top right section. As a PROTAC engages its target protein and E3 ligase a ubiquitination event occurs on the POI that leads to its degradation. The cycle regenerates the ligase components post degradation.

PROTACs were pioneered by the Crews and Deshaies laboratories in the early 2000s and were targeted to degrade MetAP-2 which plays a role in endothelial cell proliferation.[10,11] The design of "Protac-1" was characterized by a small molecule ligand (ovalacin) bound to a 6-carbon linker that was attached to a 10-mer peptide moiety. The peptide portion of Protac-1 was derived from the protein IκBα whose role in the NF-κB pathway was discussed in chapter 1. By utilizing the phosphomimic sequence DRHDS$_P$GLDS$_P$M from IκBα, Protac-1 was able to recruit the E3 ligase complex SCF-β^-^{TRCP} and lead to the subsequent ubiquitination and degradation event of Met-AP-2 in cell lysate. The accomplishment of this targeted degradation was significant for the reason that Met-AP-2 was not known to naturally interact with that specific E3 ligase complex or be part of a degradation event, such as IκBα, highlighting the redirection of PPIs to achieve this goal. Although this initial study was carried out in vitro, the results

demonstrated that peptides with high affinity sequences could be utilized to target individual POIs for PROTAC application.

A significant advance in the PROTAC field came from the recognition that small molecule ligands of E3 ligases could replace the peptides in the initial PROTACs.[12,13] As previously discussed, thalidomide has been extensively studied and shown to interact with the E3 ligase Cereblon. PROTACs that utilized thalidomide and analogues (pomalidomide, lenalidomide) as warheads to target BRD4 been shown to be effective modulators of c-Myc.[14] Other small molecules such as AHPC have been shown to also be effective recruiters of the E3 ligase complex VHL and PROTACs containing this ligand have been effective at targeting receptors such as CCR9.[15] Thalidomide, AHPC and their derivatives have comprised the main motifs to target E3 ligases. Notably, there are at least 250 Cullin-RING E3 ligases that have degradation roles in cells but have yet to be functionally explored due to the efficiency of targeting the ones previously mentioned.[16]

The work described in this chapter focuses on employing the techniques described above and developing targeted PROTACs for NEMO. What we learned from the previous chapter was that the short NBD peptides (TALDWSWLQTE) have a weak affinity for interacting with NEMO and thus require high concentrations for cell activity. The main hypothesis driving this work is **targeted degradation PROTAC technology will increase the effects of a peptide to effectively inhibit the NF-κB pathway**.[17] As discussed in chapter 2, NEMO contains 11 cysteine residues throughout its domains in addition to 61 other residues that can all be potential sites for ubiquitination. It resides mostly in the cytoplasm of the cell which makes crossing the cell membrane the only

barrier a peptide-PROTAC must overcome. In addition, NEMO's main role as a scaffolding protein to the IKK complex that lacks enzymatic activity makes it a great target for point of intervention.

C. Results and Discussions

Design and synthesis of NBD-PROTACs: Phase 1

The design of first-generation NBD-PROTACs centered upon the 3 functional portions of PROTACs. The POI ligand was held constant by using the NBD sequence from IKKβ. We considered utilizing E3 recruiter peptide ligands such as the 10-mer sequence from IκBα DRHDS$_P$GLDS$_P$M used in the design of PROTAC-1. Other peptide E3 recruiters have also been studied that target the VHL domain such as the sequence ALAPYIP derived from HIF1α [19]or the sequence LDPETGEYL derived from NrF2[20] to target the Keap1 E3 ligase.[17,21] However, because our POI recruiter motif is also a peptide that additionally requires a CPP for cell entry, we presumed that utilizing those E3 recruiter motifs would result in a large peptide with significantly attenuated cell permeability (Figure 3.2). These concerns prompted the design of peptide-small molecule PROTAC hybrids that would be much smaller in size. Thus, E3 recruiter

molecules pomalidomide (E3 ligase target cereblon, 150 nM affinity) and AHPC (E3

ligase target VHL, nM affinity) were incorporated into the design (Figure 3.3).
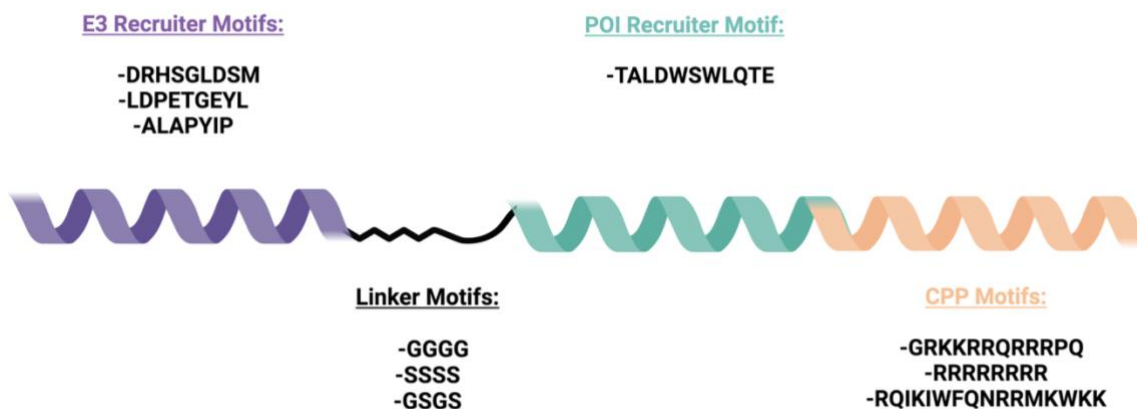
Figure 3.2 Peptide-based PROTACs. Peptide-PROTAC design for NEMO NBD recruiter would involve the following components shown above. The E3 recruiter motifs allow variability of ligases, the linkers give different flexibilities and spatial separation, and the CPPs each have different cell permeability characteristics.

Designing functional PROTACs where both recruiting ligands interact with their

respective targets largely depends on the formation of a stable ternary complex, and

there is considerable evidence that the linker heavily influences this association. A

commonly used linker is a 6-carbon hydrophobic linker, commercially available

appended to both pomalidomide and AHP. An additional design consideration is the

incorporation of a CPP. In prior work, we found the cationic sequences to be effective

CPPs for NEMO-binding peptides and peptidomimetics. Thus, my first-generation

NEMO-PROTACs (NPs) were designed to test the impact of the E3 ligase recruiter

identity and the placement of a cationic TAT CPP (Figure 3.3).
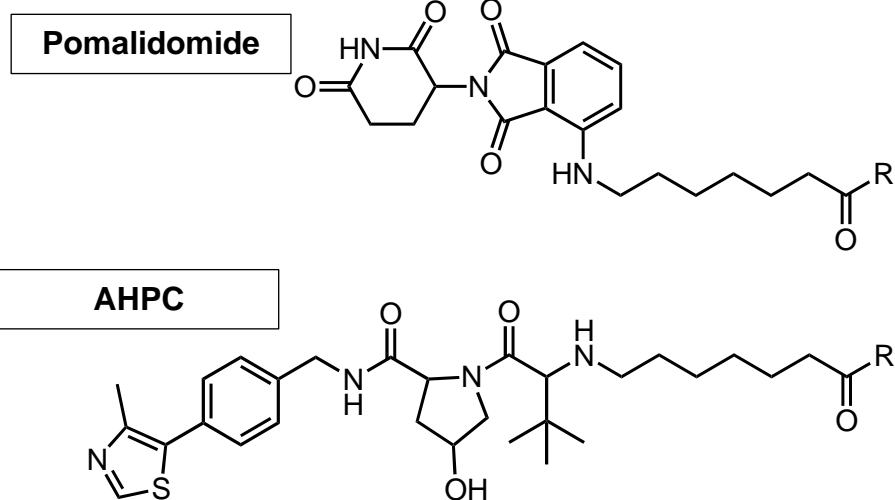
Pomalidomide

AHPC

E3 Recruiter	R	Name
Pomalidomide	TALDWSWLQTEGGGRKKRRQRRRPQ	NP-1
Pomalidomide	GRKKRRQRRRPQGGTALDWSWLQTE	NP-2
AHPC	TALDWSWLQTEGGGRKKRRQRRRPQ	NP-3
AHPC	GRKKRRQRRRPQGGTALDWSWLQTE	NP-4

Figure 3.3 Phase 1 NBD-PROTACs. The library of PROTACs made for phase 1 are shown above. Pomalidomide and AHP were used as small molecule E3 recruiter motifs which were connected to the POI peptide recruiter motif by a standard C6-carbon linker. The regions highlighted in red represent the NBD sequence which are separated by a small Gly spacer to the TAT region in blue.

PROTACs NP1-4 were prepared using standard solid-phase synthesis protocols, with identify and purity verified by mass spectrometric analysis and HPLC (see Materials section). Coupling of the pomalidomide-linker warhead to the NBD derivatives was straightforward, as was the purification of the resulting conjugates. A physical property of pomalidomide is its conjugated aromatic system which provides a UV absorbance at 425 nm. This, in addition to the Trp residues of the NBD sequence, facilitated the purification and isolation of NP 1 and 2. In contrast, the AHPC-linker

warhead was more challenging to couple to the peptide. Additionally, the lack of

significant UV absorbance of AHPC complicated detection of the NP-3 and NP-4 during

HPLC purification. Finally, both conjugates displayed poor solubility and were thus

difficult to isolate. Nonetheless, all four were successfully synthesized and proceeded to

testing

Functional assessment of NP1-4

There are a number of methods for assessing the activity of potential PROTACS

described in the literature. These include indirect methods, in which degradation of the

POI is coupled to an output that is readily measured, such as luminescence, as well as

direct methods that visualize the change in concentration of the POI. The latter methods

are typically lower throughput. Due to the small number of compounds to be tested,

however, I elected to use Western blot analysis of NEMO from treated cells for the

functional assessment of NPs 1-4. PC3 cells were chosen as the test cell line for this

part of the study due to reports that NF-κB. transcription factors are constituently active

in that cell line. Since our assay centered upon degradation of NEMO, we designed an

initial experiment in which we tested a baseline expression of NEMO protein in the PC3

cells first.

The first step was to determine cell density and growth conditions under which

NEMO could be readily detected by Western blot. Towards that end, I plated PC3 cells

at varying cell densities (250, 125, and 62.5K cells/well), let them form surface

attachments overnight, and then collected them the next day for extraction. The cells

were lysed using NE-PER reagent to obtain cytoplasmic extracts and protein

concentration in the lysate was quantified using a BCA assay. We then loaded varying

amounts (µg) of each sample onto an SDS page gel and proceed to analyze though

Western blot with corresponding antibodies. We found that culturing 6-well plates

loaded with 125,000 cells/well and then loading 10 µg per well of SDS page gel was an

ideal condition that led to a readily visible signal corresponding to NEMO in PC3 cells

(Figure 3.4).
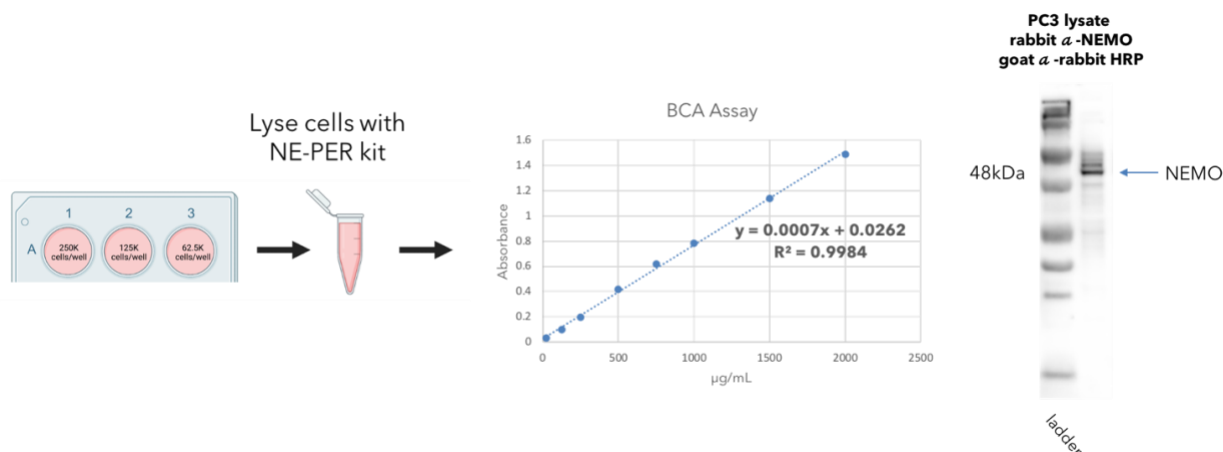
Figure 3.4 Western blot analysis workflow. The workflow for analyzing NEMO degradation in PC3 cells is shown above. PC3 cells were plated in a 6-well plate, lysed with NE-PER reagent, quantified and standardized to BSA utilizing a BCA assay, loaded onto and SDS-page gel, and treated with antibodies on a nitrocellulose membrane.

Based upon the above results, PC3 cells were cultured in a 6-well plate with

125,000 cells/well and the next day treated with increasing concentrations of NP1-4.

Studies have shown it takes roughly 2-4 hours[22] for peptide molecules to escape

endosomes post treatment and we therefore incubated the cells with the NPs for 3

hours. The results shown in Figure 3.5 indicate that none of the compounds are

effective degraders of NEMO. NP2-4, for example, induced little to no change in NEMO

at concentrations up to 50 µM and all three showed evidence of toxicity as

concentrations increased. Treatment of PC3 cells with NP-1 did lead to a small

decrease in NEMO at 50 µM without a concomitant decrease in GAPDH, suggesting

some PROTAC activity.

Given the modest affinity of the NEMO-binding peptides used for this initial study $(K_{DS} > 100\mu M)$, it is not surprising that activity was not observed at low micromolar concentrations. Increasing treatment concentration or time to boost activity was not feasible due to toxicity concerns in the PC3 cells, however. Nonetheless, some initial conclusions could be drawn from these experiments. First, no activity was observed with either of the PROTACS containing AHPC as the E3 recruiter moiety (NP-3, NP-4). These results coupled with the synthetic and solubility difficulties encountered with AHPC-functionalized peptides meant that AHPC was not used in the next PROTAC design. Second, the studies of NEMO-binding peptides outlined in Chapter 2 provided sequences with significantly increased affinity for NEMO relative to the ones used in NP1-4. Thus, it seemed possible to increase the quite modest activity of NP-1 by altering the NEMO-targeting sequence.
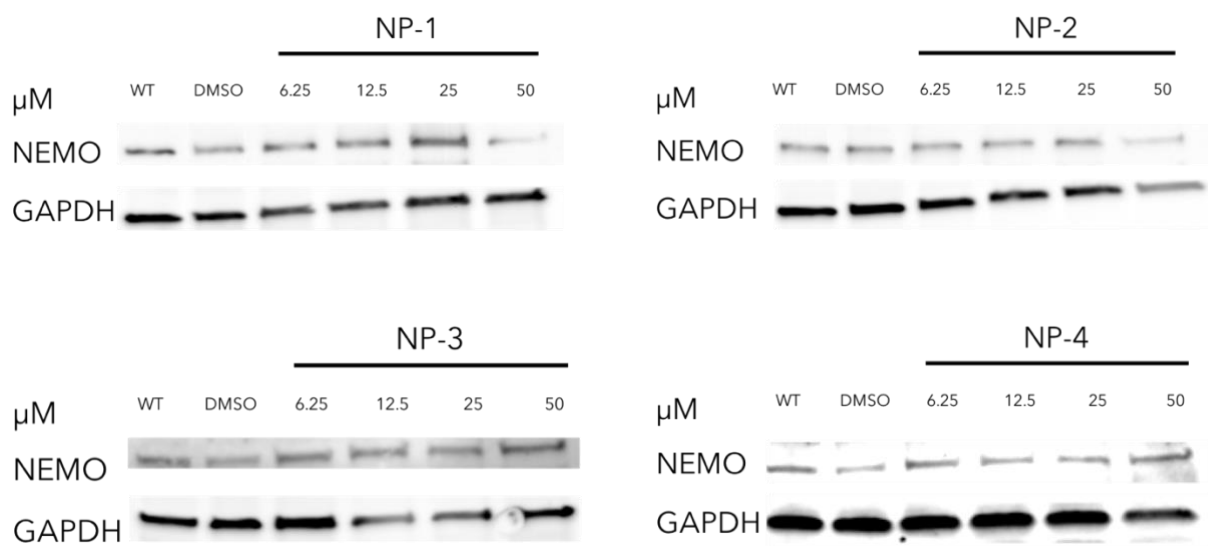
Figure 3.5 PC3 cells treated with NPs. PC3 cells were treated with NPs 1-4. Treatment with all PROTACs shows minimal level of degradation with exception to high concentrations of NPs 1-2 that possess the pomalidomide handle. No activity was observed with AHP handle (NP3-4). GAPDH was tracked as a housekeeping gene to observe negative off target effects of toxicity. DMSO levels were kept under 0.1% in all experiments.

Design of NBD-PROTACs: Phase 2

We hypothesized from the results of phase 1 that the affinity between NEMO and the POI recruiter motif needed to be increased. To address this the design was altered to include the 45-mer construct that we tested in chapter 2 (IKKwt) with a binding affinity of 200 nM. Several NPs were then designed to test additional variables. As can be seen in Figure 3.6, two different linkers were tested as well as the positioning of the TAT CPP. The resulting structures, NP-5 through NP-8 were synthesized using solid-phase synthetic procedures, purified, and characterized as was done for the Phase 1 analogs (see Methods for details).
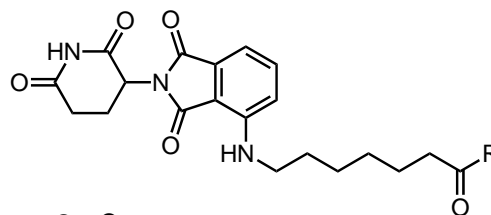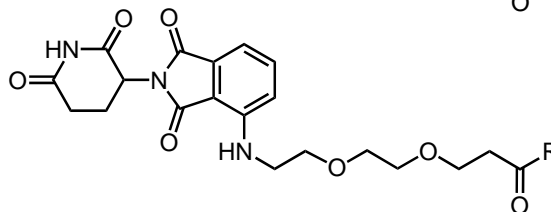
E3 Recruiter	R	Name
Pomalidomide- C6 Linker	βAPAKKSEELVAEHNLCTLLENAIQDTVREQDQSFTA LDWSWLQTEGGGRKKRRQRRRPQ	NP-5
Pomalidomide- C6 Linker	βAGRKKRRQRRRPQGGPAKKSEELVAEHNLCTLLEN AIQDTVREQDQSFTALDWSWLQTE	NP-6
Pomalidomide- (PEG)2 Linker	βAPAKKSEELVAEHNLCTLLENAIQDTVREQDQSFTA LDWSWLQTEGGGRKKRRQRRRPQ	NP-7
Pomalidomide- (PEG)2 Linker	βAGRKKRRQRRRPQGGPAKKSEELVAEHNLCTLLEN AIQDTVREQDQSFTALDWSWLQTE	NP-8

Figure 3.6 Phase 2 NBD-PROTACs. The library of PRTOACs made for phase 2 are shown above. Pomalidomide small molecule E3 recruiter motifs were connected to the POI peptide recruiter motif by either a C6- carbon or (PEG)2 linker. The regions highlighted in red represent the NBD sequence which are separated by a small Gly spacer to the TAT region in blue.

Affinity assessment of Phase 2 NBD-PROTACs

Given the results of Phase 1 and the design changes made in Phase 2, assessing the affinity of NP-5 through -8 for NEMO was critical. To do this, a competition binding assay was used, with fluorescein-labeled IKK peptide used as the tracer (K_D = 1 μM). Additionally, a mutant version of the IKK peptide with significantly attenuated affinity (K_D>100μM) was used as a negative control. As shown in Figure 3.7, all of the Phase 2 NPs were found to have submicromolar IC_{50}s against the wild type IKK sequence. The most effective inhibitors – and therefore binders – were NP-6 and NP-8, in which the TAT sequence precedes the NEMO-binding sequence. This highlights the possibility that the PROTACs have the potential to displace the natural interaction that occurs between NEMO and the IKK complex and lead to degradation. It was somewhat surprising the linker effects were minimal, given the identical activities of NP-6 and NP-8.

NP/Peptide	Composition	IC_{50} (μM)
NP-5	Pom-C6-IKK-TAT	0.30 ± 0.04
NP-6	Pom-C6-TAT-IKK	0.10 ± 0.09
NP-7	Pom-PEG-IKK-TAT	0.20 ± 0.02
NP-8	Pom-PEG-TAT-IKK	0.10 ± 0.02
Acyl-IKKwt		0.20 ± 0.01
Acyl-IKKmut(W739A W741A)		NA
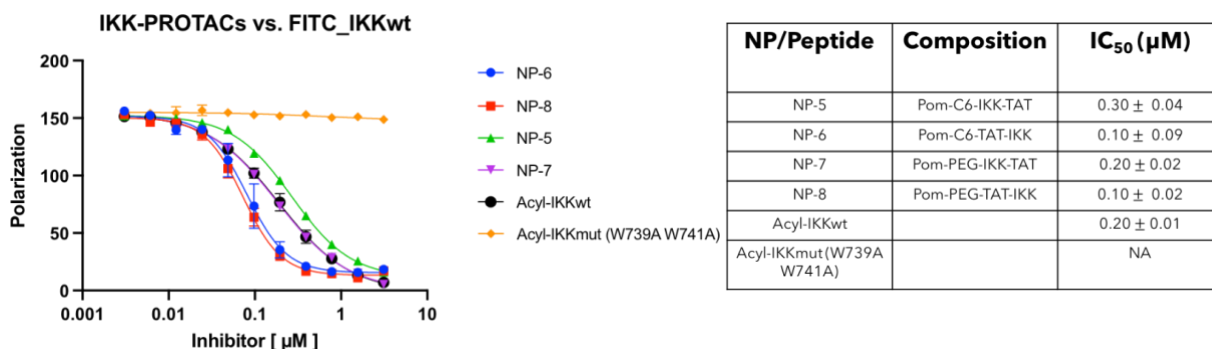
Figure 3.7 Competitive binding assay of NPs. The library of NPs 5-8 was tested against a FITC-tagged NBD peptide construct (IKKwt) bound to NEMO. Experiments were performed in triplicate with the indicated error (SDOM). NPs relative displacement ability were compared to the dynamic range between the acylated WT IKK peptide and its mutant. NPs that localize the NBD sequence on the C-terminus (6 and 8) displace the tracer better than those that localize it on the N-terminus (5 and 7). The linker type between relative constructs affects the binding ability as well.

Effect of TAT positionality on Binding

The results from the previous section prompted us to investigate further the relationship between TAT and the NBD sequence and how their localization relative to each other affect binding to NEMO. As described in Chapter 2, Pei and co-workers reported that a cationic CPP incorporated into a NEMO binder unexpectedly increased the affinity of the molecule through interaction with a nearby negatively charged surface residues 88-91.

To test this in our system, I synthesized isomeric constructs that omitted the E3 recruiters and respective linkers. By doing this, we could test if the terminus of the peptide-PROTAC plays a larger role in target binding as well as the orientation between TAT and the NBD (Figure 3.8). The NBD sequence localized at the C-terminus resulted in tighter binding. Additionally, the peptide Acyl-TAT-IKK binds 4x better than the WT sequence and 2x better than the structural isomer Acyl-IKK-TAT. Also of note is that a comparison of this data with that of Figure 3.7 indicates that the added functionality of the PROTAC attenuates affinity.

TAT Postion Effect

Legend:
- Acyl-TAT_IKK
- Acyl-IKK_TAT
- Acyl_IKKmut (W739A W741A)
- Acyl_IKKwt

Peptide	IC$_{50}$ (µM)
Acyl-IKKwt	0.40 ± 0.01
Acyl-TAT-IKK	0.10 ± 0.02
Acyl-IKK-TAT	0.20 ± 0.02
Acyl-IKKmut (W739A W741A)	NA
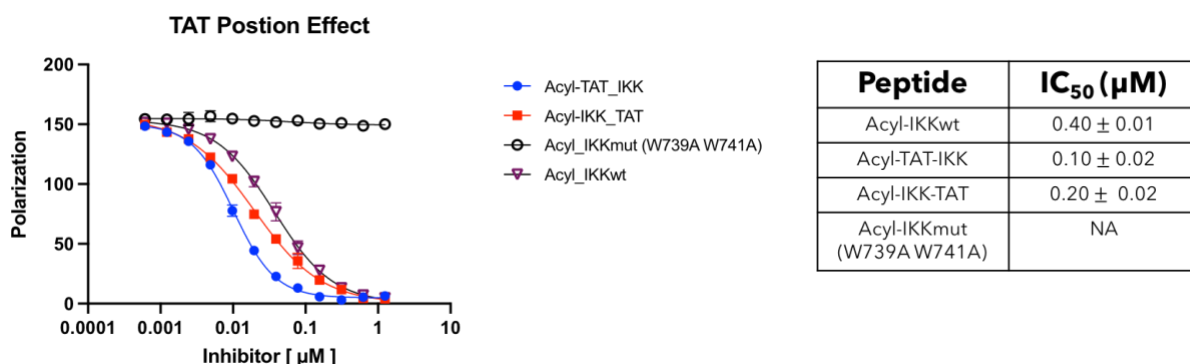
Figure 3.8 Competitive binding assay of large NBD peptides. The library of large NBD peptides were tested against a FITC-tagged NBD peptide construct (IKKwt) bound to NEMO. Experiments were performed in triplicate with the indicated error (SDOM). The peptides relative displacement ability was compared to the dynamic range between the acylated WT IKK peptide and its mutant. The NBD peptide that localized the NBD sequence on the C-terminus (Acyl-TAT-IKK) displaced the tracer better than the structural isomer.

Due to Western blotting being a semi-quantitative experiment that requires significant optimization, we decided to test the activity of the Phase 2 PROTACs through a more robust assay. Utilizing HEK-293T cells where the NF-κB. transcription factors were transfected with a luciferase gene (BPS Bioscience) we were able to measure the effects of the NPs as a response to the suppressed activity NF-κB..

Our first goal was to find the most efficient way to stimulate pathway activation to achieve a signal readout in relation to dosing with the characteristically large NPs. As has been previously reported, large cargo such as peptides require a time scale of hours to for cell entry.[23] NF-κB activity is dependent upon upstream signaling, and there are many reported ways to stimulate activation like those involving the use TNFα, IL-1β, LPS, virulent agents and oxidative chemicals. Based on literature precent, TNFα and IL-1β were chosen for our studies.

The experimental setup involved plating the cells overnight, and the next day treating with 10 ng/mL of stimulant for various time periods. The cells were then lysed with a reagent that contained substrate luciferin that produces light when processed by the luciferase enzyme. From these results we learned that the time points and stimulating agent made a significant difference in pathway activity. Neither stimulant activated the pathway to a measurable effect after treatment for 1 hour (Figure 3.9), requiring longer time points. However, the activation of the pathway by TNFα is substantially greater, with almost 3x higher luminescence at the longest stimulation

point.[24,25] Thus, we selected the 3-hour stimulation time for TNFα for the functional

assessment.

Stimulant Timepoints (10ng/mL)
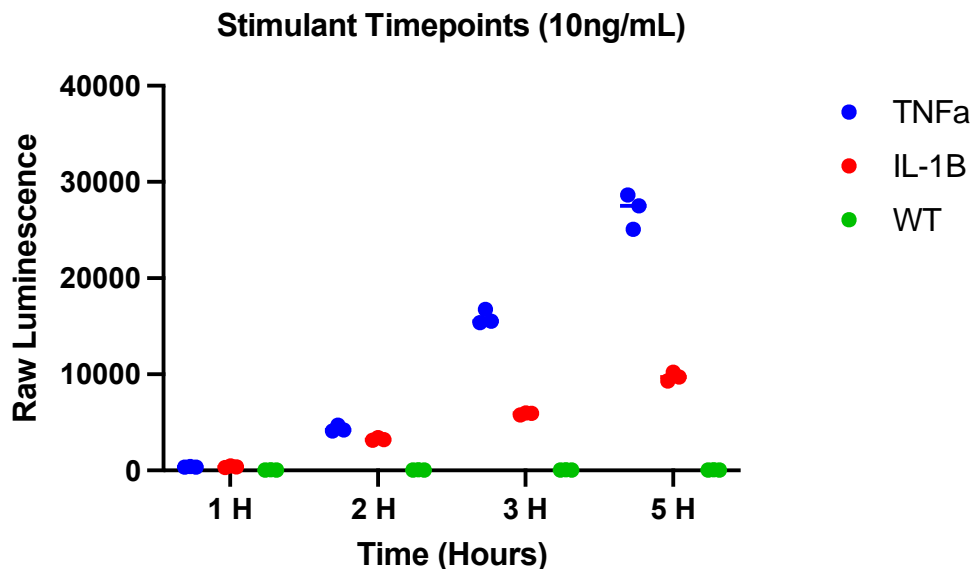
Figure 3.9 Stimulation of the NF-κB pathway. The experiment above depicts different stimulants and timepoints used to activate NF-κB translational activity. HEK-293Ts were stably transfected with luciferase prior to experiment. Post stimulation, cells were treated with lysis buffer and D-luciferin substrate to measure luminescence. Experiments were performed in triplicate.

We proceeded to test the activity of an elongated NBD peptide (Acyl-IKK-TAT) in

the context of TNFα activation. Experiments were conducted by dosing for two

timepoints (1 and 3 hours) with peptide concentrations (µM) 10-fold units apart. We

found that the activity of the NBD peptide showed a dose response for the treated

timepoints, (Figure 3.10) with the longer dosing time have a greater effect. With these

optimized conditions in mind, we proceeded to test how the NPs affected activity under

the same conditions.

A

1 Hour Dose / 3 Hour Stimulation (TNFα)

B

3 Hour Dose / 3 Hour Stimulation (TNFα)
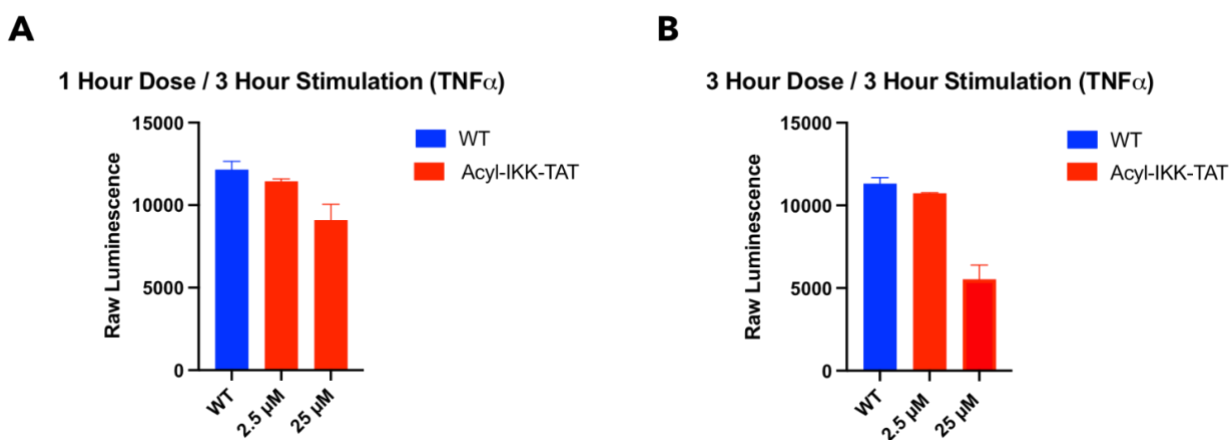
Figure 3.10 Dosing of HEK-293T cells with NBD peptides. HEK-293Ts were plated at a concentration of 45,00 cells/well and allowed to incubate overnight. **A)** The cells were treated with NBD peptide at respective concentrations for 1 hour and then stimulated with TNFα for 3. **B)** Cells were treated with NBD peptide at respective concentrations for 3 hour and then stimulated with TNFα for 3. The workup for these experiments was the same as the stimulation experiments and were done in triplicate.

NBD-PROTAC activity in HEK-293T cells

After the finding both a stimulation and dosing timepoint where we could see inhibition activity of the NBD peptide, we proceeded to test how the NPs affected activity of NF-κB. We kept the experimental setup the same in which we treated the HEK293Ts with the NPs for 3 hours and stimulated for an additional 3 with TNFα. The activation of NF-κB through TNFα stimulation provided a large activation potential that allowed us to study any effects the NPs exerted. We found that all the NPs resulted in decreased activity of NF-κB, albeit to a small degree. Interestingly, NP-8 had the largest impact on inhibitory activity relative to the other NPs which coincided with the results of the competitive FP experiments. Analyzing by comparative linker type (NP-5 and 6) the same trend can be seen where the PROTAC that contains the NBD sequence on the C-terminus is more effective.

NPs Effect on NFκB Activity
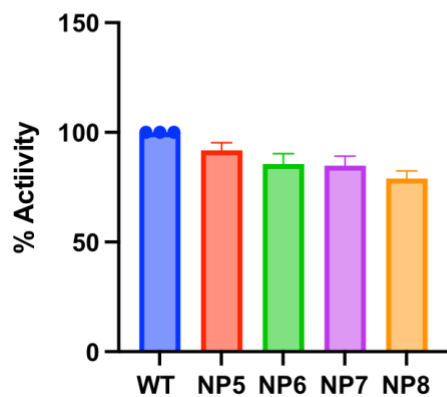
NP	Composition	Activity (%)
NP-5	Pom-C6-IKK-TAT	92 ± 3
NP-6	Pom-C6-TAT-IKK	86 ± 7
NP-7	Pom-PEG-IKK-TAT	85 ± 5
NP-8	Pom-PEG-TAT-IKK	79 ± 3

Figure 3.11 Dosing of HEK-293T cells with NPs. HEK-293Ts were plated at a concentration of 45,00 cells/well and allowed to incubate overnight. The cells were treated with NPs (25 µM) for 3 hours followed by an additional 3 hours of stimulation with TNFα. The % activity of the NPs were normalized to WT cells that were treated with media and stimulated in the same format. The workup for these experiments were kept constant and done in triplicate with the standard deviation between values shown.

D. Assessment and Future Directions

The goal of the experiments in this chapter was to convert NEMO binding peptides into bifunctional PROTAC molecules. Critical to the design was the use of higher affinity NEMO-binding peptides, with IKK derivatives (NP-7, NP-8) exhibiting inhibition in cell culture. Moving forward, Western blot analysis will be important for testing if the observed inhibition is due to degradation, simple inhibition, or a combination of the two. Such data will be critical to further optimize NEMO PROTAC activity. For example, changes in experimental protocol, such as longer PROTAC treatment times, may be important for effective degradation to be obtained. As outlined in Chapter 2, I identified NEMO-binding peptide analogs with considerably improved affinity for NEMO and the incorporation of these sequences into the PROTAC design could enhance activity (Figure 3.12). Finally, analyzing the cell penetration and localization of the PROTACs by fluorescence microscopy will also be critical.

Pomalidomide-C6 Linker

Pomalidomide-(PEG)2 Linker
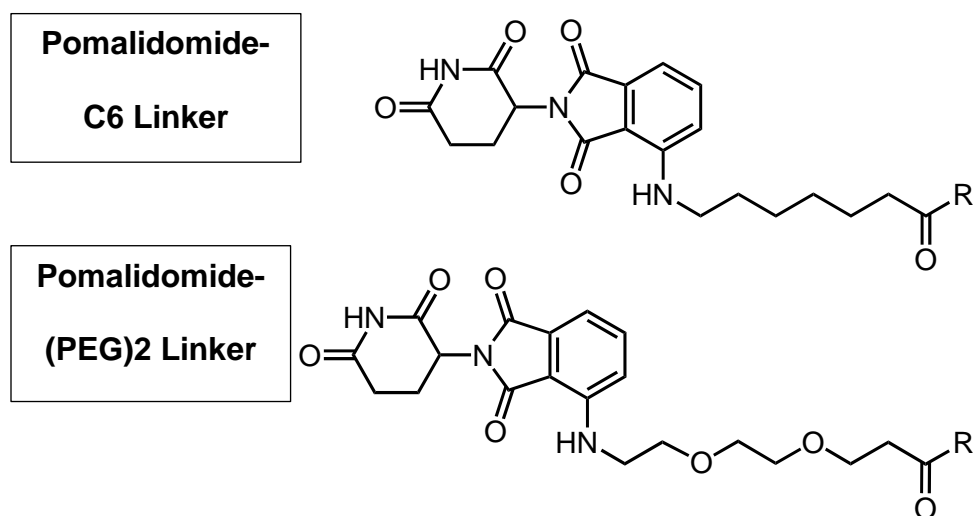
E3 Recruiter	R	Name
Pomalidomide	βASFTALDW^{1}SW^{1}LQTEGGGRKKRRQRRRPQ	NP-9
Pomalidomide	βAGRKKRRQRRRPQGGSFTALDW^{1}SW^{1}LQTE	NP-10

W^1= 6-chloro-Trp

Figure 3.12 Phase 3 NBD-PROTACs. The library of PRTOACs for phase 3 are shown above. Pomalidomide small molecule E3 recruiter motifs are connected to the POI peptide recruiter motif by either a C6- carbon or (PEG)2 linker. The regions highlighted in red represent the NBD sequence which are separated by a small Gly spacer to the TAT region in blue. The NBD sequence is modified to a slightly larger construct than those in phase 1 and include substituted Trp residues that increased the affinity to its protein target.

E. Materials and Methods

Reagents and Instrumentation

      Chemical and biological reagents were obtained from commercial sources and were utilized without additional modifications (unless otherwise specified). DNA, protein, peptide, and O.D. concentrations were determined using a Thermo Scientific NanoDrop One Spectrophotometer.

Protein Expression and Purification:

      Protocols were followed exactly as written in Chapter 2: Methods and Materials of this dissertation.

Synthesis of NBD peptides

      Protocols were followed exactly as written in Chapter 2: Methods and Materials of this dissertation unless stated otherwise.

Table 3.1. Sequences of peptides used in chapter 3

Peptide	Sequence (N'-C')
IKKwt	FITC-βAla-PAKKSEELVAEHNLCTLLENAIQDTVREQDQSFTALDWSWLQTE
Acyl-IKKwt	Acyl-βAla-PAKKSEELVAEHNLCTLLENAIQDTVREQDQSFTALDWSWLQTE
Acyl-IKK-TAT	Acyl-A^{B}PAKKSEELVAEHNLCTLLENAIQDTVREQDQSFTALDWSWLQTEGGGRKKRRQRRRPQ

Acyl-TAT-IKK	Acyl-A^{B}GRKKRRQRRRPQGGPAKKSEELVAEHNLCTLLENAIQDTVREQD QSFTALDWSWLQTE
Acyl-IKKmut	Acyl-βAla-PAKKSEELVAEHNLCTLLENAIQDTVREQDQSFTALDASALQTE

Synthesis of NBD-PROTACs

Protocols for the peptide portion of the PROTIACs were followed exactly as written in Chapter 2: Methods and Materials of this dissertation. Addition of the linker-E3 recruiter motifs were coupled onto the N-terminus of the peptides using standard solid-phase peptide synthesis reagents. Peptide on resin was incubated overnight with a 2 mL DMF solution containing 5X HOBT, 5X HBTU, 10X DIPEA, and 2X molar equivalence of linker-ligand. The bifunctional peptides were then worked up as described in Chapter 2. The molecules that contained TAT sequences were subjected to extra cleavage solution and additionally chloride-salt-exchange was performed through repeated lyophilize freeze/thaw cycles where the purified compounds were dissolved in a 6mM HCL solution.

Table 3.1. Structure of NPs used in chapter 3

NP	Structure
1	
2	
3	
4	
5	
6	
7	

| 8 | |
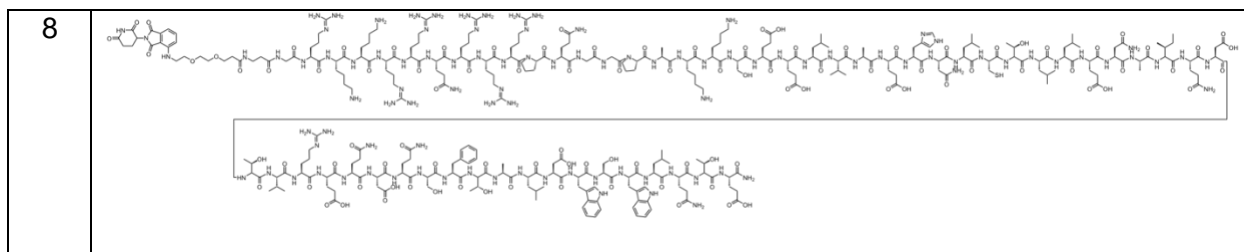
Western Blot Degradation Assay

Western blot degradation assays were performed after extracting cell lysate from PC-3 cells with NE-PER reagent (Thermo Fisher Scientific, cat #: 78833). The lysates were quantified using a BCA a assay. that was standardized to BSA and then an equal amount (10 µg) of each sample was subjected to heat denaturation at 95 ⁰C with equal amounts of BME and LDS loading dye for 10 minutes. The samples were then loaded onto an SDS PAGE 4-12% bis-tris gel for and run at 150 V for 1 hour. Post-run, the gel was transferred to nitrocellulose PDVF membrane using a Bio-Rad Trans-Blot Transfer System following standard protocols. The membrane was then blocked for 1 hour at room temperature using SuperBlock™ Blocking Buffer in PBS (Thermo Scientific, 37515). After 1 hour, the blocking buffer was removed and primary NEMO antibody (Santa Cruz 166398) was added (1:1000 dilution with 1% Tween 20 in SuperBlock™) and incubated overnight at 4⁰C with gentle shaking. The next day, the primary antibody was discarded, and the membrane was washed 3X with PBST buffer for 5 minutes each. The secondary antibody mouse anti rabbit HRP (Santa Cruz 525408) was added to the membrane (1:1000 dilution with 1% Tween 20 in SuperBlock™) and incubated at room temperature for 1 hour. The secondary antibody was removed after an hour and the 3 washing steps were repeated again. HRP substrate (Thermo Scientific, 34095) was then added to the membrane and incubated for 1 minute at room temperature

following standard protocols. The blot was then visualized using Chemiluminescence on an Azure Biosystems c600 imager. Further analysis was done on Fiji software.

Competitive Binding Assay

Competitive binding assays were performed in triplicate with a final well volume of 20 µL in a low volume, non-binding 384-well black plate (Corning). NEMO protein was precomplexed with fluorescent (FITC) peptide using two-fold the concentrations of the protein and peptide to reach 50% of the tracer bound in binding buffer (200 mM NaCl, 50mM Tris, 0.01% Triton X-100 (V/V), 1mM DTT). Non-fluorescent peptides were dissolved in DMSO and diluted in assay buffer and serially diluted down two-fold with assay buffer going down the plate to row (16µL per well). The pre-complexed peptide-protein complex was then added to the well for a final volume of 20 µL (Row P should contain only the peptide-protein complex with no inhibitor molecules and was used as a standardized control). The plate was allowed to incubate for 30 minutes at room temperature and after was read on a PHERAStar multi-mode plate reader using polarized excitation at 485 nm with emission intensity measured through a parallel and 72 perpendicularly polarized 535 nm filter. Polarization values were plotted against log [inhibitor] and fit into a non-linear regression curve utilizing Prism's built-in equation "log(inhibitor) vs response-variable slope (four parameters)". The IC_{50} values were calculated using the IC_{50} values from Prism results. Each data point is an average 3 technical replicates with the error representing the standard deviation between them.

Mammalian cell culture and luciferase assay

The luciferase assays were carried out using stably transfected HEK-293T cells (BPS Bioscience). Cells were cultured in standard 10 cm dishes using DMEM media (Gibco, cat #: 11965092) supplemented with 10 % FBS, 1%Penn/Strep, and 1% Hygromycin. Cells were grown under standard conditions at 37ºC with 5% CO_2.

The experimental setup involved plating cells in a white opaque 96-well plate at a cell density of 45,000 cells/well in 45 µL of media and allowed to form cell attachment overnight. The next day, the cells were treated with either 5 µL of molecule, DMSO, or media, and allowed to incubate for 3 hours at 37ºC. After the 3-hour dosing time, the cells were stimulated with 5 µL of either TNFa or IL-1B (10ng/mL) for a total volume of 55 µL and were incubated for additional 3 hours and incubated at 37ºC. The cells were then lysed with ONE-Step™ Luciferase Assay System (BPS Bioscience, 60690) and allowed to incubate for 15 minutes at room temperature. The plate was then read on a luminometer to obtain the raw luminescence of each well. The luminescence of each variable group was then normalized to the WT group of cells that was treated only with media which was set to 100 %. Each data point is an average 3 technical replicates with the error representing the standard deviation between them.

F. References

1. Deribe, Y. L., Pawson, T. & Dikic, I. Post-translational modifications in signal integration. *Nat. Struct. Mol. Biol. 2010 176* **17**, 666–672 (2010).

2. Komander, D. The emerging complexity of protein ubiquitination. doi:10.1042/BST0370937

3. Shi, C. S. & Kehrl, J. H. TRAF6 and A20 regulate lysine 63-linked ubiquitination of Beclin-1 to control TLR4-induced Autophagy. *Sci. Signal.* **3**, (2010).

4. Sakamoto, K. M. *et al.* Protacs: Chimeric molecules that target proteins to the Skp1–Cullin–F box complex for ubiquitination and degradation. *Proc. Natl. Acad. Sci.* **98**, 8554–8559 (2001).

5. Dong, G., Ding, Y., He, S. & Sheng, C. Molecular Glues for Targeted Protein Degradation: From Serendipity to Rational Discovery. *J. Med. Chem.* **64**, 10606–10620 (2021).

6. Ito, T., Ando, H. & Handa, H. Teratogenic effects of thalidomide: molecular mechanisms. *Cell. Mol. Life Sci.* **68**, 1569–1579 (2011).

7. Sievers, Q. L. *et al.* Defining the human C2H2 zinc finger degrome targeted by thalidomide analogs through CRBN. *Science (80-.).* **362**, (2018).

8. Maniaci, C. & Ciulli, A. Bifunctional chemical probes inducing protein–protein interactions. *Curr. Opin. Chem. Biol.* **52**, 145–156 (2019).

9. Kozicka, Z. & Thomä, N. H. Haven't got a glue: Protein surface variation for the design of molecular glue degraders. *Cell Chem. Biol.* **28**, 1032–1047 (2021).

10. Sakamoto, K. M. *et al.* Protacs: Chimeric molecules that target proteins to the Skp1-Cullin-F box complex for ubiquitination and degradation. (2001).

11.	Yeh, J. R. J., Mohan, R. & Crews, C. M. The antiangiogenic agent TNP-470 requires p53 and p21CIP/WAF for endothelial cell growth arrest. *Proc. Natl. Acad. Sci.* **97**, 12782–12787 (2000).

12.	Toure, M. & Crews, C. M. Small-Molecule PROTACS: New Approaches to Protein Degradation. *Angew. Chemie Int. Ed.* **55**, 1966–1973 (2016).

13.	An, S. & Fu, L. Small-molecule PROTACs: An emerging and promising approach for the development of targeted therapy drugs. *EBioMedicine* **36**, 553–562 (2018).

14.	Zhang, F. *et al.* Discovery of a new class of PROTAC BRD4 degraders based on a dihydroquinazolinone derivative and lenalidomide/pomalidomide. *Bioorg. Med. Chem.* **28**, 115228 (2020).

15.	Huber, M. E. *et al.* A Chemical Biology Toolbox Targeting the Intracellular Binding Site of CCR9: Fluorescent Ligands, New Drug Leads and PROTACs. *Angew. Chemie - Int. Ed.* **61**, (2022).

16.	Reichermeier, K. M. *et al.* PIKES Analysis Reveals Response to Degraders and Key Regulatory Mechanisms of the CRL4 Network. *Mol. Cell* **77**, 1092-1106.e9 (2020).

17.	Ma, S. *et al.* Non-small molecule PROTACs (NSM-PROTACs): Protein degradation kaleidoscope. *Acta Pharm. Sin. B* **12**, 2990–3005 (2022).

18.	Arkin, M. M. R. & Wells, J. A. Small-molecule inhibitors of protein–protein interactions: progressing towards the dream. *Nat. Rev. Drug Discov. 2004 34* **3**, 301–317 (2004).

19.	Jiang, Y. *et al.* Development of Stabilized Peptide-Based PROTACs against Estrogen Receptor α. (2017). doi:10.1021/acschembio.7b00985

20. Lu, M.-C. *et al.* Binding thermodynamics and kinetics guided optimization of potent Keap1-Nrf2 peptide inhibitors †. (2015). doi:10.1039/c5ra16262a

21. Lu, M. *et al.* Discovery of a Keap1-dependent peptide PROTAC to knockdown Tau by ubiquitination-proteasome degradation pathway. *Eur. J. Med. Chem.* **146**, 251–259 (2018).

22. Nakase, I., Kobayashi, S. & Futaki, S. Endosome-disruptive peptides for improving cytosolic delivery of bioactive macromolecules. *Pept. Sci.* **94**, 763–770 (2010).

23. Varkouhi, A. K., Scholte, M., Storm, G. & Haisma, H. J. Endosomal escape pathways for delivery of biologicals. *J. Control. Release* **151**, 220–228 (2011).

24. Rex, J. *et al.* IL-1β and TNFα differentially influence NF-κB activity and FasL-induced apoptosis in primary murine hepatocytes during LPS-induced inflammation. *Front. Physiol.* **10**, (2019).

25. Kwon, H.-J. *et al.* Tumor Necrosis Factor Alpha Induction of NF-B Requires the Novel Coactivator SIMPL. *Mol. Cell. Biol.* **24**, 9317–9326 (2004).

Chapter 4

Conclusions and Future Directions

A. Rationale

The NF-κB pathway becomes constituently active in cancer, autoimmune disorders, and in infectious diseases such as COVID-19 and has thus been the focus of much drug-discovery research.[1,2] Targeting NF-κB activity is challenging due to the complexity of the different activation pathways and apparent crosstalk between the pathways themselves. Additionally, many of the constituent pathway proteins and protein complexes are classed as 'undruggable'.[3] The transcription factors in the pathway, for example, have large intrinsically disordered regions and the well-folded domains lack discrete binding sites.[4] The kinases within the pathways are the more traditional targets and effective modulators have been developed. However, selectivity for particular arms in the pathway has been problematic since many of the kinases play multiple roles. IKKα, for example, is a prime therapeutic target but it activates both the canonical and non-canonical pathway; thus IKKα inhibitors block both desired and desired parts of NF-κB activity.[5]

This dissertation focused primarily on regulating NF-κB transcriptional activity through modulation of the IKK pathway by targeting NEMO. NEMO was chosen as a target because of the critical role it plays as a scaffold protein that functions to recruit both IKK and IKKβ for phosphorylation.[6] In addition, it functions exclusively within the

canonical pathway. Lastly, it has no kinase enzymatic activity which prevents off-target events that occur with traditional kinase inhibitors from happening.[7] However, there are no apparent small molecule binding sites, meaning that targeting the NEMO PPI binding surfaces is necessary for the development of modulators. The main goal of this thesis focused on mimicking key features from NEMO binding partners in order to block NEMO's function in the NF-κB pathway.

B. Conclusions

Crystallographic studies of NEMO in complex with its IKK binding partners reveal a large interaction surface between the proteins.[8] However, work by Whitty and others suggested the importance of a loop region present in both IKKα and IKKβ for recognition of NEMO, indicating that peptidomimetics of this structure could be effective NEMO inhibitors.[9] In earlier work from our lab, an IKK-derived sequence internally braced to stabilize a loop-like conformation (NBD$_2$) was found to interact with NEMO in cells and block its activity.[10]

To test the hypothesis that the internal brace increased the affinity of the peptide sequence for NEMO, we developed an expression and purification protocol of full-length NEMO and a fluorescence polarization assay. Analysis of NBD$_2$ and various derivatives revealed that the synthetic brace does not affect the binding affinity relative to the native sequence; however, a TAT cell-penetrating peptide (CPP) incorporated for cellular studies negatively impacted binding. From these studies I concluded that the enhanced cellular activity observed with NBD$_2$ was due to its increased resistance to proteolysis from the synthetic brace.

In search of other strategies for increasing the affinity of IKK-derived peptidomimetics I examined a series of IKK peptides and mutants (Chapter 2). From this I confirmed that an 11-residue sequence (IKK 735-745) is the minimal sequence for detectable NEMO binding. The affinity can be increased significantly (2-fold) by extending the sequence to Ser733, which I hypothesize enables a productive H-bond interaction. Additionally, 3 aromatic residues- F734, W739, and W741 are critical for binding. I found that by substituting Trp residues 739 and 741 for those that contained electron withdrawing chloro substituents on position 6 of the indole ring, I increased the binding affinity at least 100-fold relative to the WT sequence. These results will guide future NBD-peptide derivates to target the complex for inhibition, including the PROTACs described in Chapter 3.

NEMO appears to be an excellent candidate for targeted degradation, and in Chapter 3 my strategy to convert NEMO binders to PROTACs is outlined. I found that the NEMO binding peptides were largely tolerant of the additional functionality needed to incorporate both a CPP and an E3 ligase recruiter, although the position of the CPP did impact affinity for NEMO. The lead PROTAC, NP-8, which contains an elongated NBD sequence and PEG linker shows the most promise to functionally inhibit the NF-κB activity. It is however, still a very large peptide sequence and we suspect that further optimization of this region by applying the results from Chapter 2 will result in a better PROTAC molecule. Additionally, as outlined in more detail below, I suspect that the cell environment plays a key role in determining the effectiveness of a PROTAC and this is an important direction to examine in future iterations of the project.

C. Future Directions

Cell environment contributing to PROTAC efficacy

As noted above, the current NEMO PROTACs underperform in downregulating NEMO activity. Certainly, additional studies of NP-8 will reveal the extent to which cell trafficking and time-dependence of NEMO degradation affect the observed activity. Beyond PROTAC structure, additional variables include cell type, protein levels, and the NEMO turnover will likely also be critical. To examine this further, I analyzed PROTACs in the literature that have well-documented functional degradative activity and utilized the opensource depmap portal to examine knockdown effects of POIs in cancer cell lines.[11] Not surprisingly, I noted a correlation between protein levels in cells and proliferation activity post POI KO.

Depmap portal allows users to analyze data sets of various cancer cell lines and the effects on their proliferation when gene targets are treated with a knockout technique like CRISPR or RNAi. These data can be very useful and applicable to PROTAC research due to the molecules chemically inducing knockouts of targets, I surveyed the entire Depmap repository for cell lines that showed significant decreased proliferation upon knockout of NEMO by either RNAi or CRISPR techniques. I observed an interesting result by grouping the cells through lineage percentage and found that a clear majority of lung-cell type (20%) were affected in their cell proliferation when IKBKG was knocked out (Figure 4.2).[12]

Cancer Types Proliferation Activity Affected by NEMO Knockout

- 3.16% Uterus
- 0.79% Thyroid
- 1.58% Soft tissue
- 3.16% Skin
- 0.40% Prostate
- 0.79% Pleura
- 1.19% Peripheral nervous system
- 7.51% Pancreas
- 5.93% Ovary/ Fallopian tube
- 4.74% Myeloid
- 6.32% Lymphoid
- 19.76% Lung
- 3.16% Liver
- 5.93% Kidney
- 3.16% Head and Neck
- 0.40% Eye
- 8.30% Esophagous/ Stomach
- 8.30% CNS/ Brain
- 5.93% Breast
- 5.93% Bowel
- 2.37% Bone
- 0.79% Bladder/ UT
- 0.40% Billary tract
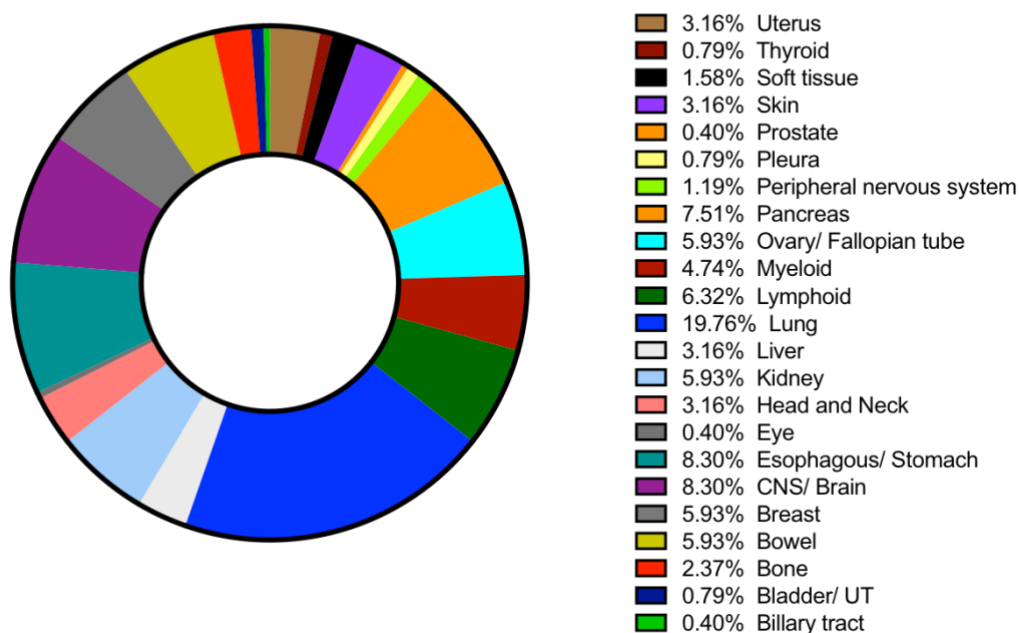
Figure 4.1 Percentage of cancer lineage affected by IKBKG knockout. The pie graph above describes the relative amounts of lineage types where both techniques had a decreased effect in the proliferation of cancer cells when IKBKG was knocked out. The sample size for this graph was 254 cells and the largest amount consisted of lung cell lineage amounting to 20% of the cell sample in the third quadrant.

This result is noteworthy, and this data will guide our future applications of

PROTAC molecules that target NEMO in a lung cancer cell type. We hope that the work

in this thesis provides a framework for building bifunctional peptide molecules to target

NEMO and that those molecules work in the appropriate cellular context.

D. References

1.   Amini-Farsani, Z. *et al.* Prediction and analysis of microRNAs involved in COVID-19 inflammatory processes associated with the NF-kB and JAK/STAT signaling pathways. *Int. Immunopharmacol.* **100**, 108071 (2021).

2.   Gilmore, T. D. & Herscovitch, M. Inhibitors of NF-κB signaling: 785 and counting. *Oncogene 2006 2551* **25**, 6887–6899 (2006).

3.   Mapp, A. K., Pricer, R. & Sturlis, S. Targeting transcription is no longer a quixotic quest. *Nat. Chem. Biol.* **11**, 891 (2015).

4.   Gilmore, T. D. Introduction to NF-κB: players, pathways, perspectives. *Oncogene 2006 2551* **25**, 6680–6684 (2006).

5.   Häcker, H. & Karin, M. Regulation and function of IKK and IKK-related kinases. *Sci. STKE* **2006**, 2023 (2006).

6.   Tarassishin, L. & Horwitz, M. S. Sites on FIP-3 (NEMO/IKKγ) Essential for Its Phosphorylation and NF-κB Modulating Activity. *Biochem. Biophys. Res. Commun.* **285**, 555–560 (2001).

7.   Hanson, S. M. *et al.* What Makes a Kinase Promiscuous for Inhibitors? *Cell Chem. Biol.* **26**, 390-399.e5 (2019).

8.   Rushe, M. *et al.* Structure of a NEMO/IKK-Associating Domain Reveals Architecture of the Interaction Site. *Structure* **16**, 798–808 (2008).

9.   Golden, M. S. *et al.* Comprehensive Experimental and Computational Analysis of Binding Energy Hot Spots at the NF-κB Essential Modulator/IKKβ Protein−Protein Interface. *J. Am. Chem. Soc* **135**, (2013).

10.   Bruno, P. A., Morriss-Andrews, A., Henderson, A. R., Brooks, C. L. & Mapp, A. K.

A Synthetic Loop Replacement Peptide That Blocks Canonical NF-κB Signaling. *Angew. Chemie Int. Ed.* **55**, 14997–15001 (2016).

11. Petrylak, D. P. *et al.* First-in-human phase I study of ARV-110, an androgen receptor (AR) PROTAC degrader in patients (pts) with metastatic castrate-resistant prostate cancer (mCRPC) following enzalutamide (ENZ) and/or abiraterone (ABI). *https://doi.org/10.1200/JCO.2020.38.15_suppl.3500* **38**, 3500–3500 (2020).

12. DepMap: The Cancer Dependency Map Project at Broad Institute. Available at: https://depmap.org/portal/. (Accessed: 4th January 2023)

Appendix

Peptide and PROTAC Characterization

Characterization of NBDwt. A). A chemical structure of the peptide with the FITC

shown in magenta. **B)** Analytical trace of the peptide monitored at 280 nm. The

analytical sample was run in a water with 0.1% TFA/ acetonitrile system. The sample
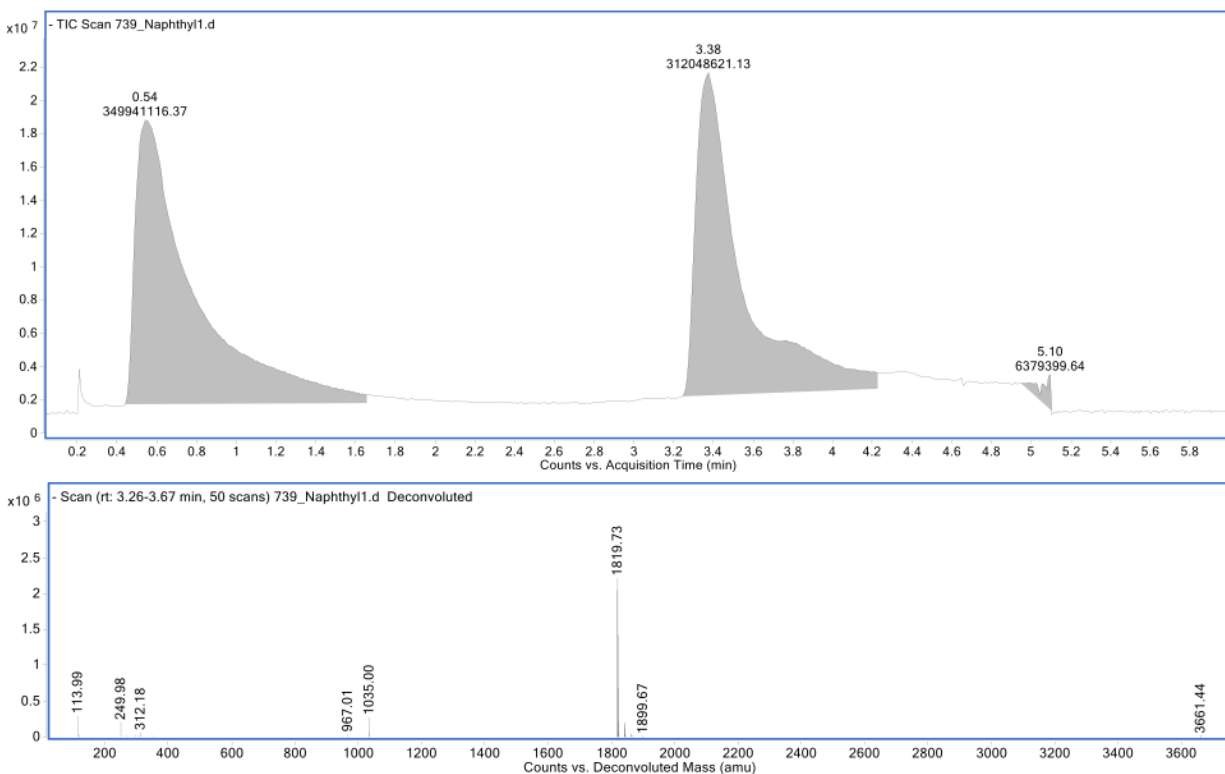
was injected with 0.1 % TFA/ acetonitrile**)** LC-MS using LC-MS qTOF. Samples were run

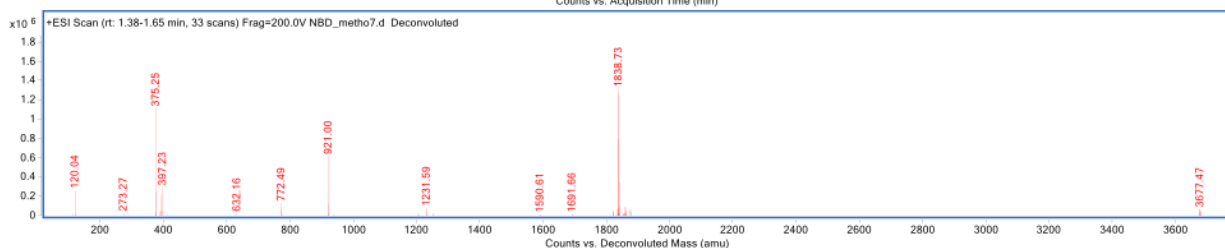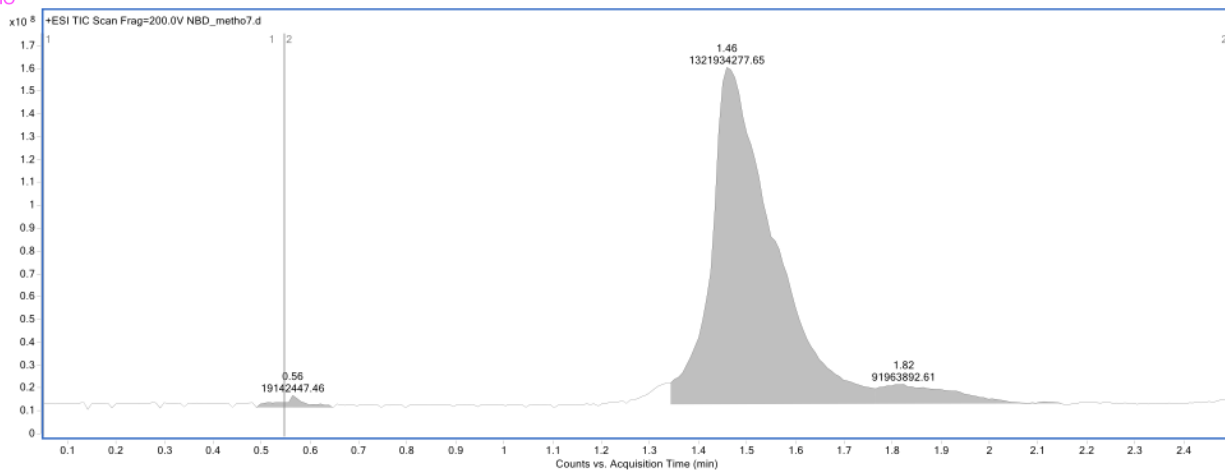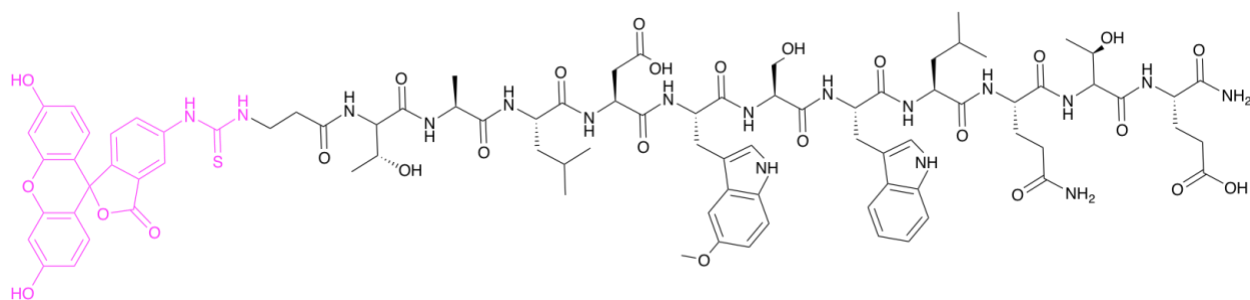in 50/50 0.1% TFA in water, and acetonitrile. Samples were injected onto a C8 column with

a C4 guard. Identity was confirmed under negative mode ionization conditions. The

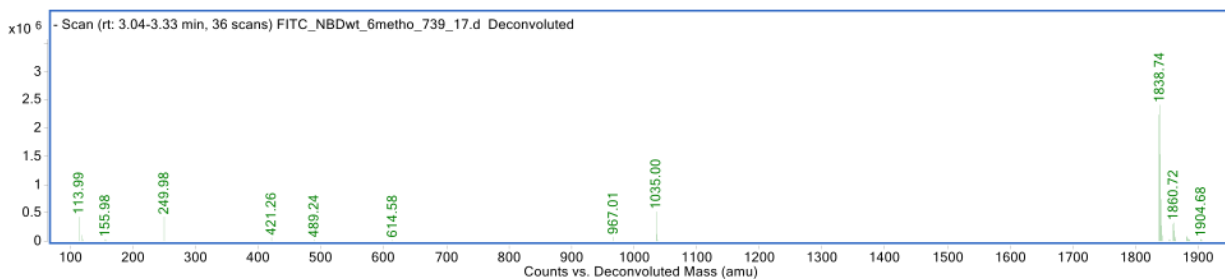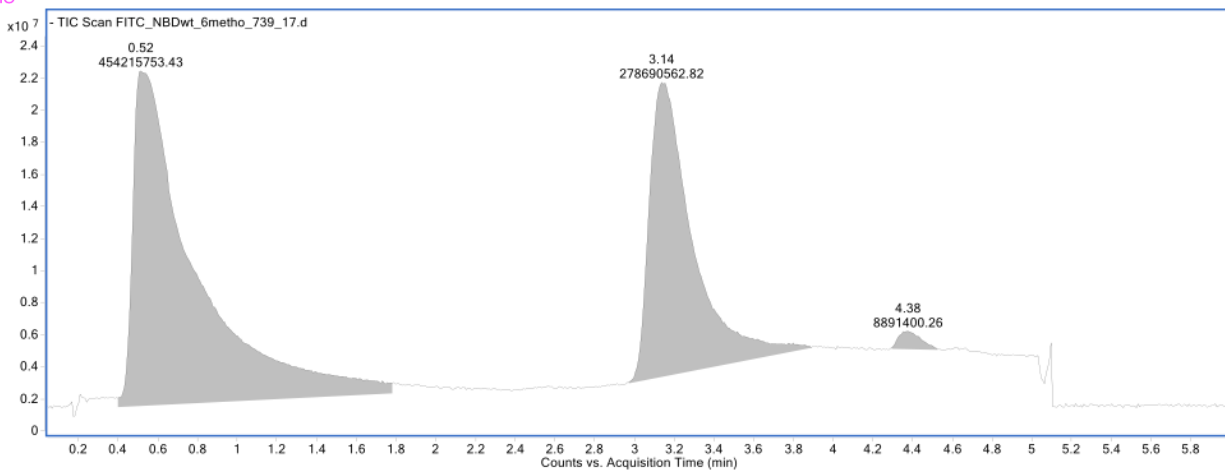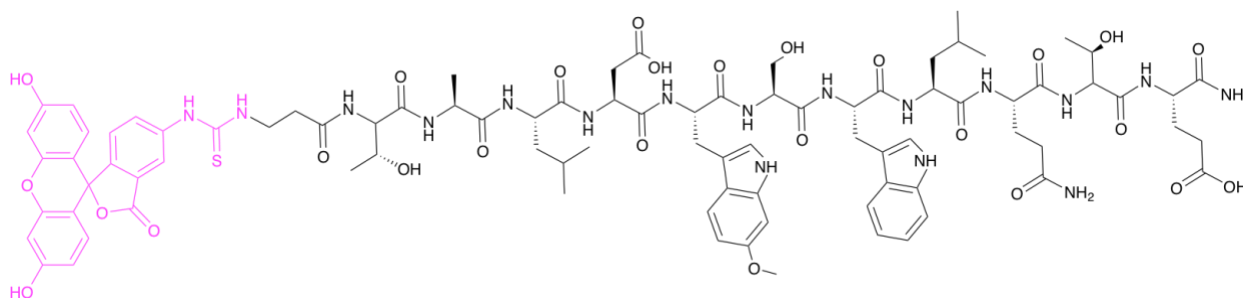expected m/z (full) is 1808.94 and the deconvoluted mass is 1808.54
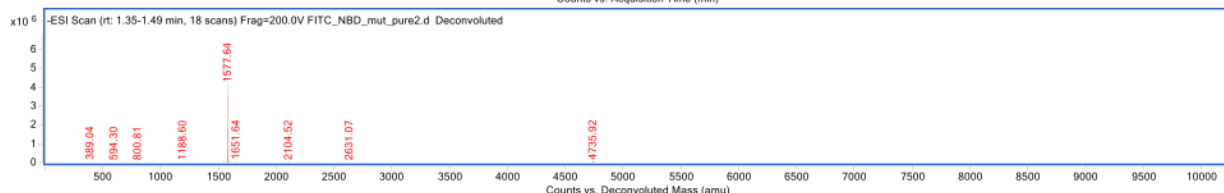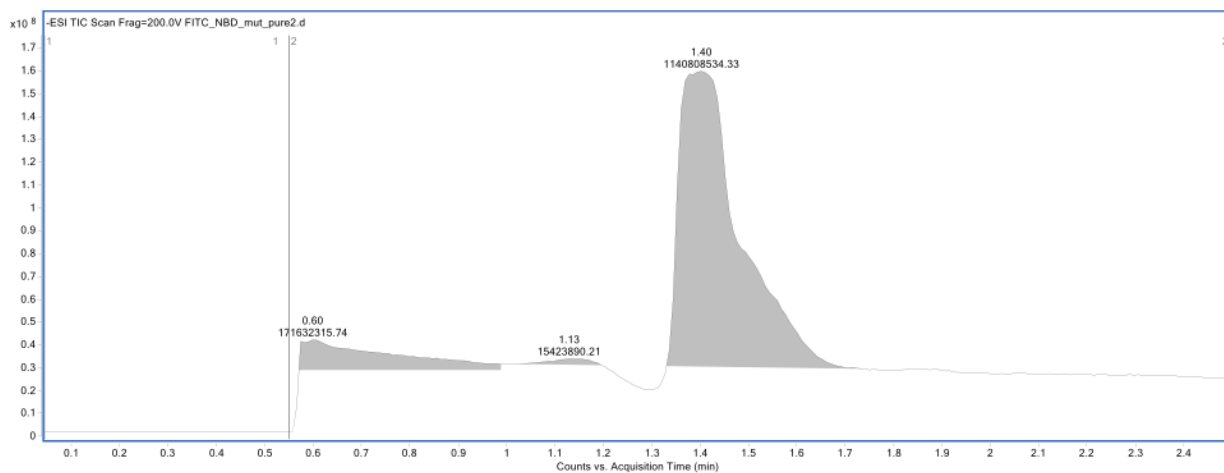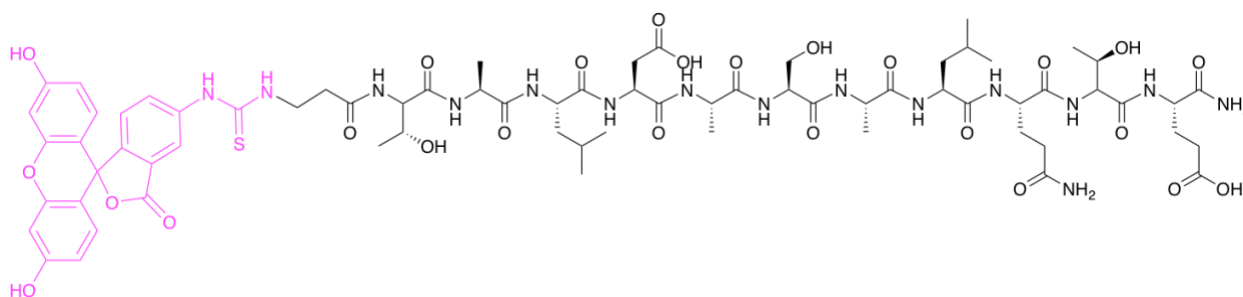
Characterization of W739A, W741A NBD Mut. A). A chemical structure of the peptide

with the FITC shown in magenta. **B)** Analytical trace of the peptide monitored at 280

nm. The analytical sample was run in a water with 0.1% TFA/ acetonitrile system. The

sample was injected with 0.1 % TFA/ acetonitrile. **C)** LC-MS using LC-MS qTOF.

Samples were run in 50/50 0.1% TFA in water, and acetonitrile. Samples were injected onto

a C8 column with a C4 guard. Identity was confirmed under negative mode ionization

conditions. The expected m/z (full) is 1578.67 and the deconvoluted mass is 1577.64.
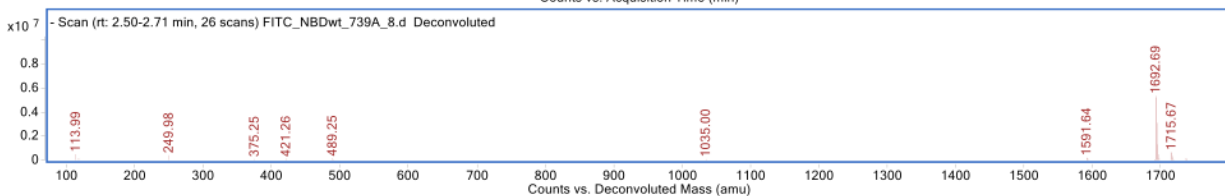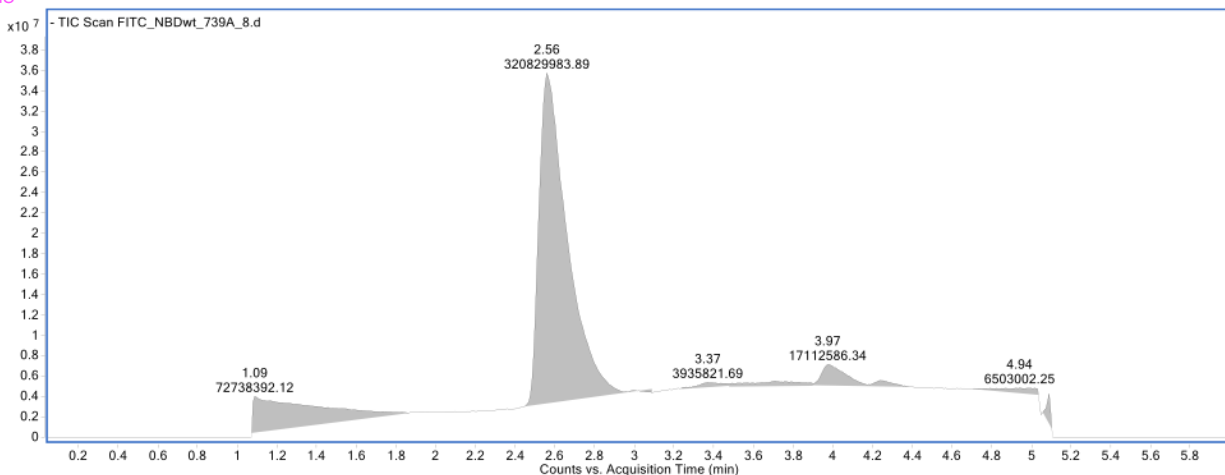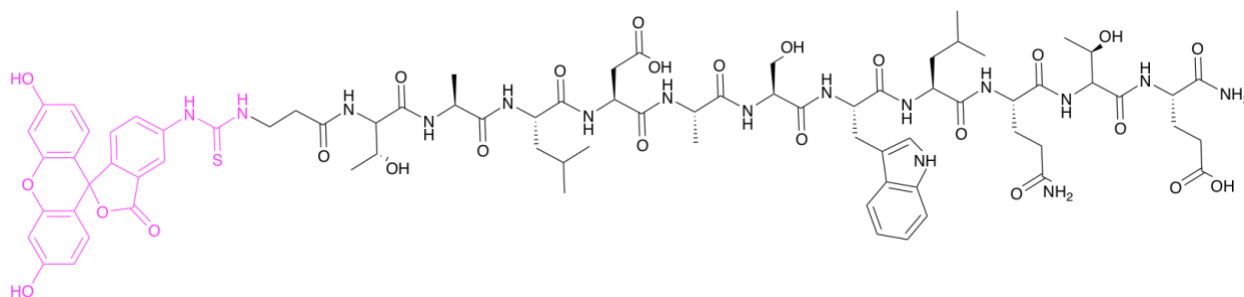
Characterization of W739A NBD Mut. A). A chemical structure of the peptide with the

FITC shown in magenta. **B)** Analytical trace of the peptide monitored at 280 nm. The
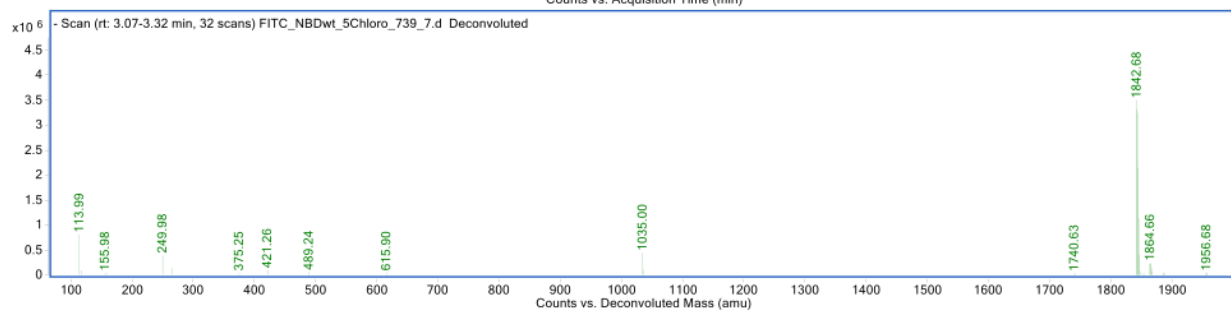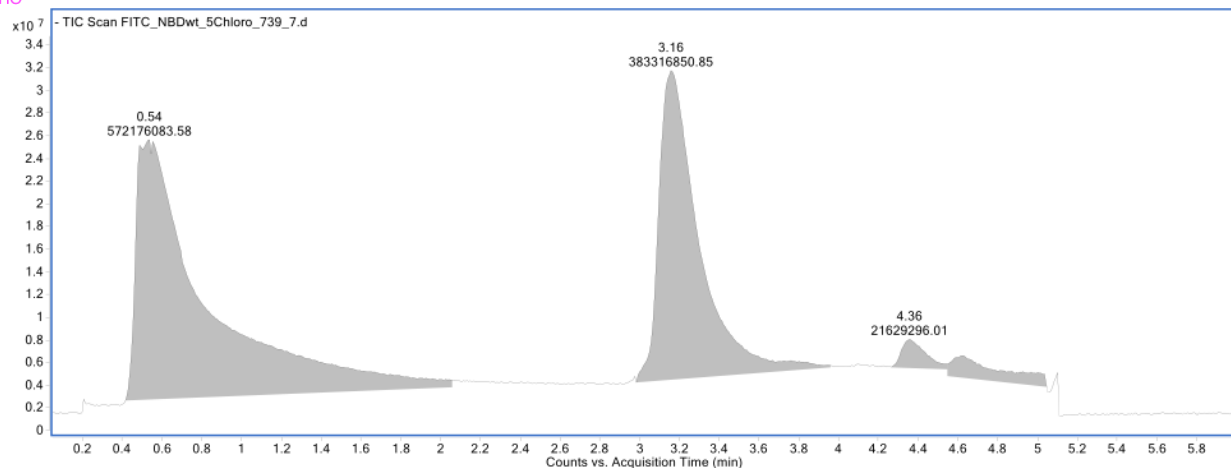
analytical sample was run in a water with 0.1% TFA/ acetonitrile system. The sample

was injected with 0.1 % TFA/ acetonitrile. **C)** LC-MS using LC-MS qTOF. Samples were

run in 50/50 0.1% TFA in water, and acetonitrile. Samples were injected onto a C8 column

with a C4 guard. Identity was confirmed under negative mode ionization conditions. The

expected m/z (full) is 1693.81 and the deconvoluted mass is 1692.59.
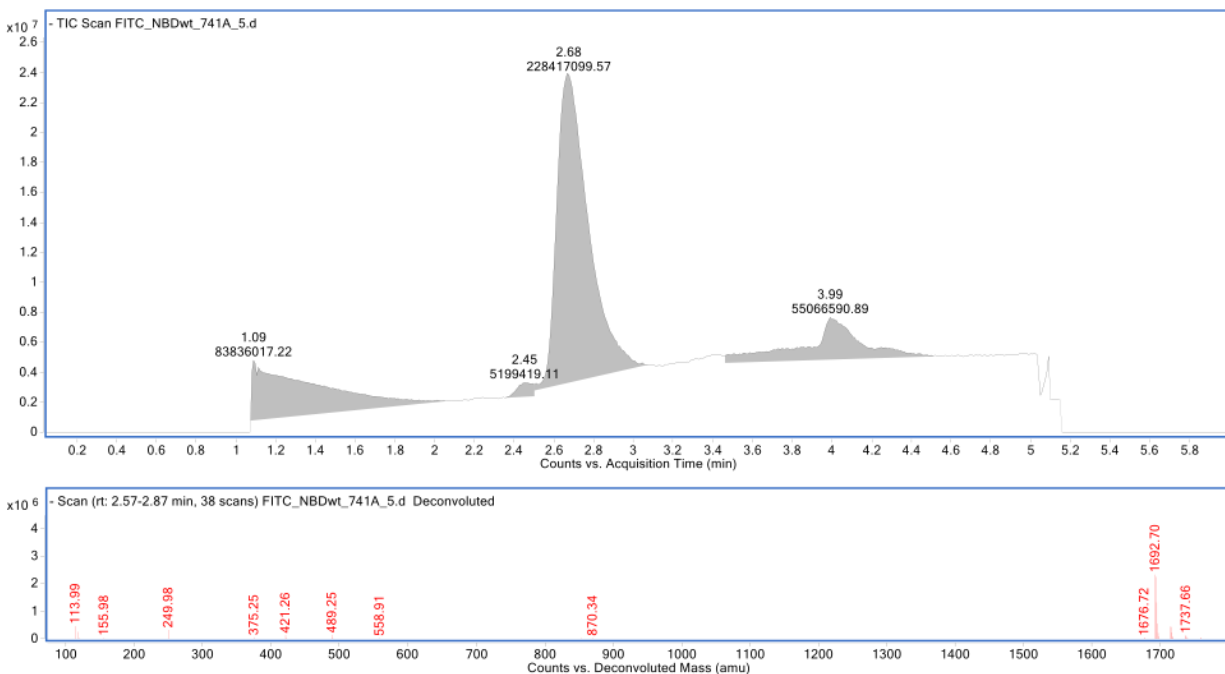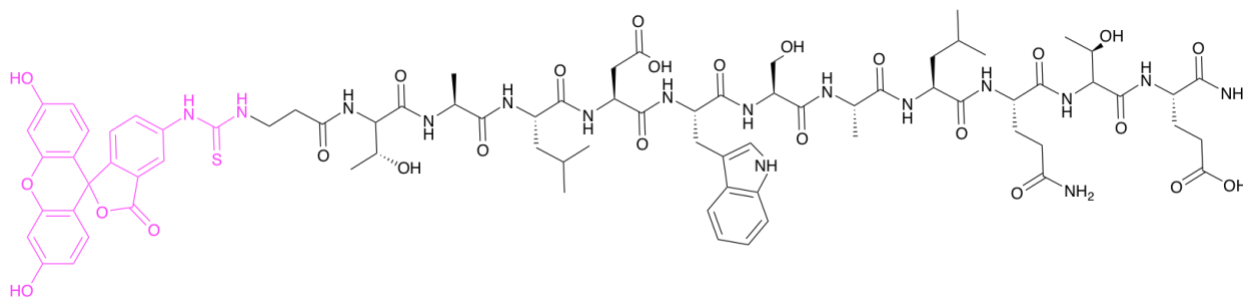
Characterization of W741A NBD Mut. A). A chemical structure of the peptide with the

FITC shown in magenta. **B)** Analytical trace of the peptide monitored at 280 nm. The
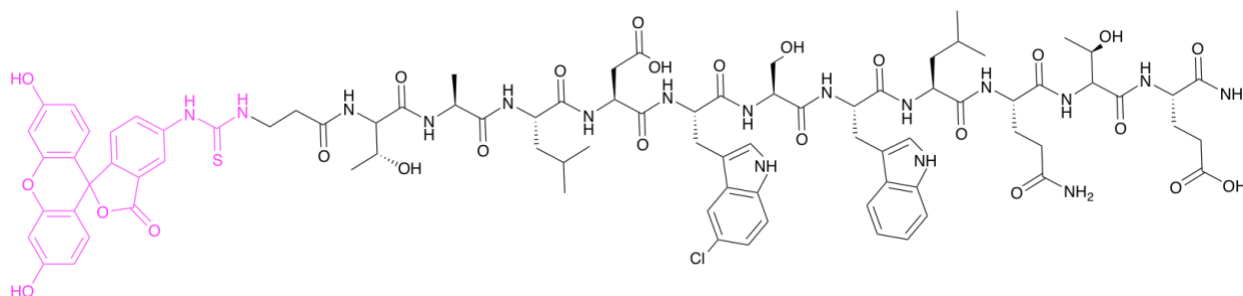
analytical sample was run in a water with 0.1% TFA/ acetonitrile system. The sample

was injected with 0.1 % TFA/ acetonitrile. **C)** LC-MS using LC-MS qTOF. Samples were

run in 50/50 0.1% TFA in water, and acetonitrile. Samples were injected onto a C8 column

with a C4 guard. Identity was confirmed under negative mode ionization conditions. The

expected m/z (full) is 1693.81 and the deconvoluted mass is 1692.70.
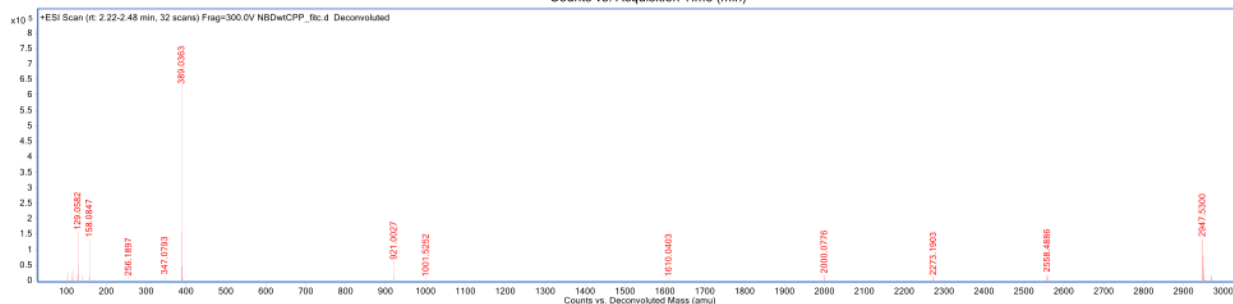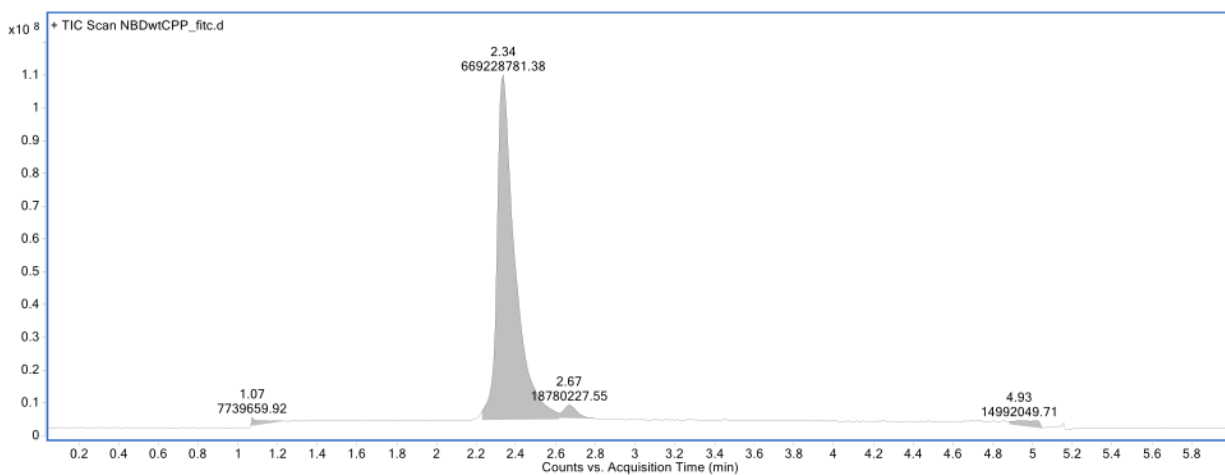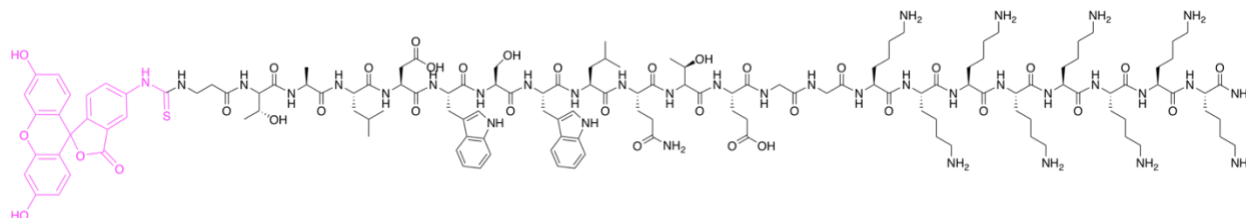
Characterization of NBDwt-PolyK. A). A chemical structure of the peptide with the

FITC shown in magenta. **B)** Analytical trace of the peptide monitored at 280 nm. The

analytical sample was run in a water with 0.1% TFA/ acetonitrile system. The sample

was injected with 0.1 % TFA/ acetonitrile. **C)** LC-MS using LC-MS qTOF. Samples were

run in 50/50 0.1% TFA in water, and acetonitrile. Samples were injected onto a C8 column

with a C4 guard. Identity was confirmed under negative mode ionization conditions. The

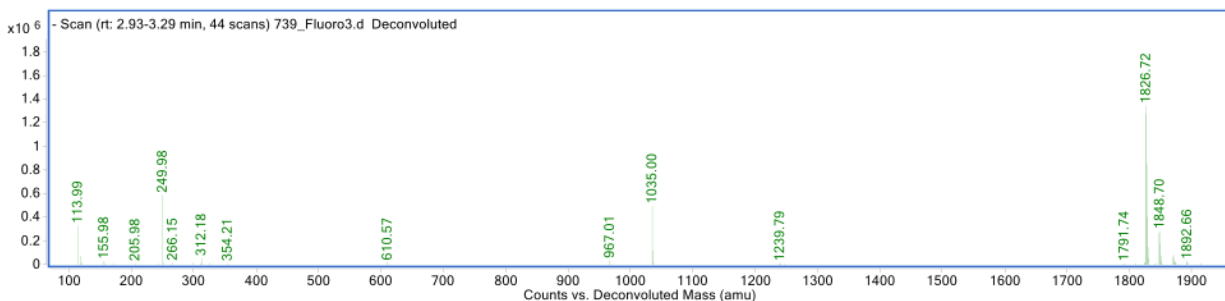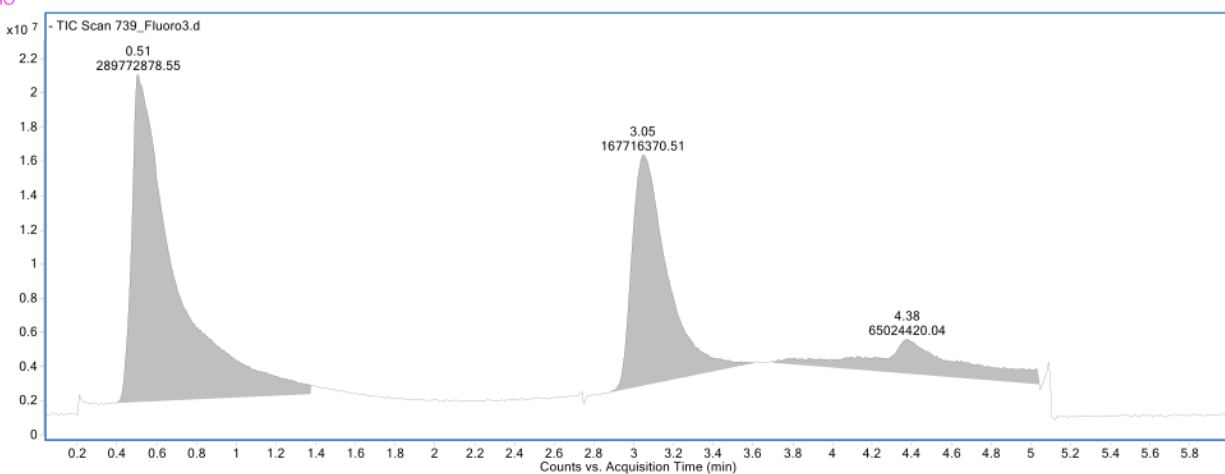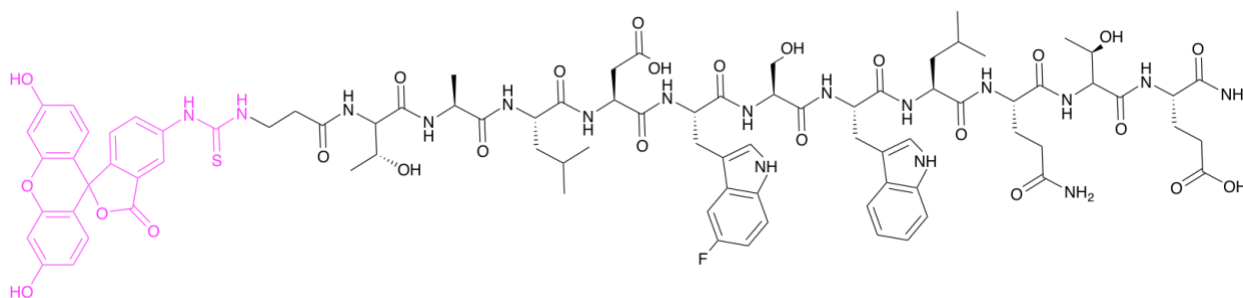expected m/z (full) is 2948.44 and the deconvoluted mass is 2947.53.
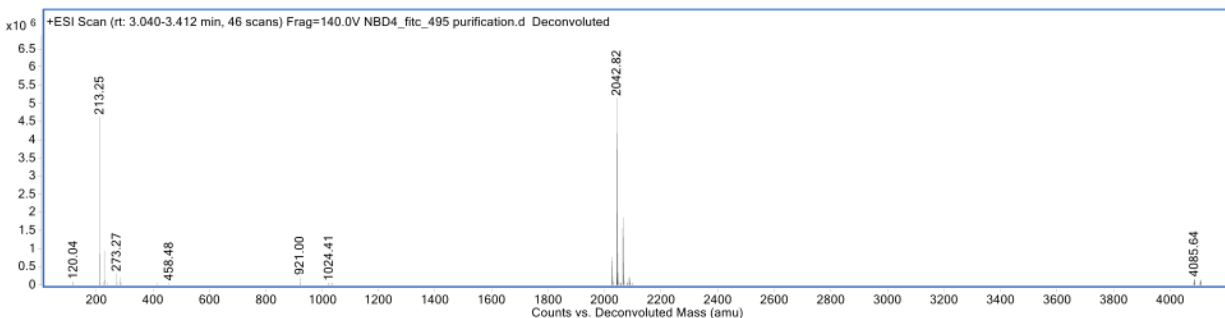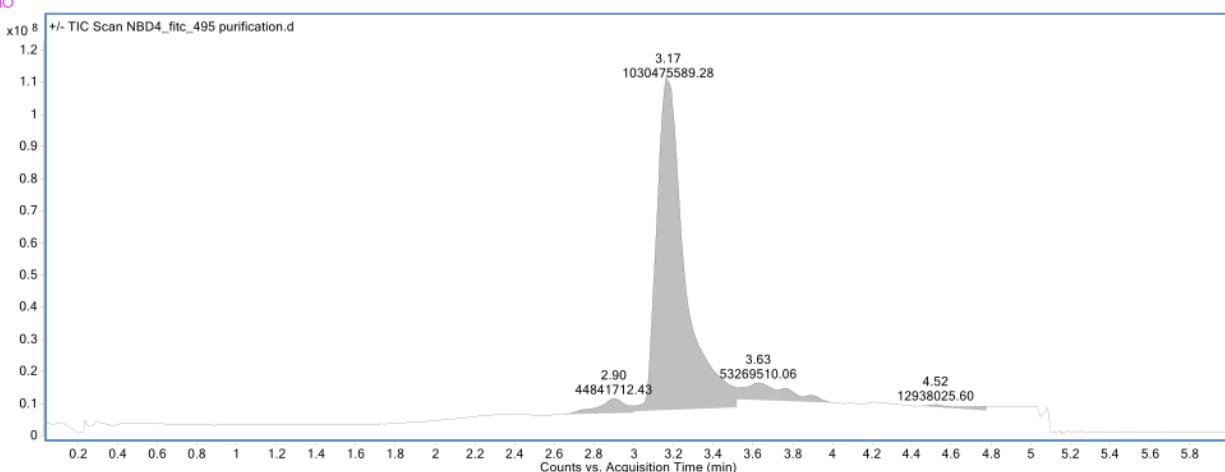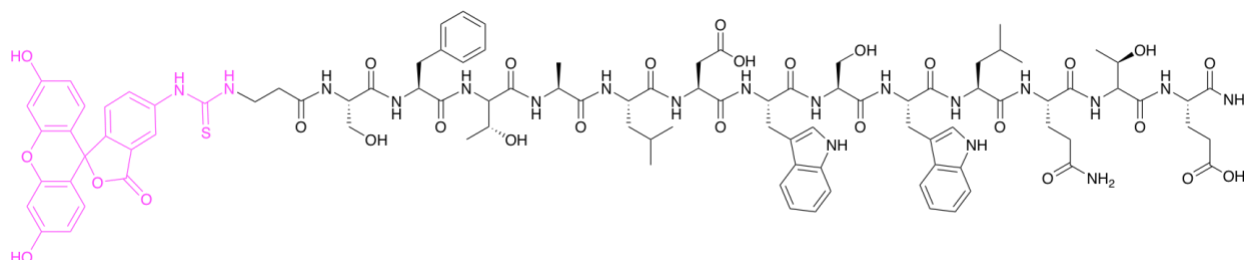
Characterization of NBD4 A). A chemical structure of the peptide with the FITC shown

in magenta. **B)** Analytical trace of the peptide monitored at 280 nm. The analytical

sample was run in a water with 0.1% TFA/ acetonitrile system. The sample was injected

with 0.1 % TFA/ acetonitrile. **C)** LC-MS using LC-MS qTOF. Samples were run in 50/50

0.1% TFA in water, and acetonitrile. Samples were injected onto a C8 column with a C4

guard. Identity was confirmed under negative mode ionization conditions. The expected m/z (full) is 2042.82 and the deconvoluted mass is 2043.20.

Characterization of NBD4mut. A). A chemical structure of the peptide with the FITC shown in magenta. **B)** Analytical trace of the peptide monitored at 280 nm. The analytical sample was run in a water with 0.1% TFA/ acetonitrile system. The sample was injected with 0.1 % TFA/ acetonitrile. The peak before 1 min corresponds to a solvent peak. **C)** LC-MS using LC-MS qTOF. Samples were run in 50/50 0.1% TFA in wat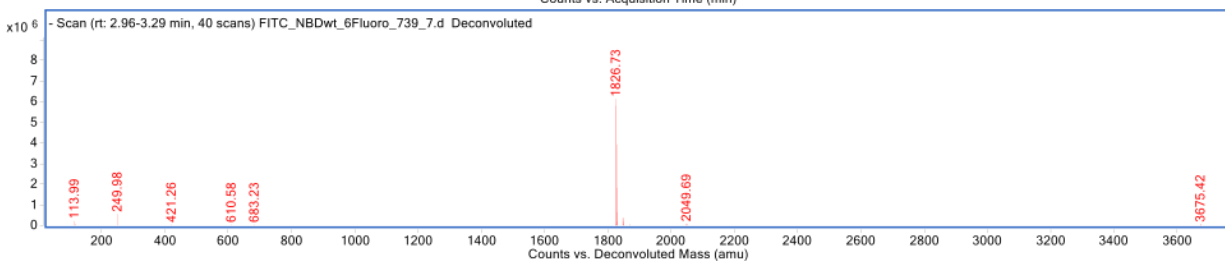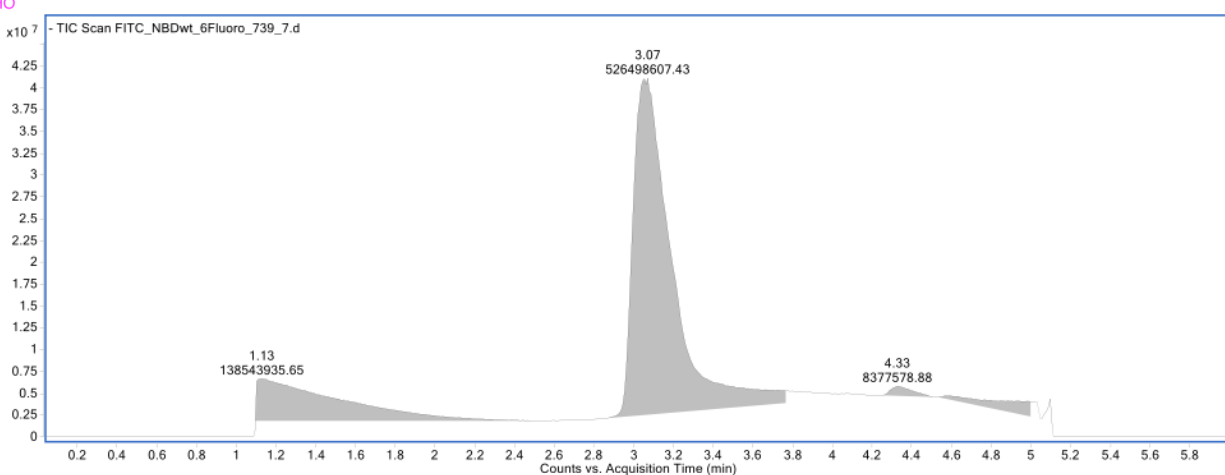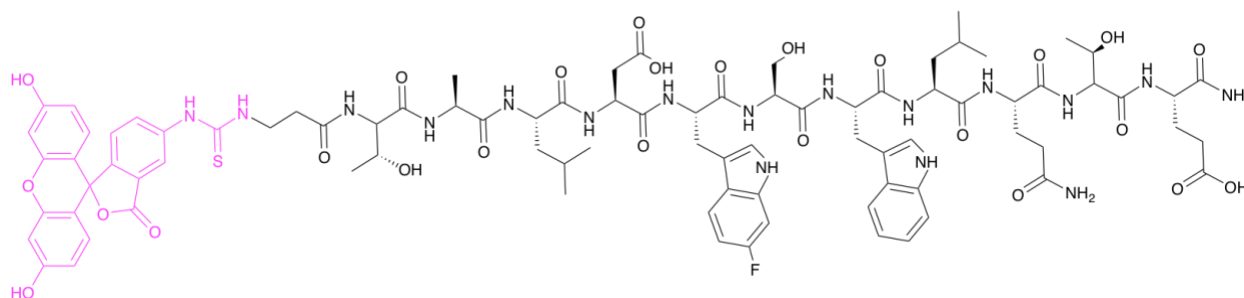er, and acetonitrile. Samples were injected onto a C8 column with a C4 guard. Identity was confirmed under negative mode ionization conditions. The expected m/z (full) is 1812.74 and the deconvoluted mass is 1812.93.

βAPAKKSEELVAEAHNLCTLLENAIQDTVREQDQSFTALDWSWLQTE−NH₂

Characterization of IKKwt. A). A chemical structure of the peptide with the FITC

shown in magenta. **B)** Analytical trace of the peptide monitored at 280 nm. The

analytical sample was run in a water with 0.1% TFA/ acetonitrile system. The sample

was injected with 0.1 % TFA/ acetonitrile. **C)** LC-MS using LC-MS qTOF. Samples were

run in 50/50 0.1% TFA in water, and acetonitrile. Samples were injected onto a C8 column

with a C4 guard. Identity was confirmed under negative mode ionization conditions. The

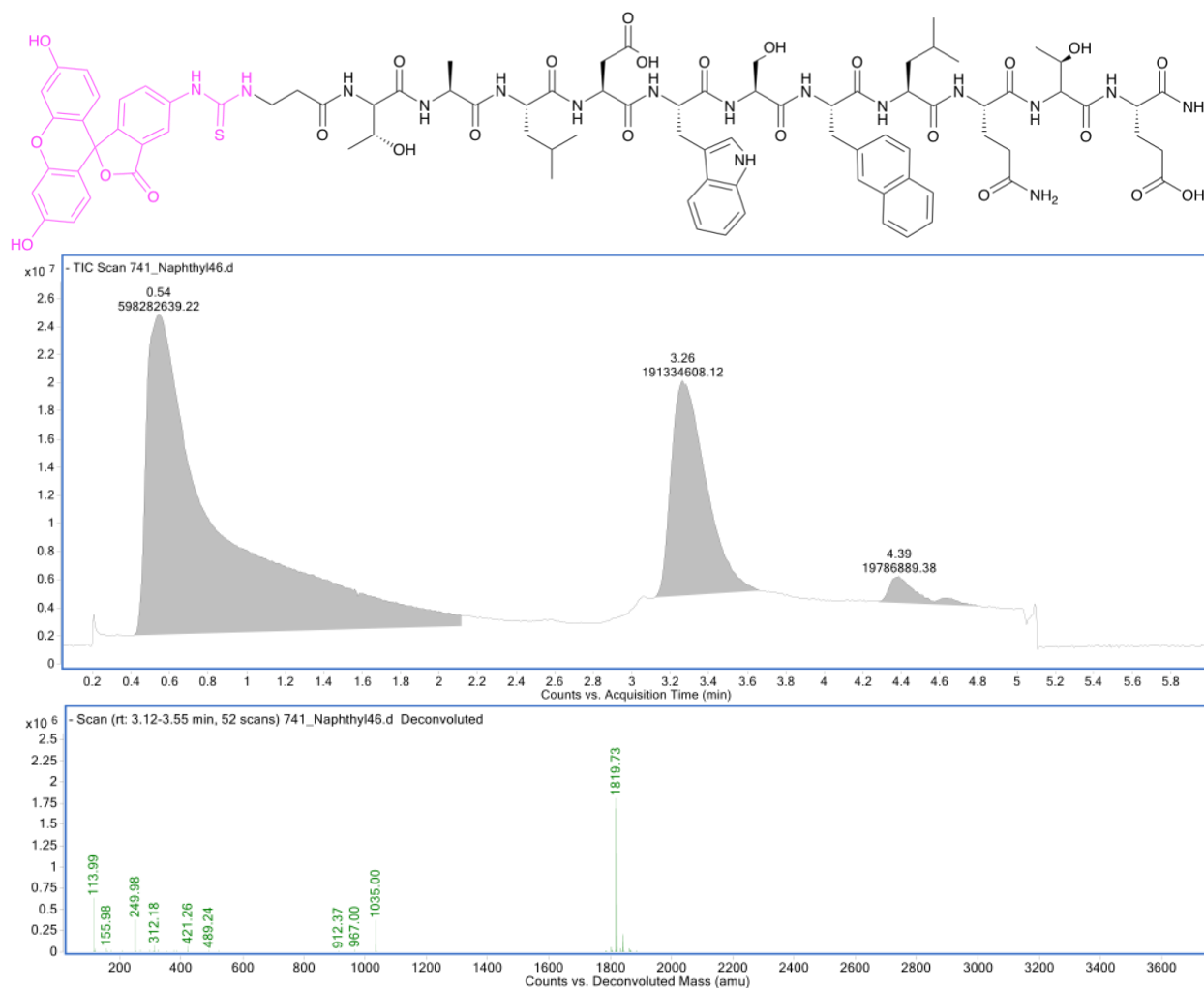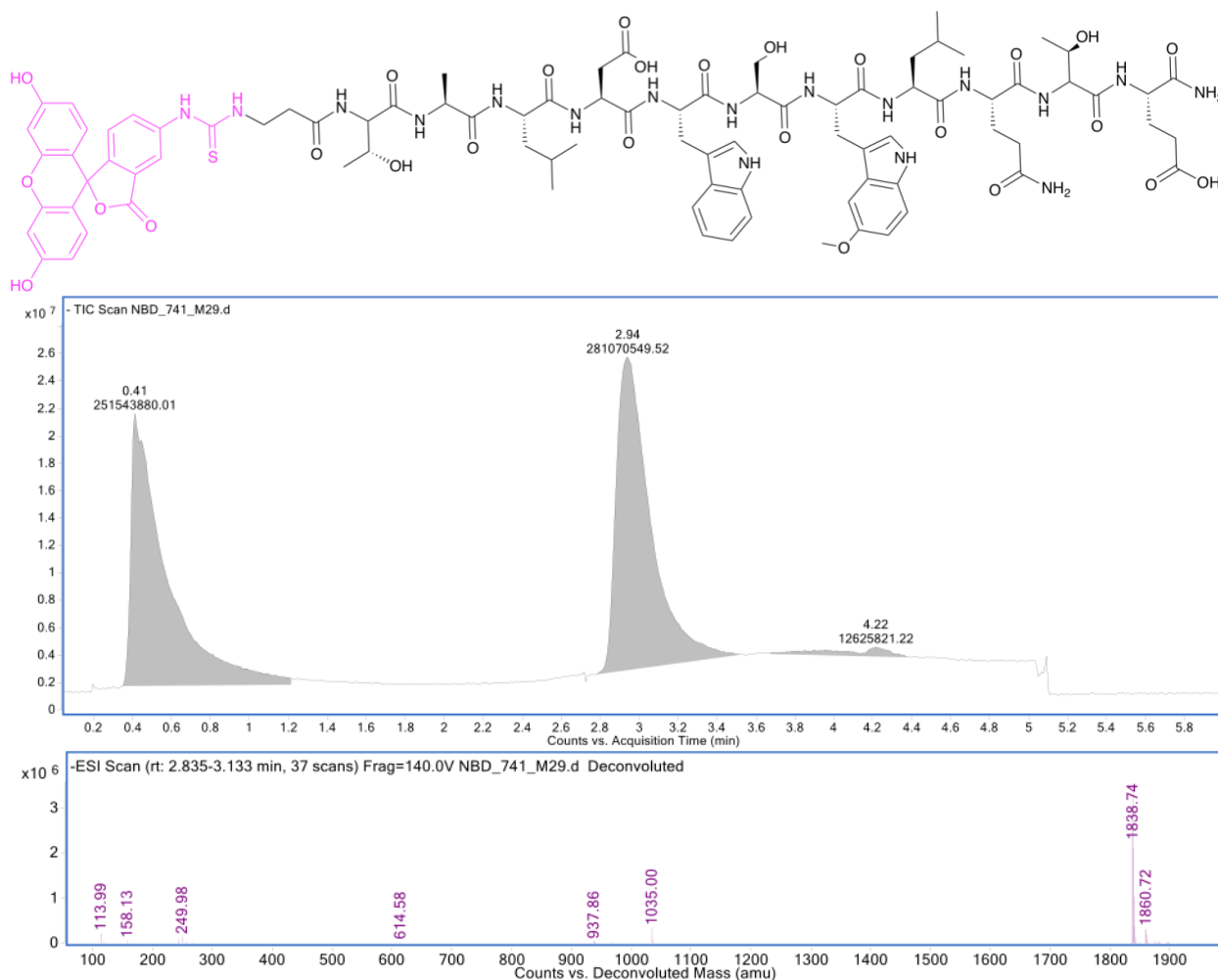expected m/z (full) is 5618.60 and the deconvoluted mass is 5619.15.
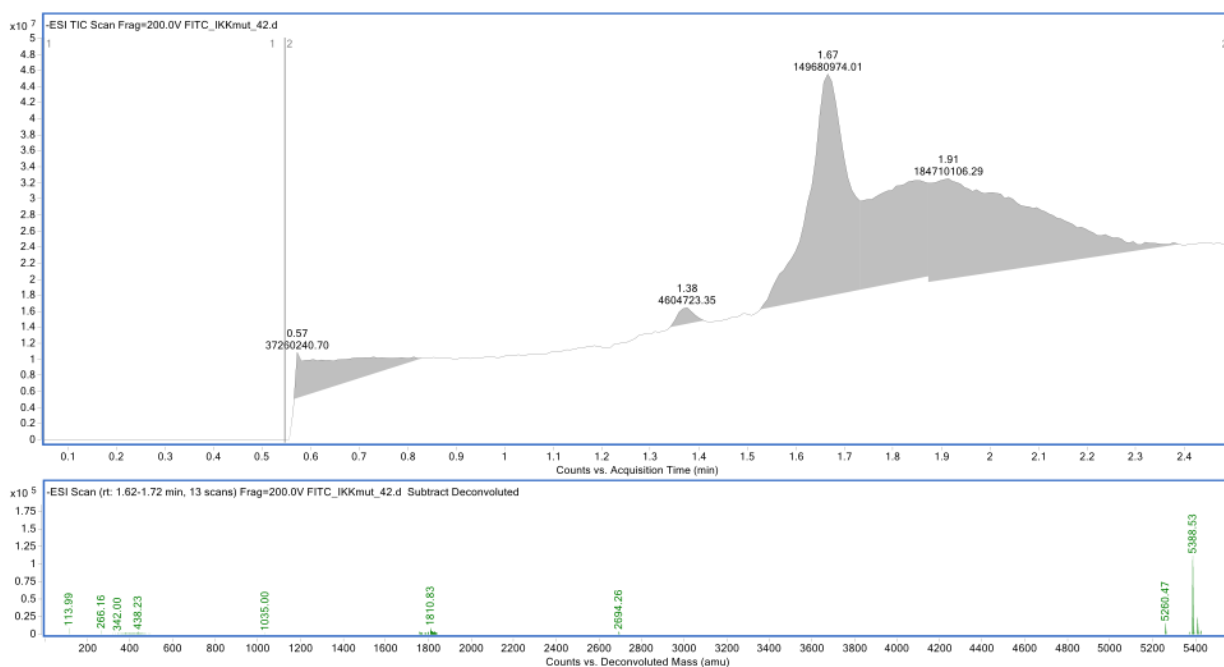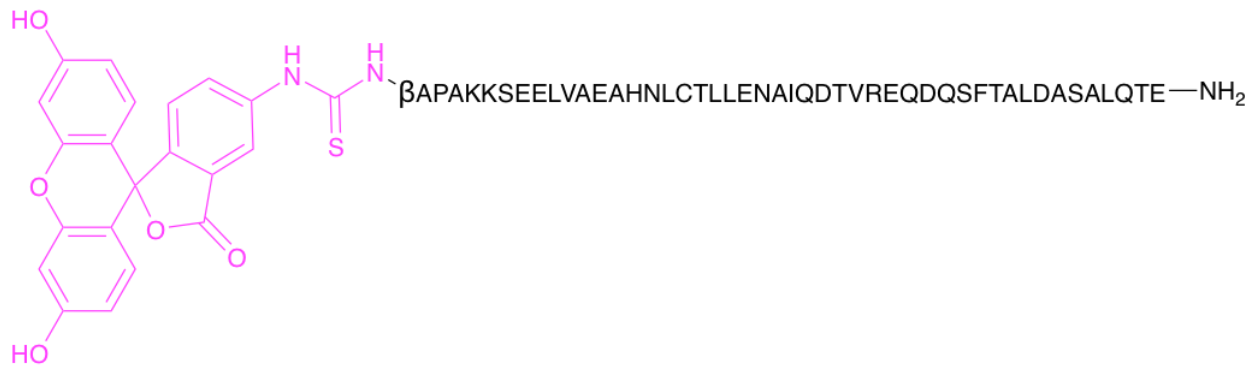
Characterization of IKKmut. A). A chemical structure of the peptide with the FITC

shown in magenta. **B)** Analytical trace of the peptide monitored at 280 nm. The

analytical sample was run in a water with 0.1% TFA/ acetonitrile system. The sample

was injected with 0.1 % TFA/ acetonitrile. **C)** LC-MS using LC-MS qTOF. Samples were

run in 50/50 0.1% TFA in water, and acetonitrile. Samples were injected onto a C8 column

with a C4 guard. Identity was confirmed under negative mode ionization conditions. The

expected m/z (full) is 5388.53 and the deconvoluted mass is 5388.88.
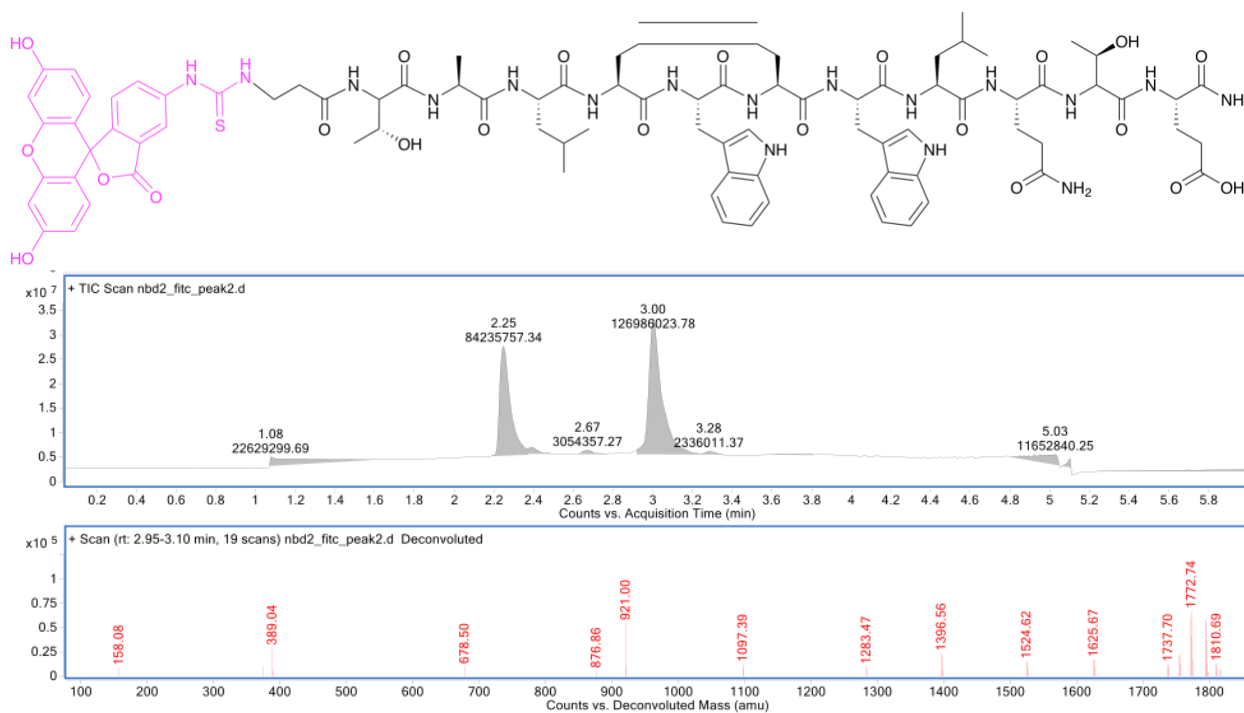
Characterization of NBD2. A). A chemical structure of the peptide with the FITC

shown in magenta. **B)** Analytical trace of the peptide monitored at 280 nm. The

analytical sample was run in a water with 0.1% TFA/ acetonitrile system. The sample

was injected with 0.1 % TFA/ acetonitrile **C)** LC-MS using LC-MS qTOF. Samples were

run in 50/50 0.1% TFA in water, and acetonitrile. Samples were injected onto a C8 column

with a C4 guard. Identity was confirmed under negative mode ionization conditions. The

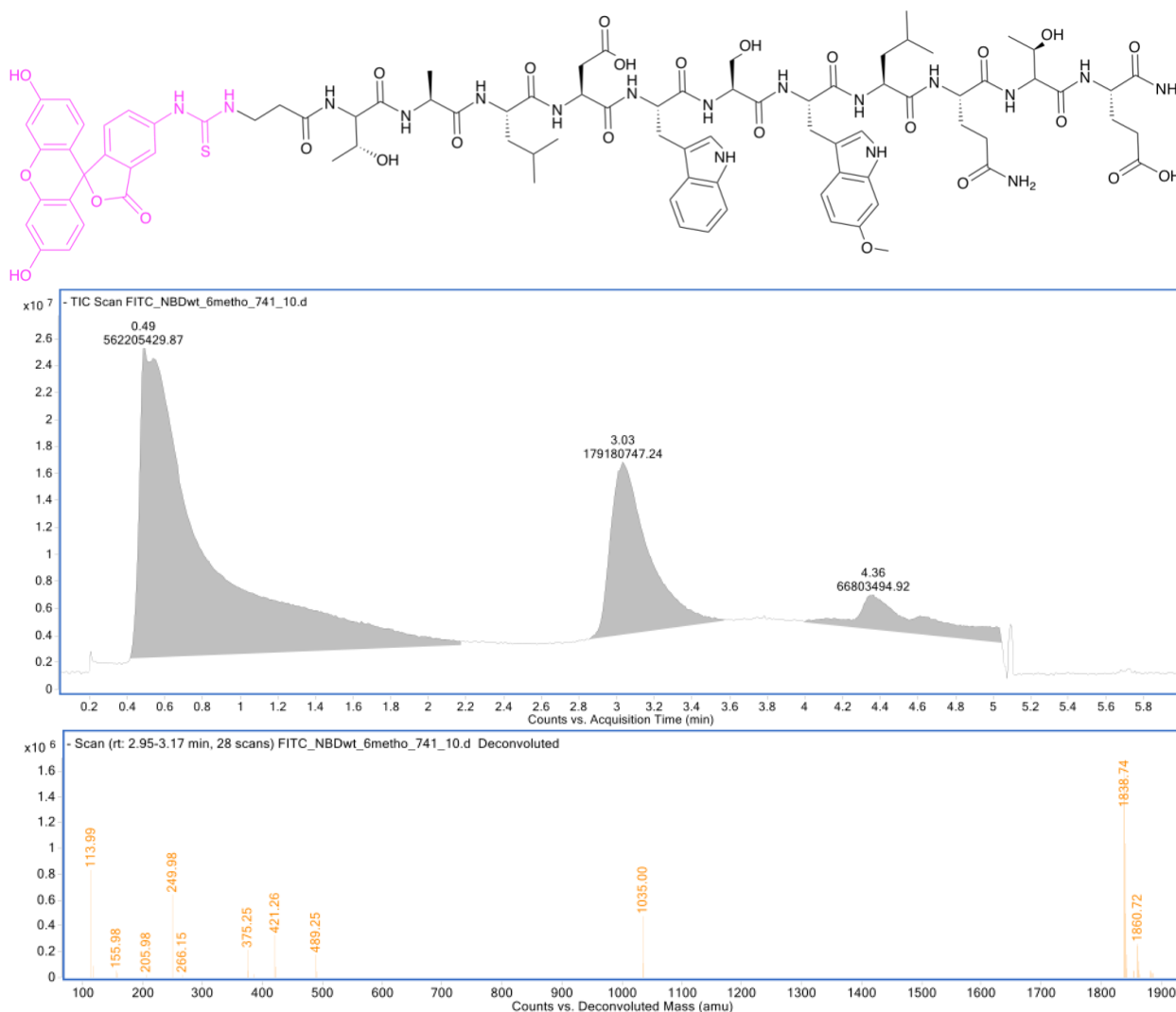expected m/z (full) is 1772.74. and the deconvoluted mass is 1772.95.
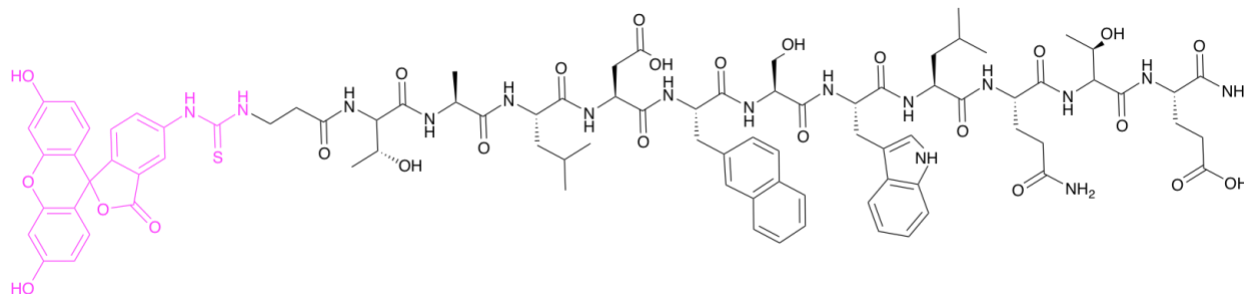
Characterization of Naphthyl-Ala-739 NBD. A). A chemical structure of the peptide

with the FITC shown in magenta. **B)** Analytical trace of the peptide monitored at 280

nm. The analytical sample was run in a water with 0.1% TFA/ acetonitrile system. The

sample was injected with 0.1 % TFA/ acetonitrile. The peak before 1 min corresponds to

a solvent peak. **C)** LC-MS using LC-MS qTOF. Samples were run in 50/50 0.1% TFA in

water, and acetonitrile. Samples were injected onto a C8 column with a C4 guard. Identity

was confirmed under negative mode ionization conditions. The expected m/z (full) is
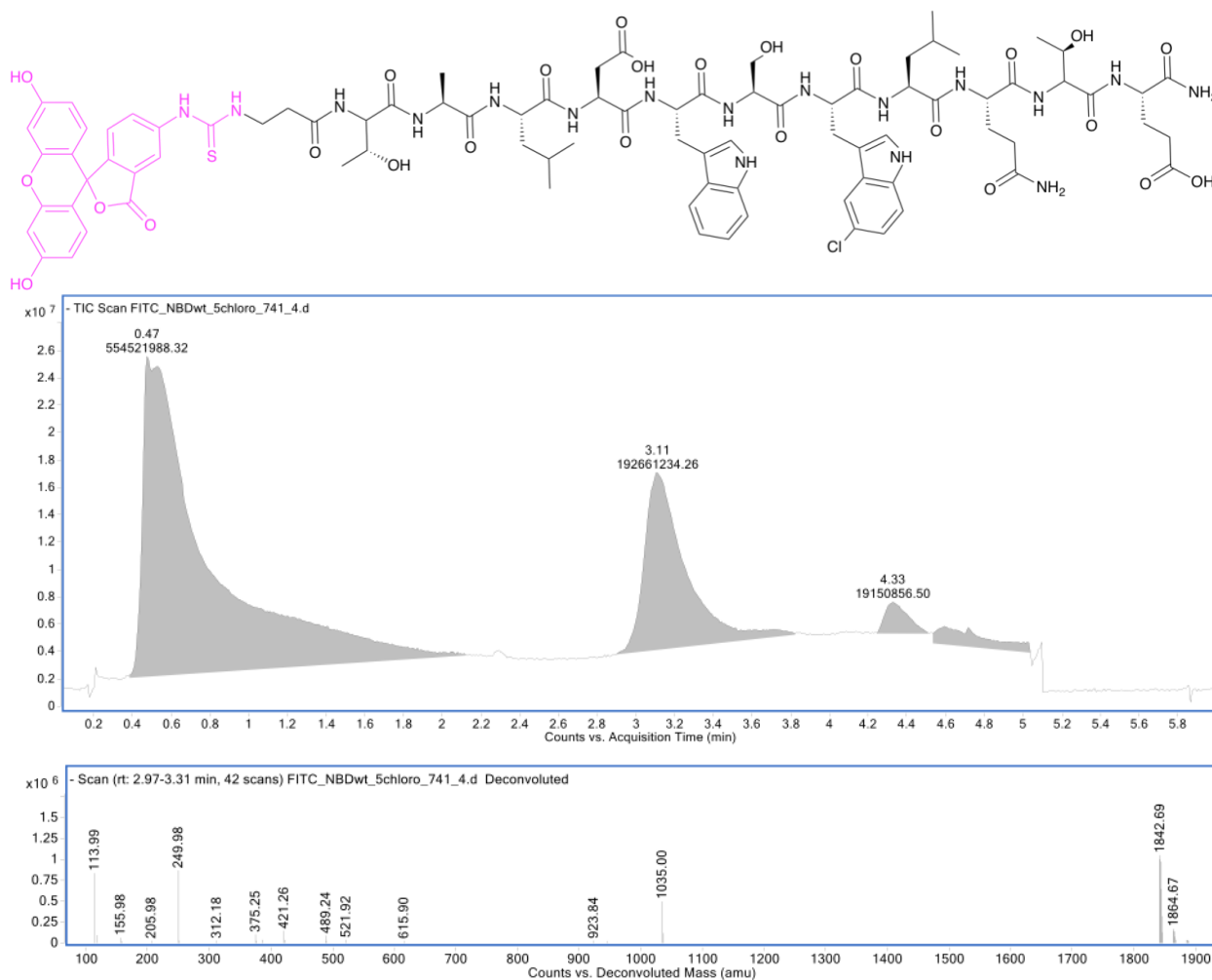
1819.96 and the deconvoluted mass is 1819.73.

Characterization of 5Methoxy-739 NBD. A). A chemical structure of the peptide with the FITC shown in magenta. **B)** Analytical trace of the peptide monitored at 280 nm. The analytical sample was run in a water with 0.1% TFA/ acetonitrile system. The sample was injected with 0.1 % TFA/ acetonitrile. **C)** LC-MS using LC-MS qTOF. Samples were run in 50/50 0.1% TFA in water, and acetonitrile. Samples were injected onto a C8 column with a C4 guard. Identity was confirmed under negative mode ionization conditions. The expected m/z (full) is 1838.97 and the deconvoluted mass is 1838.73.

Characterization of 6Methoxy-739 NBD. A). A chemical structure of the peptide with the FITC shown in magenta. **B)** Analytical trace of the peptide monitored at 280 nm. The analytical sample was run in a water with 0.1% TFA/ acetonitrile system. The sample was injected with 0.1 % TFA/ acetonitrile. The peak before 1 min corresponds to a solvent peak. **C)** LC-MS using LC-MS qTOF. Samples were run in 50/50 0.1% TFA in water, and acetonitrile. Samples were injec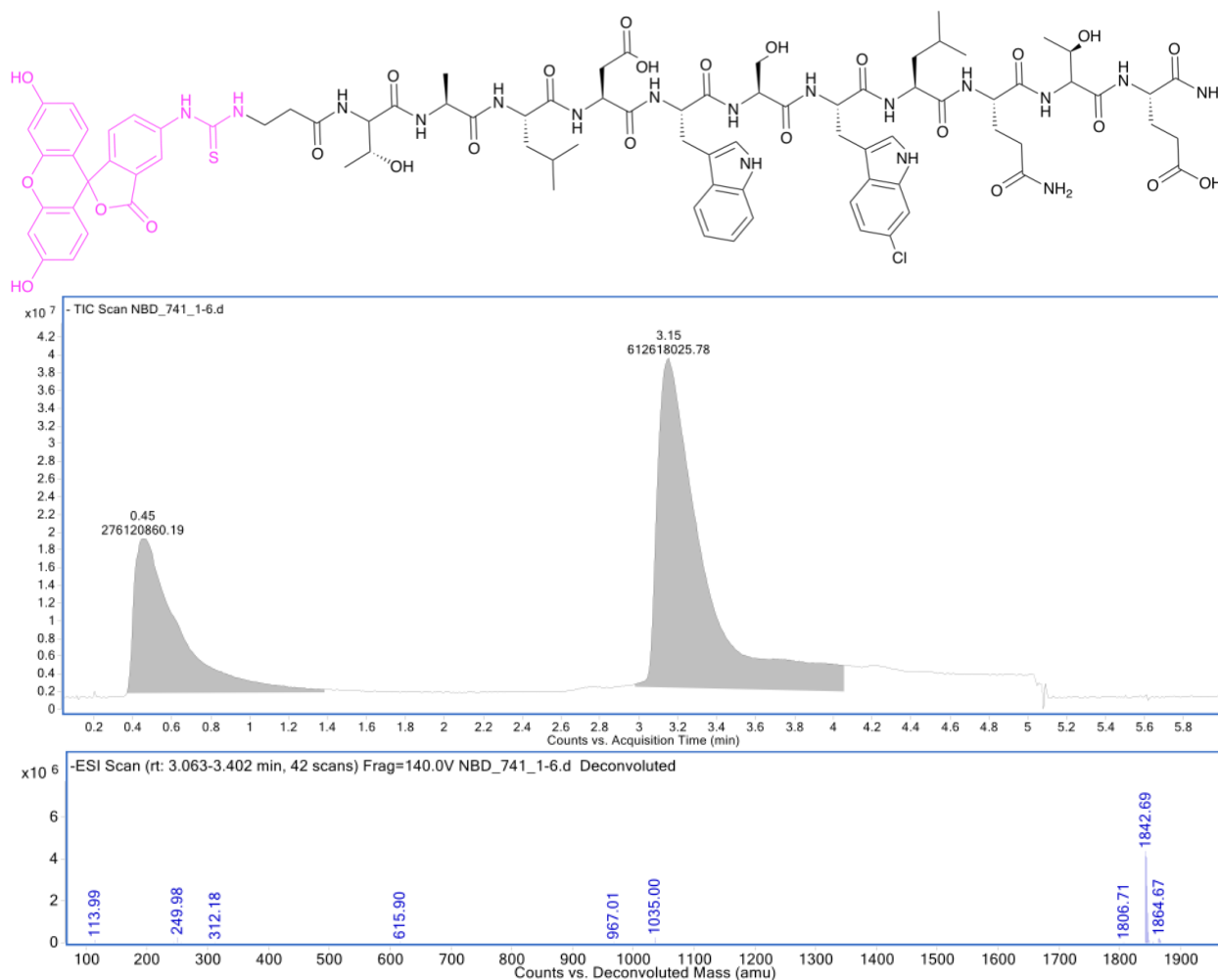ted onto a C8 column with a C4 guard. Identity was confirmed under negative mode ionization conditions. The expected m/z (full) is 1838.97 and the deconvoluted mass is 1838.74.

Characterization of 5Cl-739 NBD. A). A chemical structure of the peptide with the FITC shown in magenta. **B)** Analytical trace of the peptide monitored at 280 nm. The analytical sample was run in a water with 0.1% TFA/ acetonitrile system. The sample was injected with 0.1 % TFA/ acetonitrile. The peak before 1 min corresponds to a solvent peak. **C)** LC-MS using LC-MS qTOF. Samples were run in 50/50 0.1% TFA in water, and acetonitrile. Samples were injected o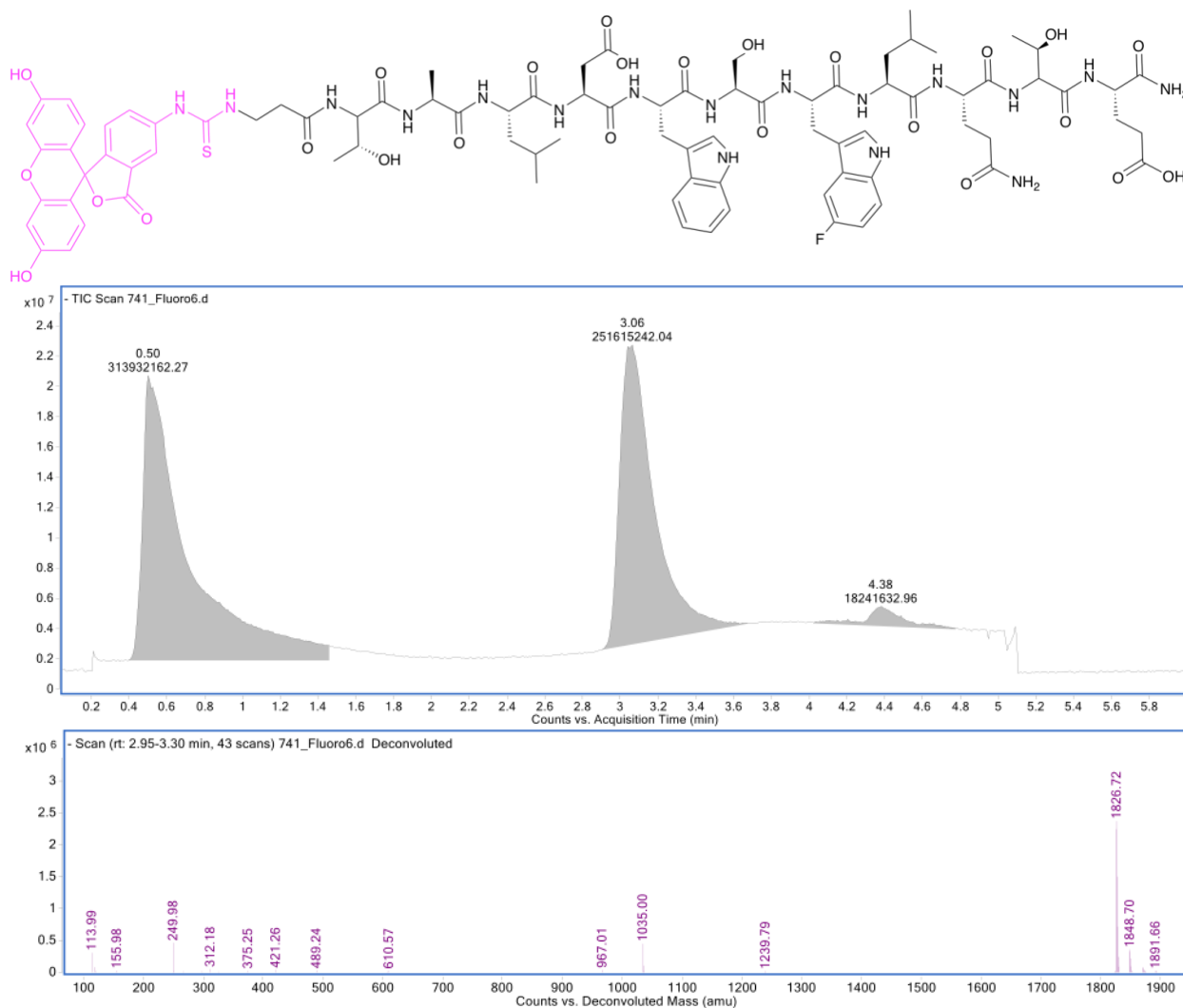nto a C8 column with a C4 guard. Identity was confirmed under negative mode ionization conditions. The expected m/z (full) is 1843.38 and the deconvoluted mass is 1842.68.
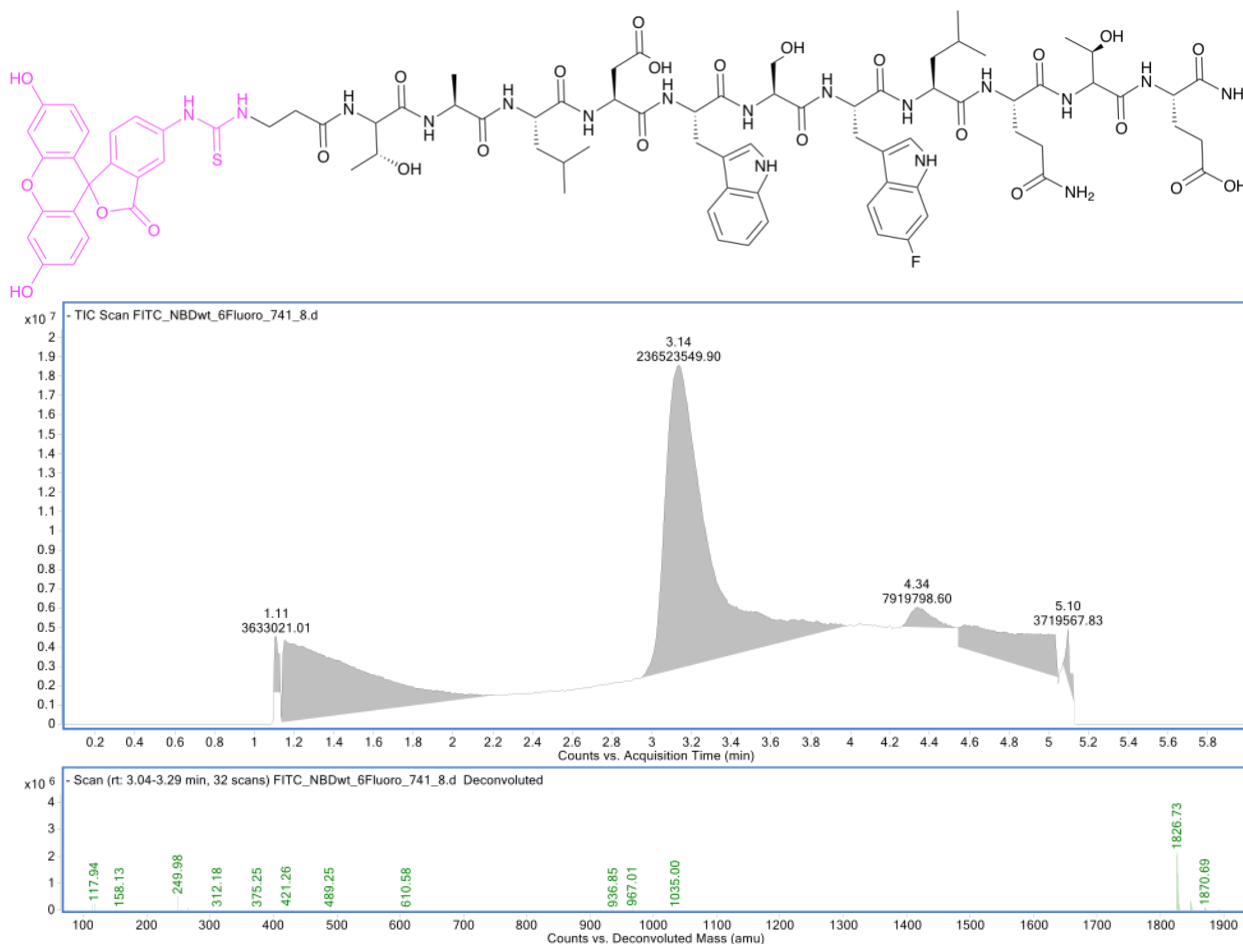
Characterization of 6CI-739 NBD. A). A chemical structure of the peptide with the

FITC shown in magenta. **B)** Analytical trace of the peptide monitored at 280 nm. The

analytical sample was run in a water with 0.1% TFA/ acetonitrile system. The sample

was injected with 0.1 % TFA/ acetonitrile. **C)** LC-MS using LC-MS qTOF. Samples were

run in 50/50 0.1% TFA in water, and acetonitrile. Samples were injected onto a C8 column

with a C4 guard. Identity was confirmed under negative mode ionization conditions. The

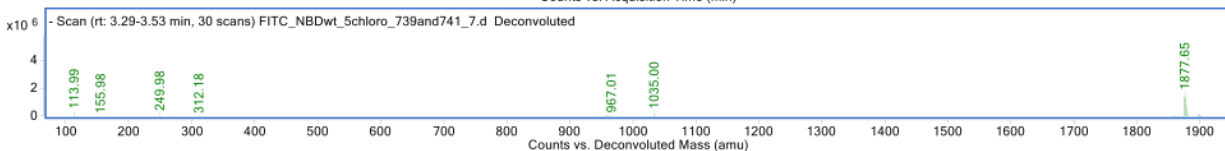expected m/z (full) is 1843.38 and the deconvoluted mass is 1843.69.

Characterization of 5F-739 NBD. A). A chemical structure of the peptide with the FITC

shown in magenta. **B)** Analytical trace of the peptide monitored at 280 nm. The

analytical sample was run in a water with 0.1% TFA/ acetonitrile system. The sample

was injected with 0.1 % TFA/ acetonitrile. The peak before 1 min corresponds to a

solvent peak. **C)** LC-MS using LC-MS qTOF. Samples were run in 50/50 0.1% TFA in

water, and acetonitrile. Samples were injected onto a C8 column with a C4 guard. Identity

was confirmed under negative mode ionization conditions. The expected m/z (full) is

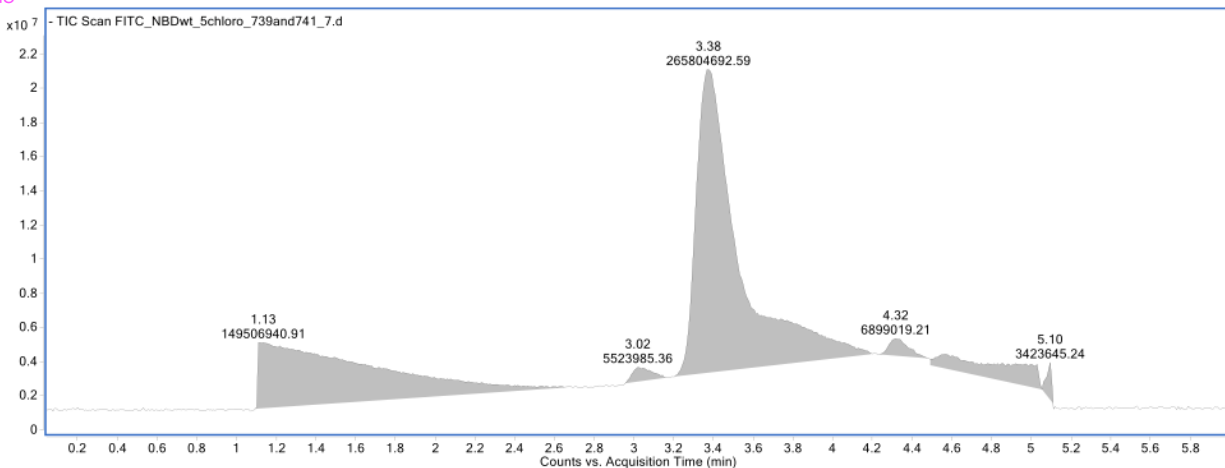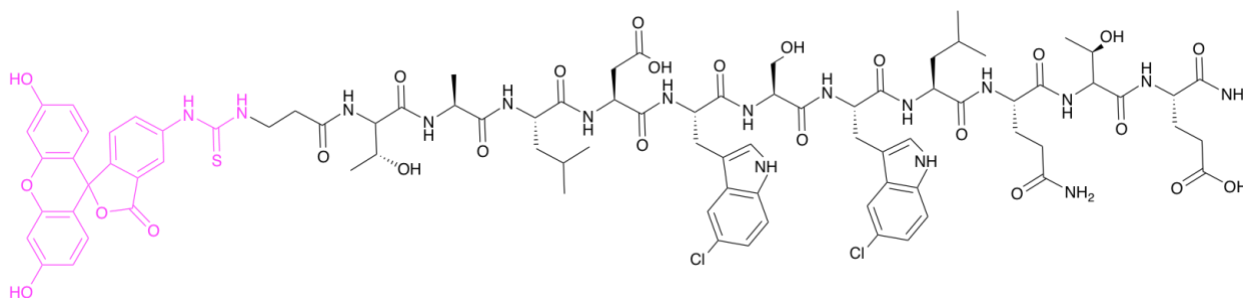1826.93 and the deconvoluted mass is 1826.72

Characterization of 6F-739 NBD. A). A chemical structure of the peptide with the FITC

shown in magenta. **B)** Analytical trace of the peptide monitored at 280 nm. The

analytical sample was run in a water with 0.1% TFA/ acetonitrile system. The sample

was injected with 0.1 % TFA/ acetonitrile. **C)** LC-MS using LC-MS qTOF. Samples were

run in 50/50 0.1% TFA in water, and acetonitrile. Samples were injected onto a C8 column

with a C4 guard. Identity was confirmed under negative mode ionization conditions. The

expected m/z (full) is 1826.93 and the deconvoluted mass is 1826.73.

Characterization of Naphthyl-Ala-741 NBD. A). A chemical structure of the peptide

with the FITC shown in magenta. **B)** Analytical trace of the peptide monitored at 280

nm. The analytical sample was run in a water with 0.1% TFA/ acetonitrile system. The

sample was injected with 0.1 % TFA/ acetonitrile. The peak before 1 min corresponds to

a solvent peak. **C)** LC-MS using LC-MS qTOF. Samples were run in 50/50 0.1% TFA in

water, and acetonitrile. Samples were injected onto a C8 column with a C4 guard. Identity

was confirmed under negative mode ionization conditions. The expected m/z (full) is 1819.96 and the deconvoluted mass is 1819.73.

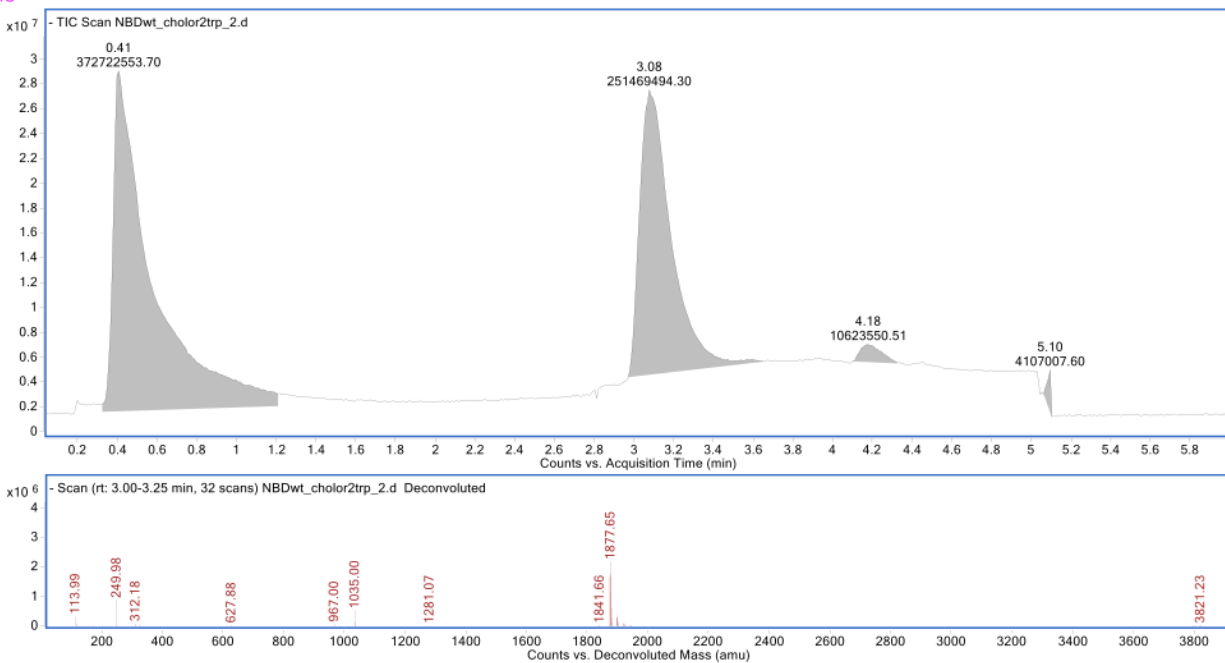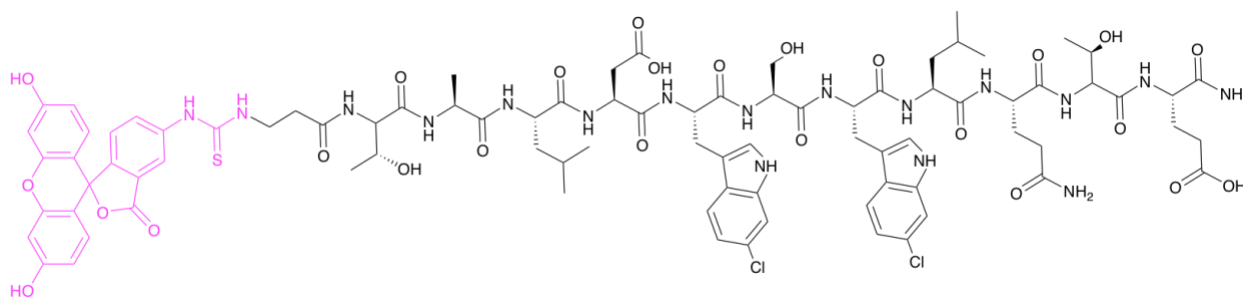**Characterization of 5Methoxy-741 NBD. A).** A chemical structure of the peptide with the FITC shown in magenta. **B)** Analytical trace of the peptide monitored at 280 nm. The analytical sample was run in a water with 0.1% TFA/ acetonitrile system. The sample was injected with 0.1 % TFA/ acetonitrile. The peak before 1 min correspond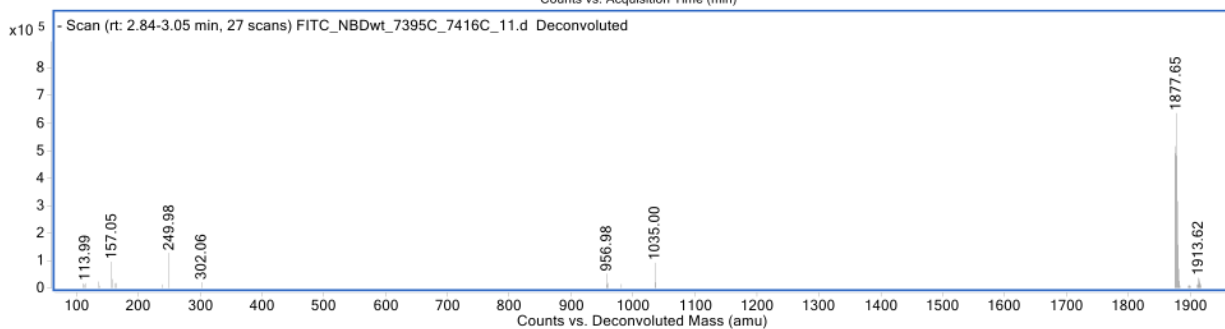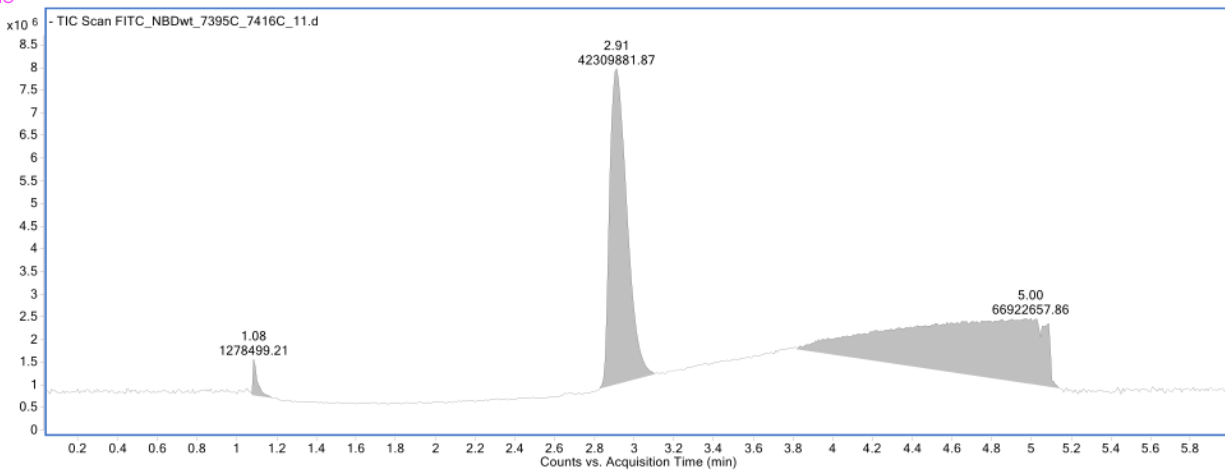s to a solvent peak. 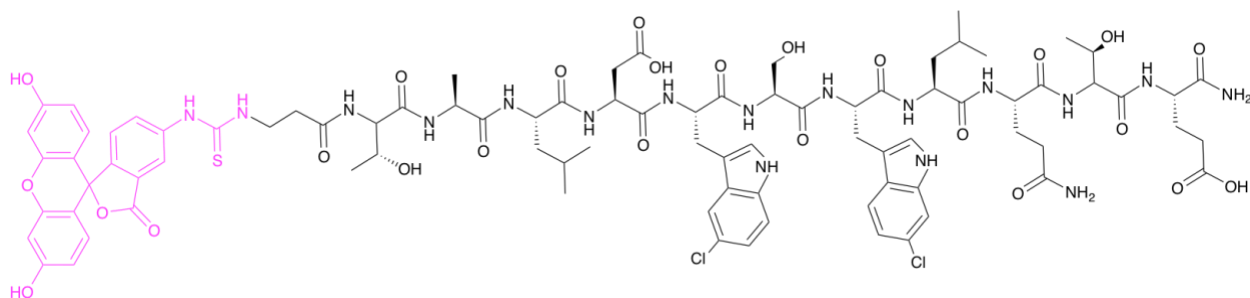**C)** LC-MS using LC-MS qTOF. Samples were run in 50/50 0.1% TFA in water, and acetonitrile. Samples were injected onto a C8 column with a C4 guard. Identity

was confirmed under negative mode ionization conditions. The expected m/z (full) is

1838.97 and the deconvoluted mass is 1838.74.

Characterization of 6Methoxy-741 NBD. A). A chemical structure of the peptide with

the FITC shown in magenta. **B)** Analytical trace of the peptide monitored at 280 nm.

The analytical sample was run in a water with 0.1% TFA/ acetonitrile system. The

sample was injected with 0.1 % TFA/ acetonitrile. The peak before 1 min corresponds to

a solvent peak. **C)** LC-MS using LC-MS qTOF. Samples were run in 50/50 0.1% TFA in

water, and acetonitrile. Samples were injected onto a C8 column with a C4 guard. Identity
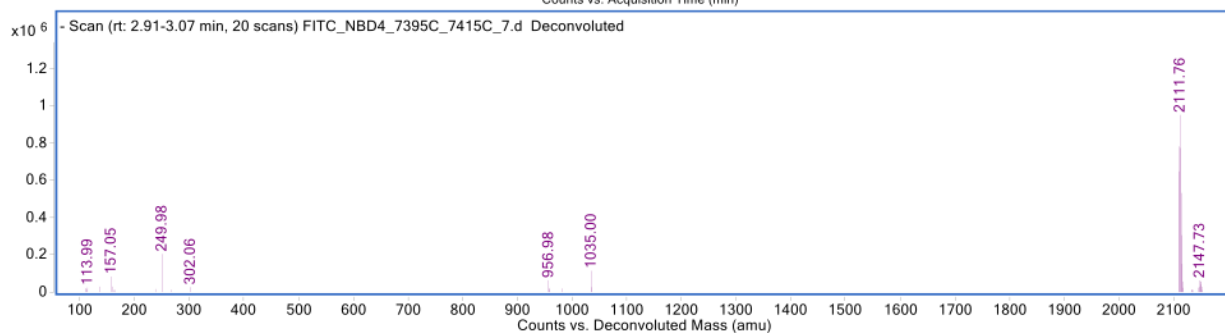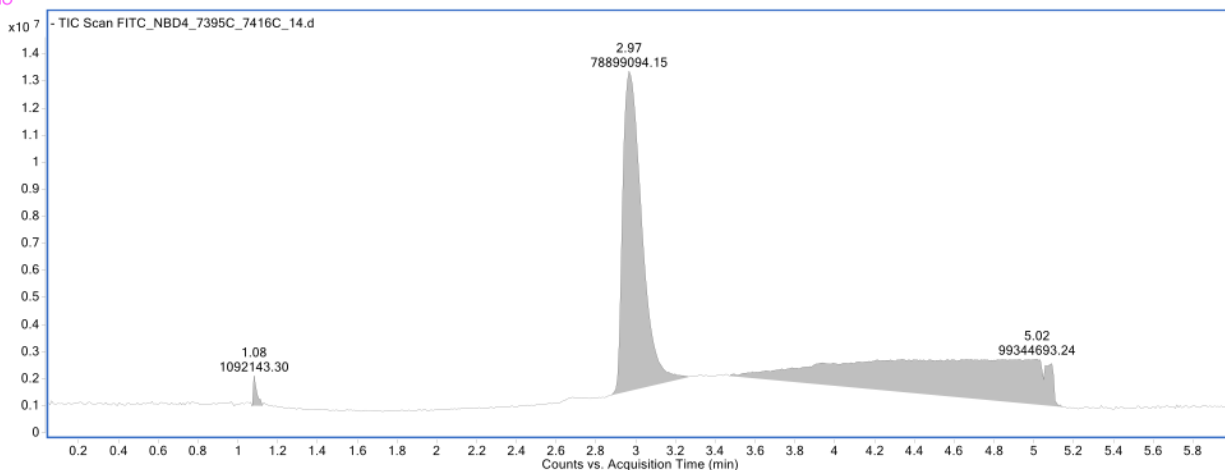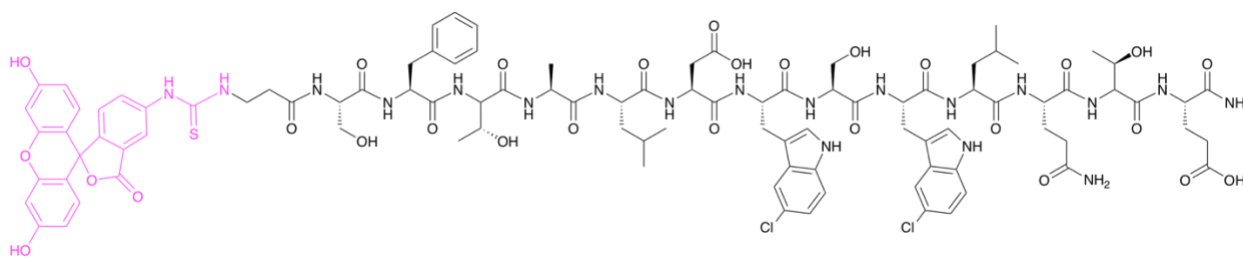
was confirmed under negative mode ionization conditions. The expected m/z (full) is 1838.97 and the deconvoluted mass is 1838.74.

Characterization of 5Cl-741 NBD. A). A chemical structure of the peptide with the FITC shown in magenta. **B)** Analytical trace of the peptide monitored at 280 nm. The analytical sample was run in a water with 0.1% TFA/ acetonitrile system. The sample was injected with 0.1 % TFA/ acetonitrile. The peak before 1 min corresponds to a solvent peak. **C)** LC-MS using LC-MS qTOF. Samples were run in 50/50 0.1% TFA in water, and acetonitrile. Samples were injected onto a C8 column with a C4 guard. Identity

was confirmed under negative mode ionization conditions. The expected m/z (full) is

1843.38 and the deconvoluted mass is 1842.69.
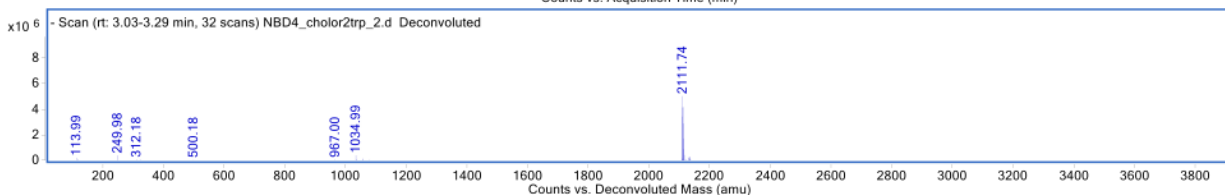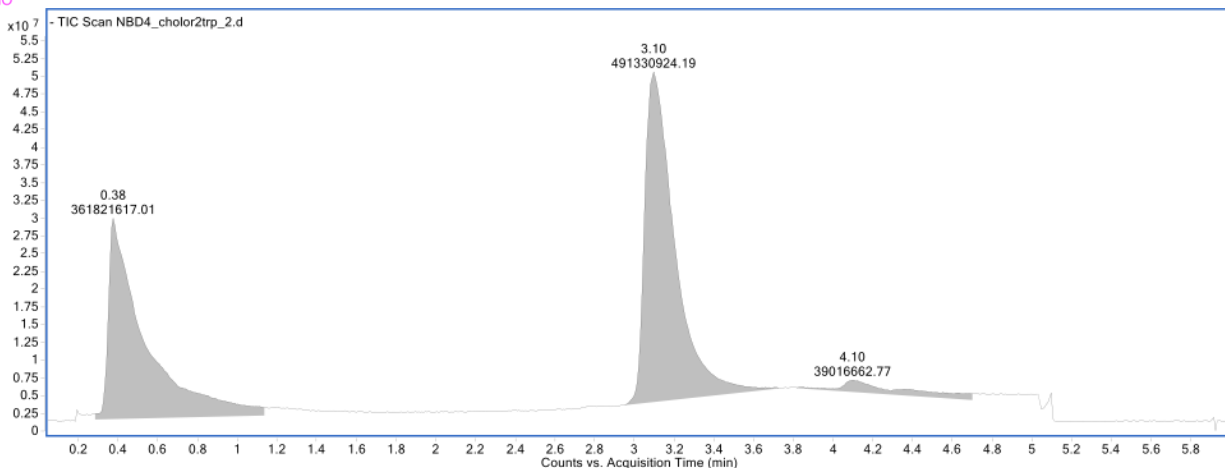

Characterization of 6Cl-741 NBD. A). A chemical structure of the peptide with the

FITC shown in magenta. **B)** Analytical trace of the peptide monitored at 280 nm. The

analytical sample was run in a water with 0.1% TFA/ acetonitrile system. The sample

was injected with 0.1 % TFA/ acetonitrile. The peak before 1 min corresponds to a

solvent peak. **C)** LC-MS using LC-MS qTOF. Samples were run in 50/50 0.1% TFA in

water, and acetonitrile. Samples were injected onto a C8 column with a C4 guard. Identity

was confirmed under negative mode ionization conditions. The expected m/z (full) is 1843.38 and the deconvoluted mass is 1842.69.
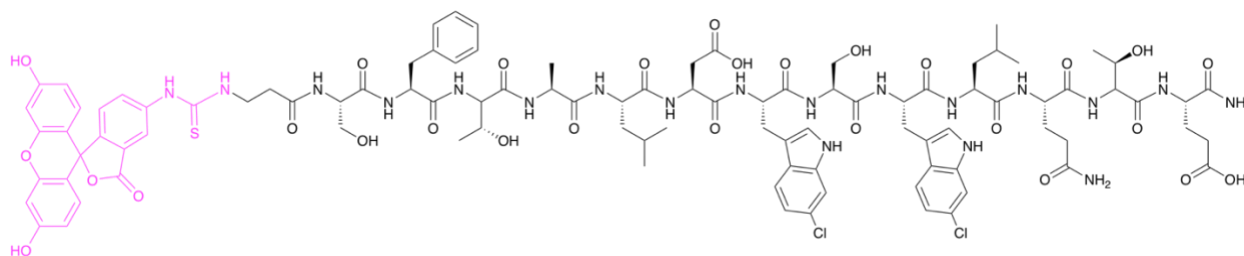

Characterization of 5F-741 NBD. A). A chemical structure of the peptide with the FITC shown in magenta. **B)** Analytical trace of the peptide monitored at 280 nm. The analytical sample was run in a water with 0.1% TFA/ acetonitrile system. The sample was injected with 0.1 % TFA/ acetonitrile. The peak before 1 min corresponds to a solvent peak. **C)** LC-MS using LC-MS qTOF. Samples were run in 50/50 0.1% TFA in water, and acetonitrile. Samples were injected onto a C8 column with a C4 guard. Identity

was confirmed under negative mode ionization conditions. The expected m/z (full) is
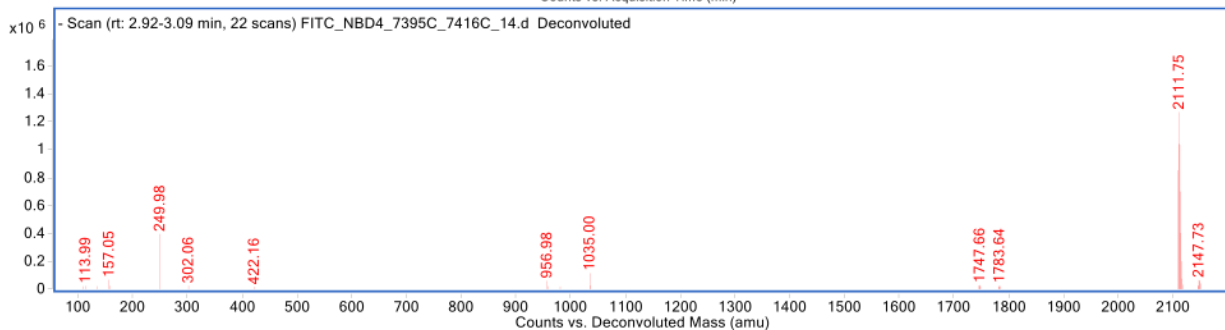
1826.93 and the deconvoluted mass is 1826.72.

Characterization of 6F-741 NBD. A). A chemical structure of the peptide with the FITC

shown in magenta. **B)** Analytical trace of the peptide monitored at 280 nm. The

analytical sample was run in a water with 0.1% TFA/ acetonitrile system. The sample

was injected with 0.1 % TFA/ acetonitrile. **C)** LC-MS using LC-MS qTOF. Samples were

run in 50/50 0.1% TFA in water, and acetonitrile. Samples were injected onto a C8 column

with a C4 guard. Identity was confirmed under negative mode ionization conditions. The

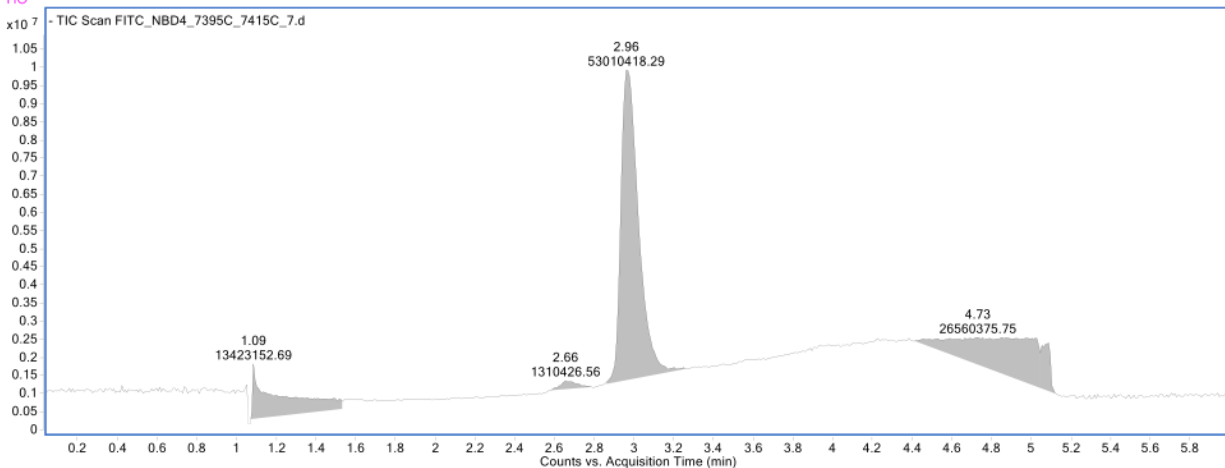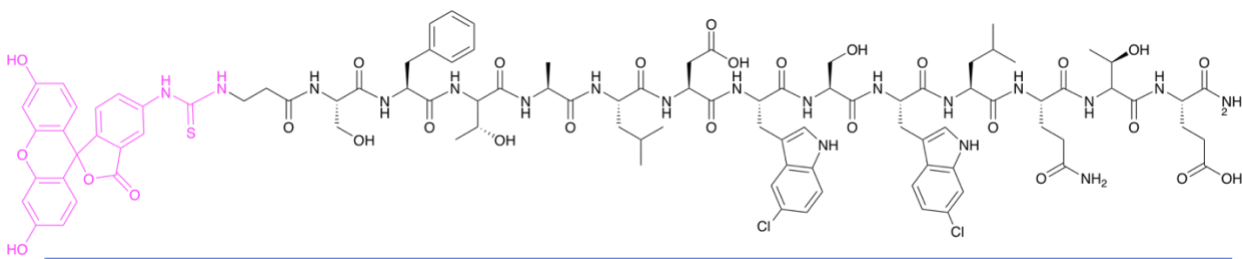expected m/z (full) is 1826.93 and the deconvoluted mass is 1826.73.

Characterization of 5CI-739, 5CI-741 NBD. A). A chemical structure of the peptide with the FITC shown in magenta. **B)** Analytical trace of the peptide monitored at 280 nm. The analytical sample was run in a water with 0.1% TFA/ acetonitrile system. The sample was injected with 0.1 % TFA/ acetonitrile. **C)** LC-MS using LC-MS qTOF. Samples were run in 50/50 0.1% TFA in water, and acetonitrile. Samples were injected onto a C8 column with a C4 guard. Identity was confirmed under negative mode ionization conditions. The expected m/z (full) is 1877.82 and the deconvoluted mass is 1877.65.
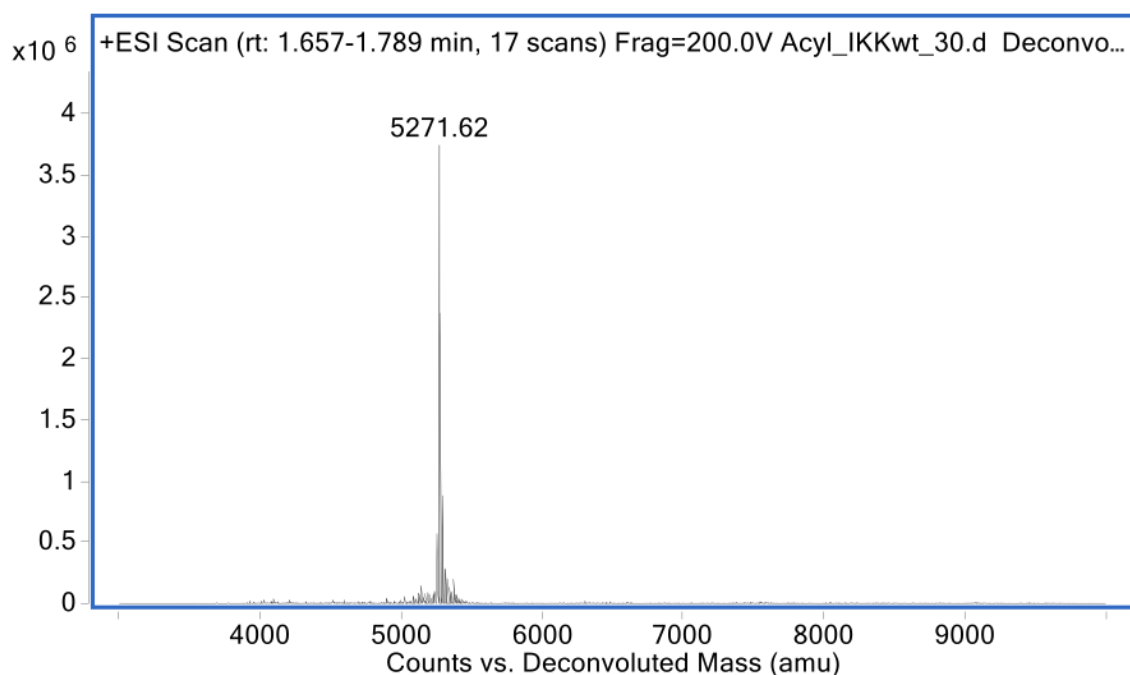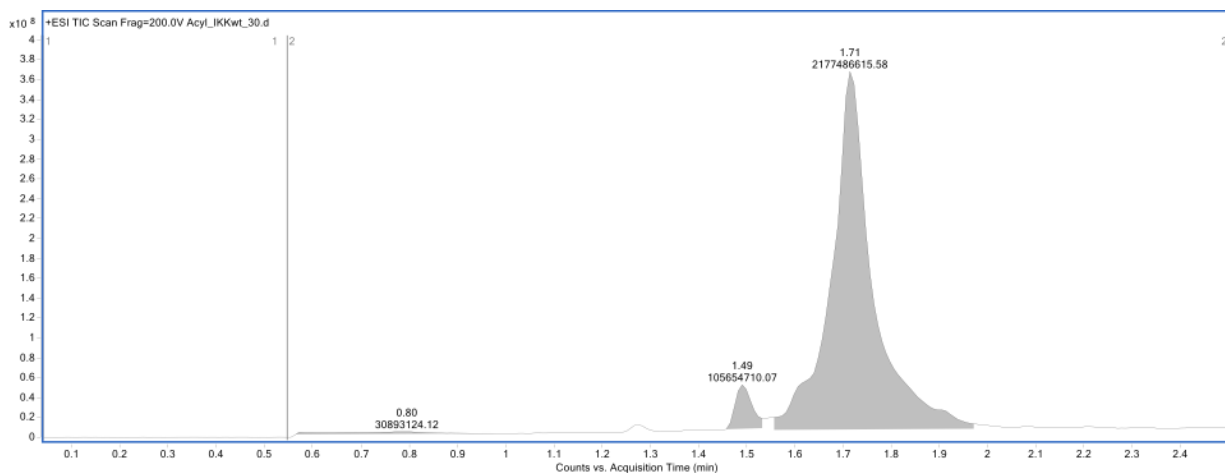
Characterization of 6Cl-739, 6Cl-741 NBD. A). A chemical structure of the peptide with the FITC shown in magenta. **B)** Analytical trace of the peptide monitored at 280 nm. The analytical sample was run in a water with 0.1% TFA/ acetonitrile system. The sample was injected with 0.1 % TFA/ acetonitrile. The peak before 1 min corresponds to a solvent peak. **C)** LC-MS using LC-MS qTOF. Samples were run in 50/50 0.1% TFA in water, and acetonitrile. Samples were injected onto a C8 column with a C4 guard. Identity was confirmed under negative mode ionization conditions. The expected m/z (full) is 1877.82 and the deconvoluted mass is 1877.65.

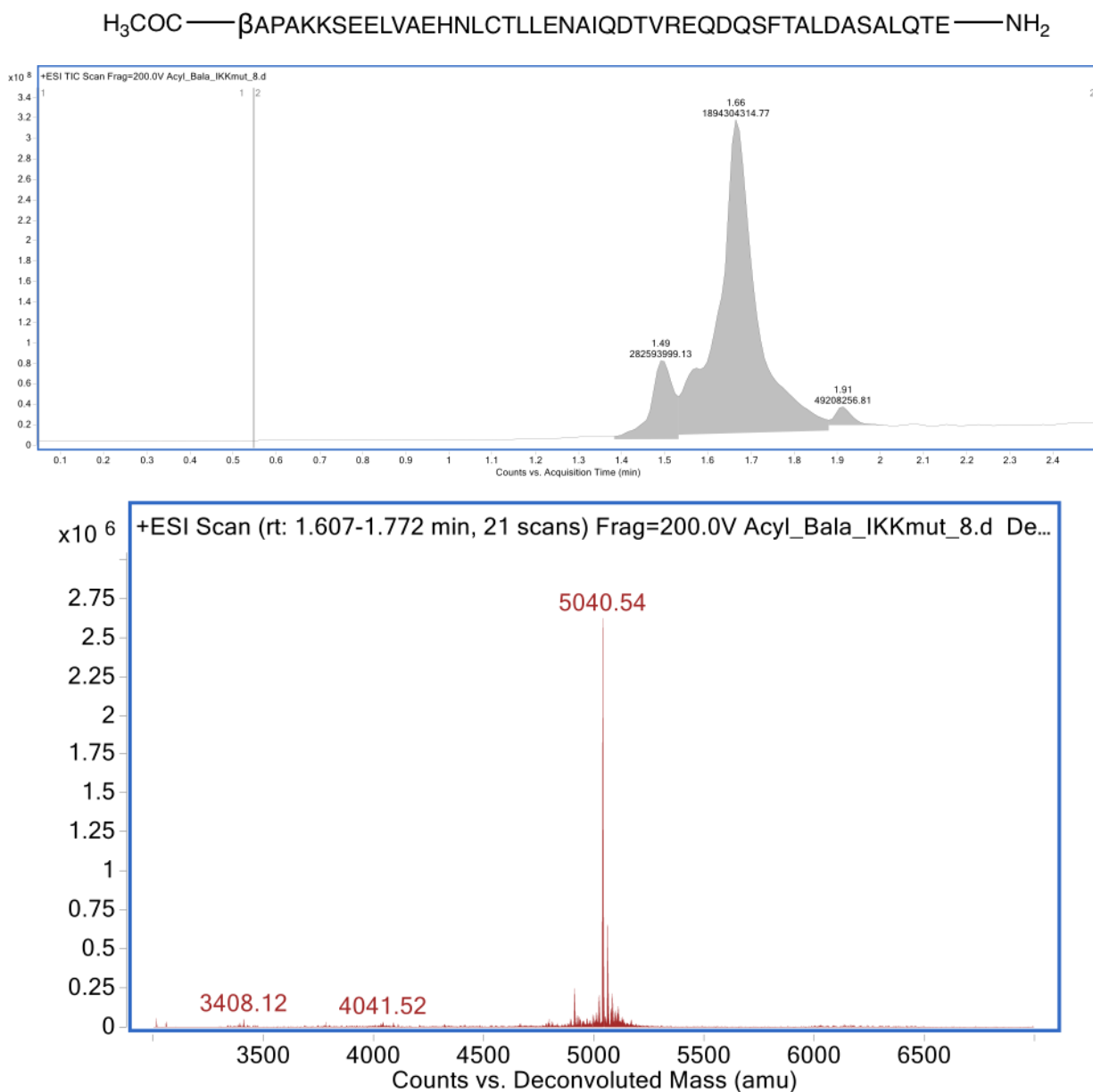**Characterization of 5Cl-739, 6Cl-741 NBD. A).** A chemical structure of the peptide

with the FITC shown in magenta. **B)** Analytical trace of the peptide monitored at 280

nm. The analytical sample was run in a water with 0.1% TFA/ acetonitrile system. The

sample was injected with 0.1 % TFA/ acetonitrile. **C)** LC-MS using LC-MS qTOF.

Samples were run in 50/50 0.1% TFA in water, and acetonitrile. Samples were injected onto

a C8 column with a C4 guard. Identity was confirmed under negative mode ionization

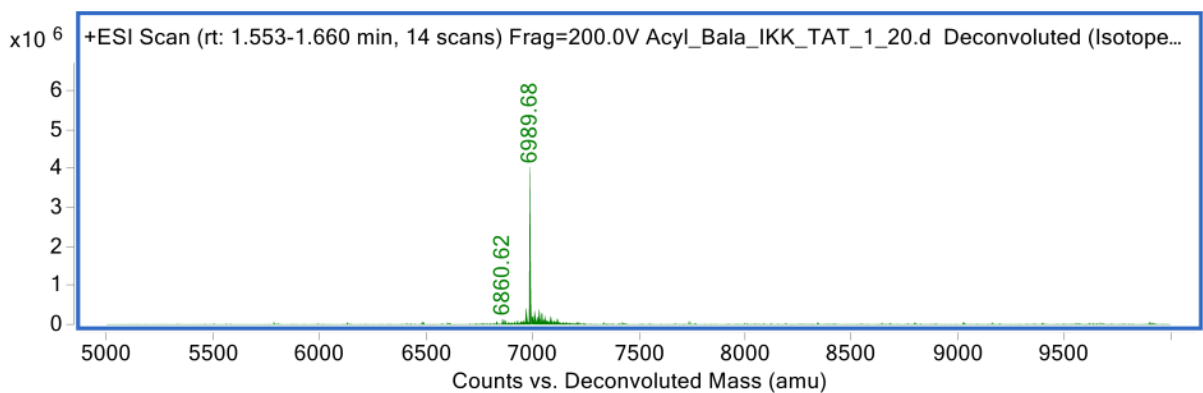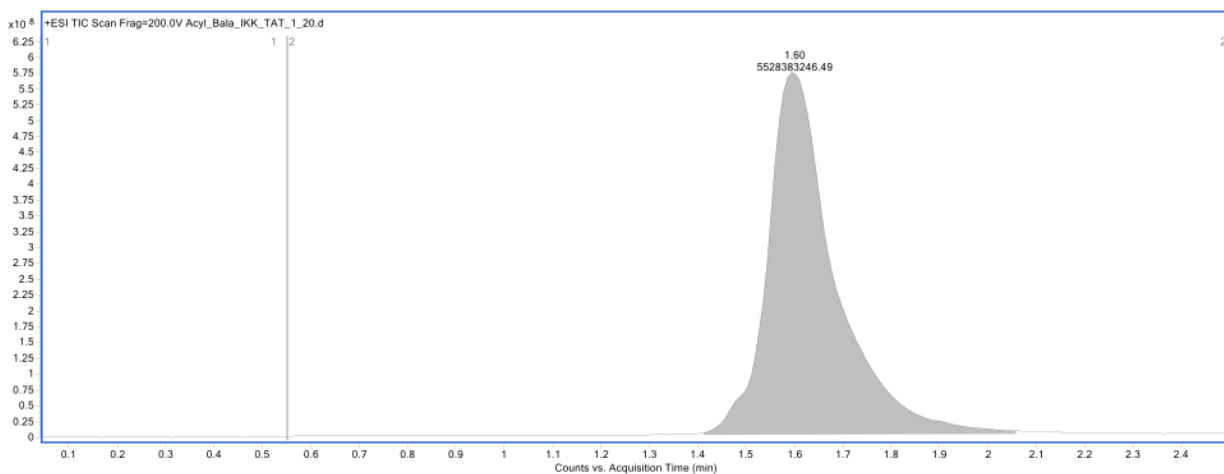conditions. The expected m/z (full) is 1877.82 and the deconvoluted mass is 1877.65.

Characterization of 5Cl-739, 5Cl-741 NBD 4. A). A chemical structure of the peptide with the FITC shown in magenta. **B)** Analytical trace of the peptide monitored at 280 nm. The analytical sample was run in a water with 0.1% TFA/ acetonitrile system. The sample was injected with 0.1 % TFA/ acetonitrile. **C)** LC-MS using LC-MS qTOF. Samples were run in 50/50 0.1% TFA in water, and acetonitrile. Samples were injected onto a C8 column with a C4 guard. Identity was confirmed under negative mode ionization conditions. The expected m/z (full) is 2112.08 and the deconvoluted mass is 2111.76.
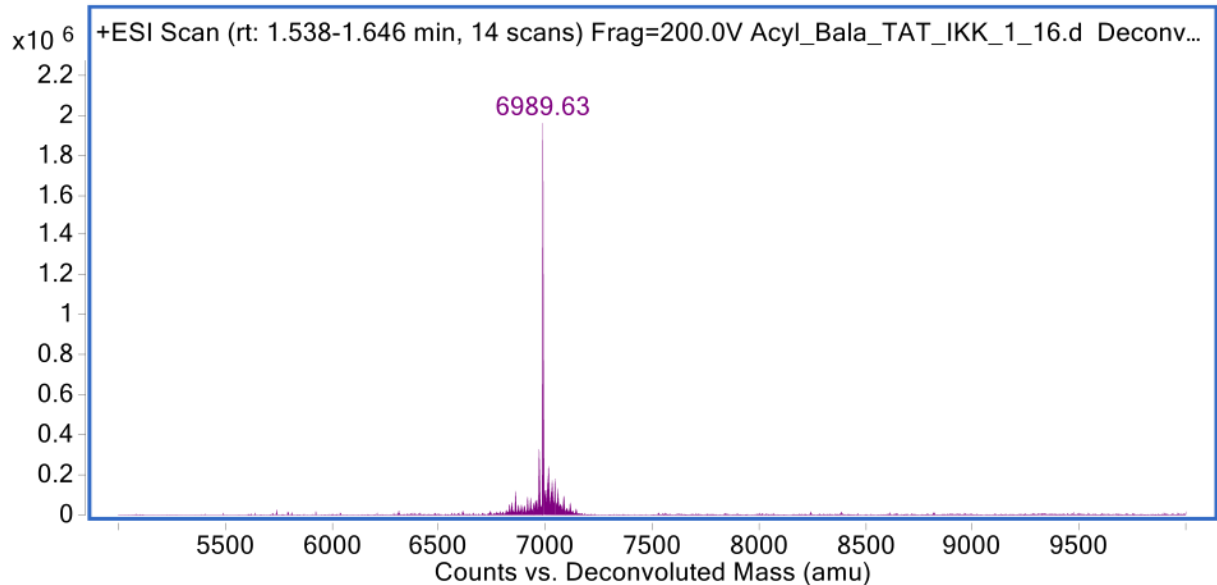
Characterization of 6Cl-739, 6Cl-741 NBD 4. A). A chemical structure of the peptide with the FITC shown in magenta. **B)** Analytical trace of the peptide monitored at 280 nm. The analytical sample was run in a water with 0.1% TFA/ acetonitrile system. The sample was injected with 0.1 % TFA/ acetonitrile. The peak before 1 min corresponds to a solvent peak. **C)** LC-MS using LC-MS qTOF. Samples were run in 50/50 0.1% TFA in water, and acetonitrile. Samples were injected onto a C8 column with a C4 guard. Identity was confirmed under negative mode ionization conditions. The expected m/z (full) is 2112.08 and the deconvoluted mass is 2111.74.
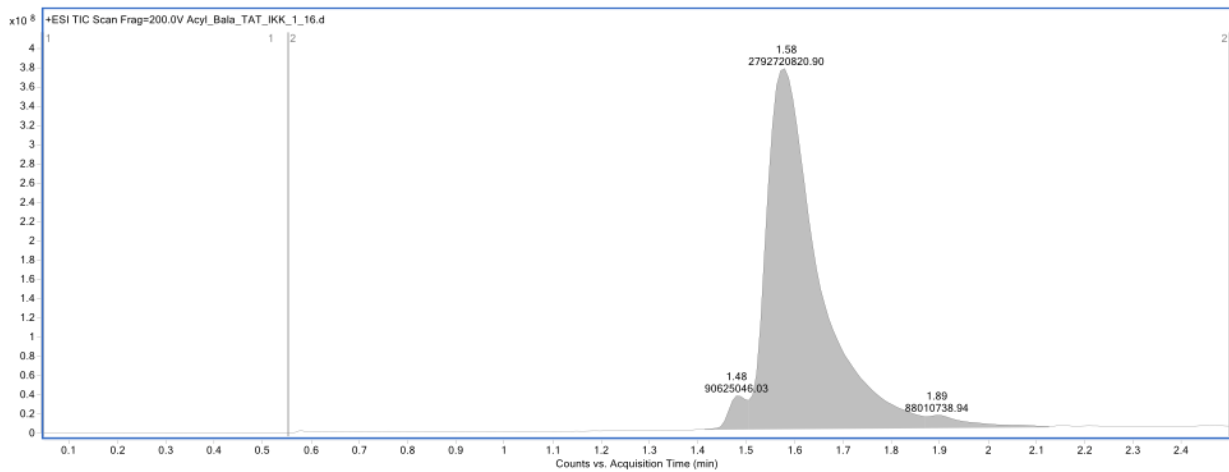
Characterization of 5Cl-739, 6Cl-741 NBD 4. A). A chemical structure of the peptide with the FITC shown in magenta. **B)** Analytical trace of the peptide monitored at 280 nm. The analytical sample was run in a water with 0.1% TFA/ acetonitrile system. The sample was injected with 0.1 % TFA/ acetonitrile. **C)** LC-MS using LC-MS qTOF. Samples were run in 50/50 0.1% TFA in water, and acetonitrile. Samples were injected onto a C8 column with a C4 guard. Identity was confirmed under negative mode ionization conditions. The expected m/z (full) is 2112.08 and the deconvoluted mass is 2111.75.

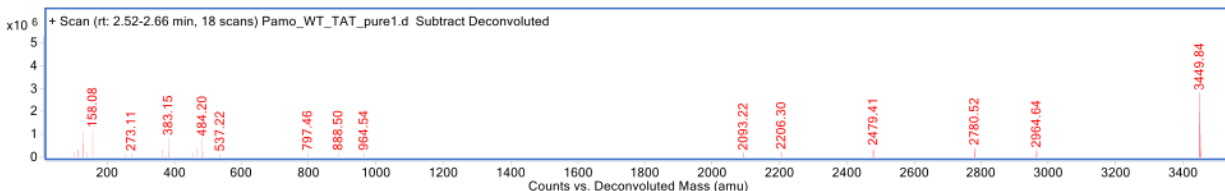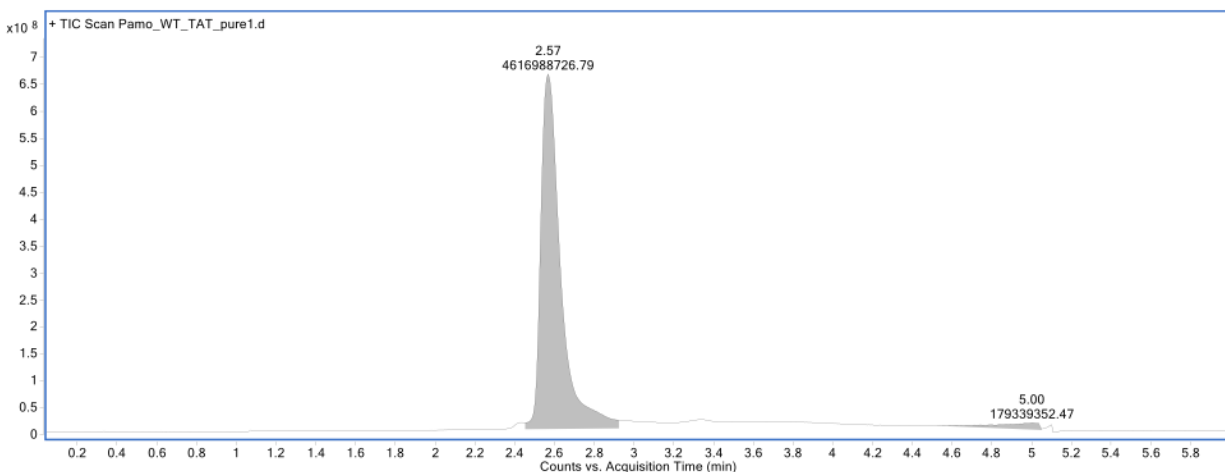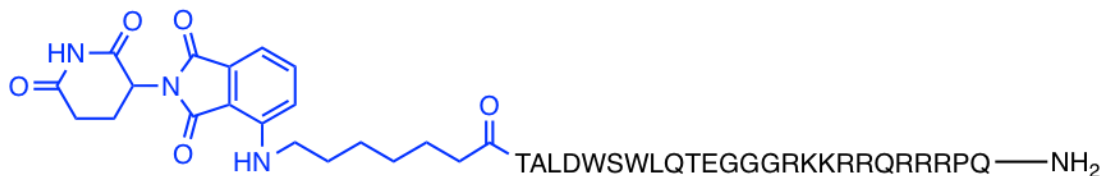H₃COC——βAPAKKSEELVAEHNLCTLLENAIQDTVREQDQSFTALDWSWLQTE——NH₂

Characterization of Acyl-IKKwt. A). A chemical structure of the peptide with the FITC

shown in magenta. **B)** Analytical trace of the peptide monitored at 280 nm. The

analytical sample was run in a water with 0.1% TFA/ acetonitrile system. The sample

was injected with 0.1 % TFA/ acetonitrile. **C)** LC-MS using LC-MS qTOF. Samples were

run in 50/50 0.1% TFA in water, and acetonitrile. Samples were injected onto a C8 column

with a C4 guard. Identity was confirmed under negative mode ionization conditions. The

expected m/z (full) is 5271.81 and the deconvoluted mass is 5271.62

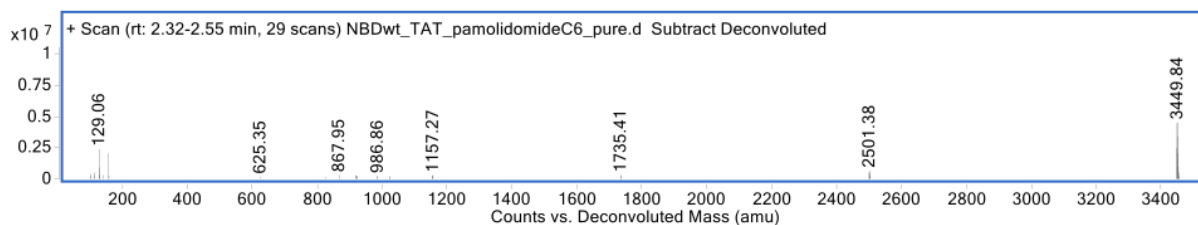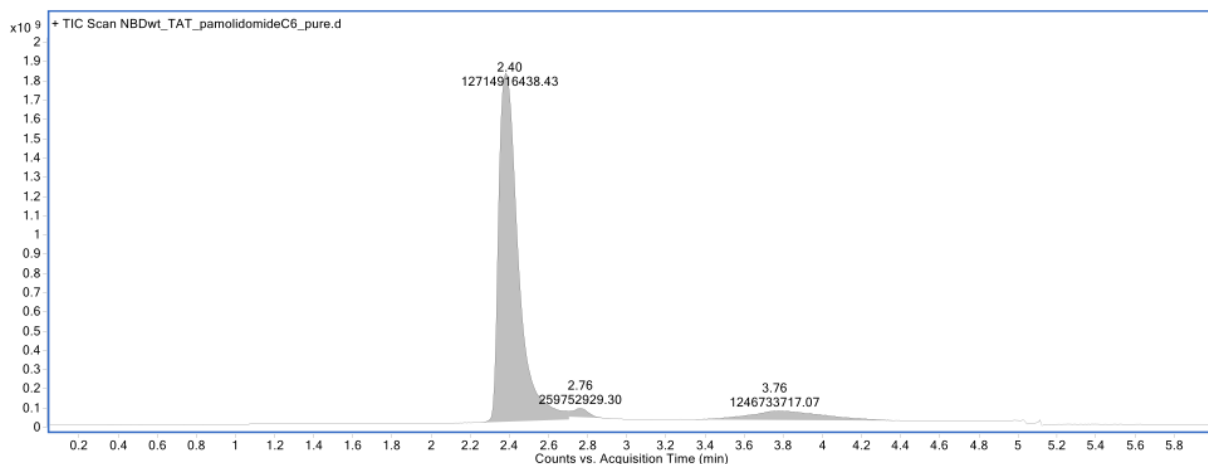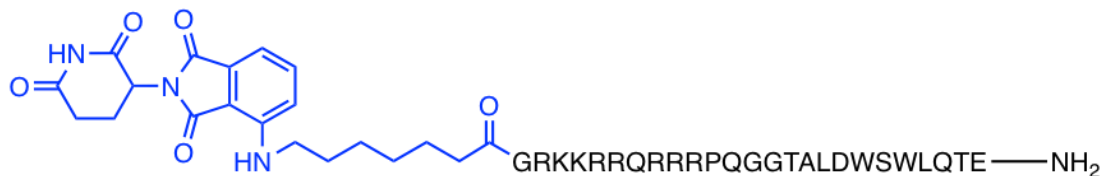H₃COC——βAPAKKSEELVAEHNLCTLLENAIQDTVREQDQSFTALDASALQTE——NH₂

Characterization of Acyl-IKKmut. A). A chemical structure of the peptide with the

FITC shown in magenta. **B)** Analytical trace of the peptide monitored at 280 nm. The

analytical sample was run in a water with 0.1% TFA/ acetonitrile system. The sample

was injected with 0.1 % TFA/ acetonitrile. **C)** LC-MS using LC-MS qTOF. Samples were

run in 50/50 0.1% TFA in water, and acetonitrile. Samples were injected onto a C8 column

with a C4 guard. Identity was confirmed under negative mode ionization conditions. The

expected m/z (full) is 5041.50 and the deconvoluted mass is 5040.54

H_3COC——βAPAKKSEELVAEHNLCTLLENAIQDTVREQDQSFTALDWSWLQTEGGGRKKRRQRRRPQ——NH_2

Characterization of Acyl-IKK-TAT. A). A chemical structure of the peptide with the

FITC shown in magenta. **B)** Analytical trace of the peptide monitored at 280 nm. The

analytical sample was run in a water with 0.1% TFA/ acetonitrile system. The sample

was injected with 0.1 % TFA/ acetonitrile. **C)** LC-MS using LC-MS qTOF. Samples were

run in 50/50 0.1% TFA in water, and acetonitrile. Samples were injected onto a C8 column

with a C4 guard. Identity was confirmed under negative mode ionization conditions. The

expected m/z (full) is 6989.83 and the deconvoluted mass is 6989.68

H₃COC——βAGRKKRRQRRRPQGGPAKKSEELVAEHNLCTLLENAIQDTVREQDQSFTALDWSWLQTE——NH₂

Characterization of Acyl-TAT-IKK. A). A chemical structure of the peptide with the

FITC shown in magenta. **B)** Analytical trace of the peptide monitored at 280 nm. The

analytical sample was run in a water with 0.1% TFA/ acetonitrile system. The sample

was injected with 0.1 % TFA/ acetonitrile. **C)** LC-MS using LC-MS qTOF. Samples were

run in 50/50 0.1% TFA in water, and acetonitrile. Samples were injected onto a C8 column

with a C4 guard. Identity was confirmed under negative mode ionization conditions. The expected m/z (full) is 6989.83 and the deconvoluted mass is 6989.63.
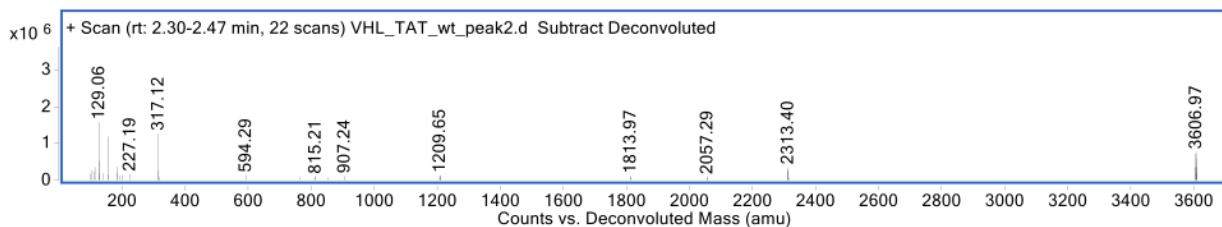

Characterization of NP-1. A). A chemical structure of the peptide with the FITC shown in magenta. **B)** Analytical trace of the peptide monitored at 280 nm. The analytical sample was run in a water with 0.1% TFA/ acetonitrile system. The sample was injected with 0.1 % TFA/ acetonitrile. **C)** LC-MS using LC-MS qTOF. Samples were run in 50/50 0.1% TFA in water, and acetonitrile. Samples were injected onto a C8 column with a C4 guard. Identity was confirmed under negative mode ionization conditions. The expected m/z (full) is 3449.90 and the deconvoluted mass is 3449.84.
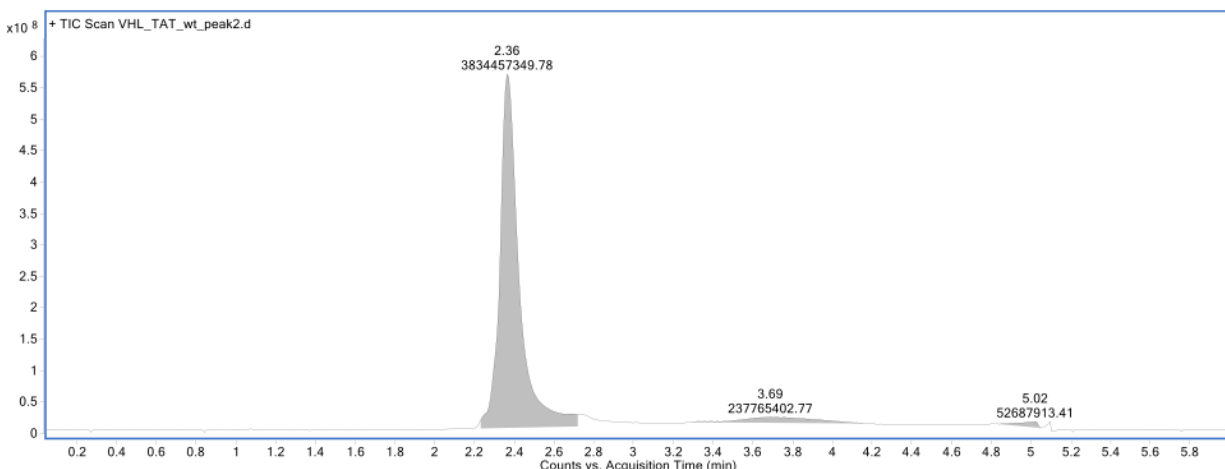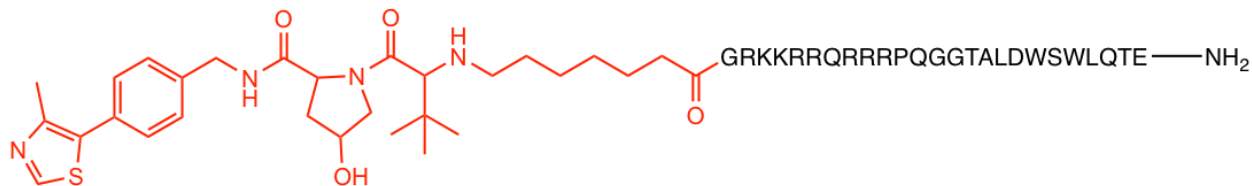
Characterization of NP-2. A). A chemical structure of the peptide with the FITC shown in magenta. **B)** Analytical trace of the peptide monitored at 280 nm. The analytical sample was run in a water with 0.1% TFA/ acetonitrile system. The sample was injected with 0.1 % TFA/ acetonitrile. **C)** LC-MS using LC-MS qTOF. Samples were run in 50/50 0.1% TFA in water, and acetonitrile. Samples were injected onto a C8 column with a C4 guard. Identity was confirmed under negative mode ionization conditions. The expected m/z (full) is 3449.90 and the deconvoluted mass is 7363.01.
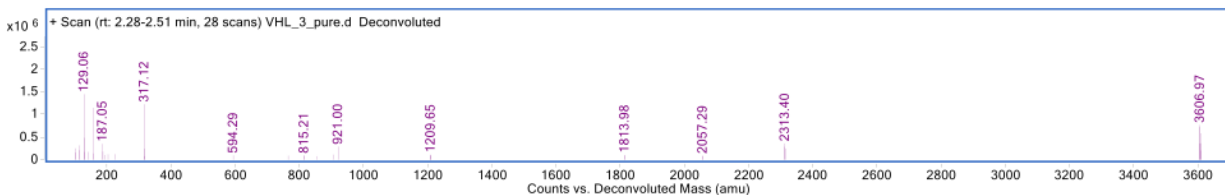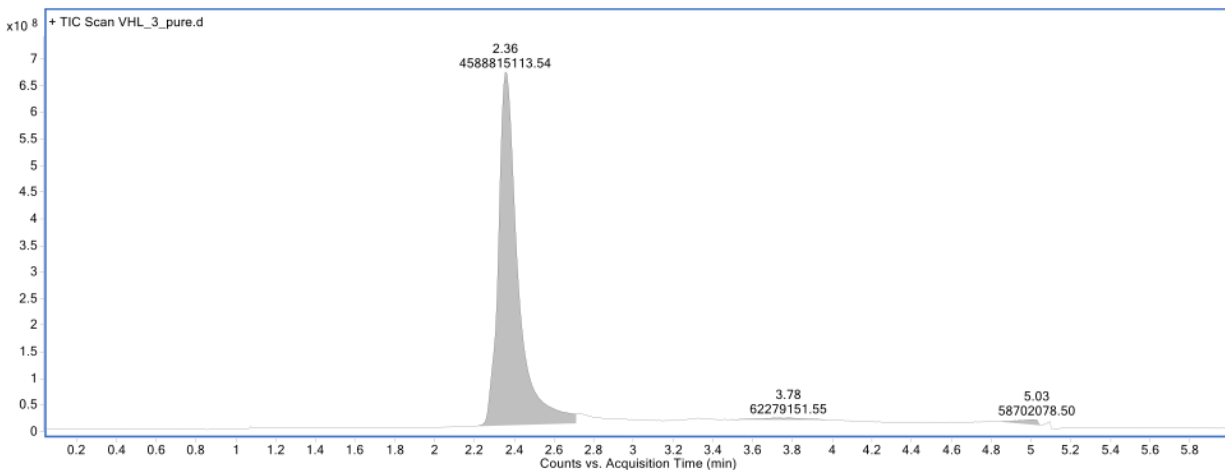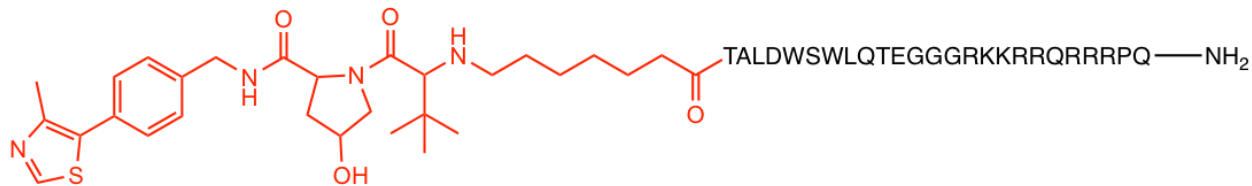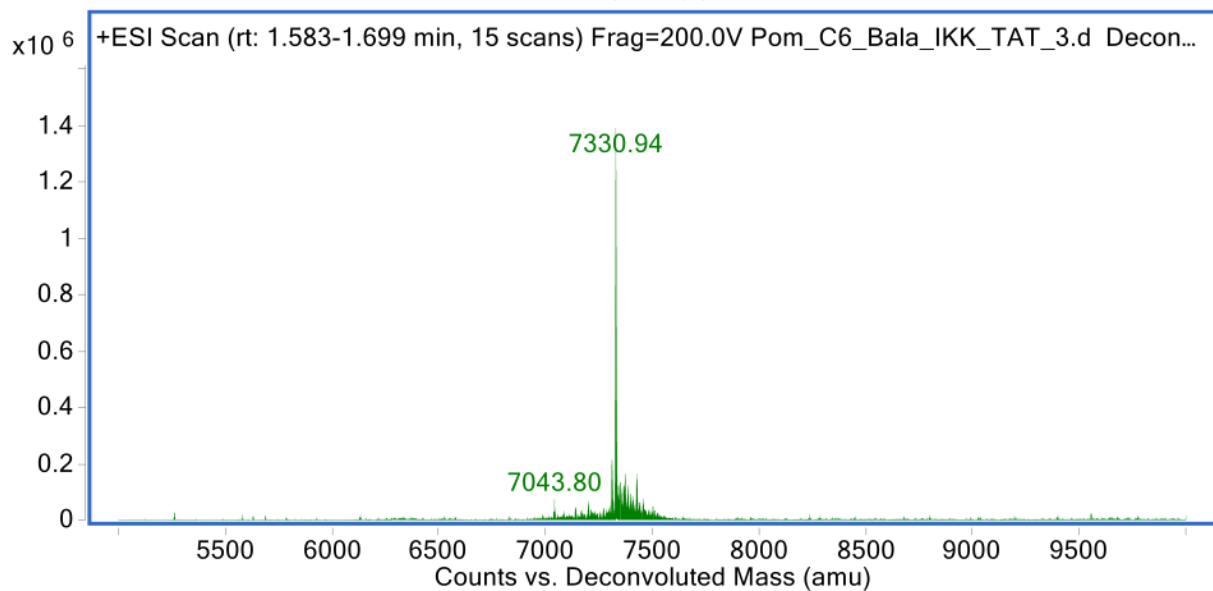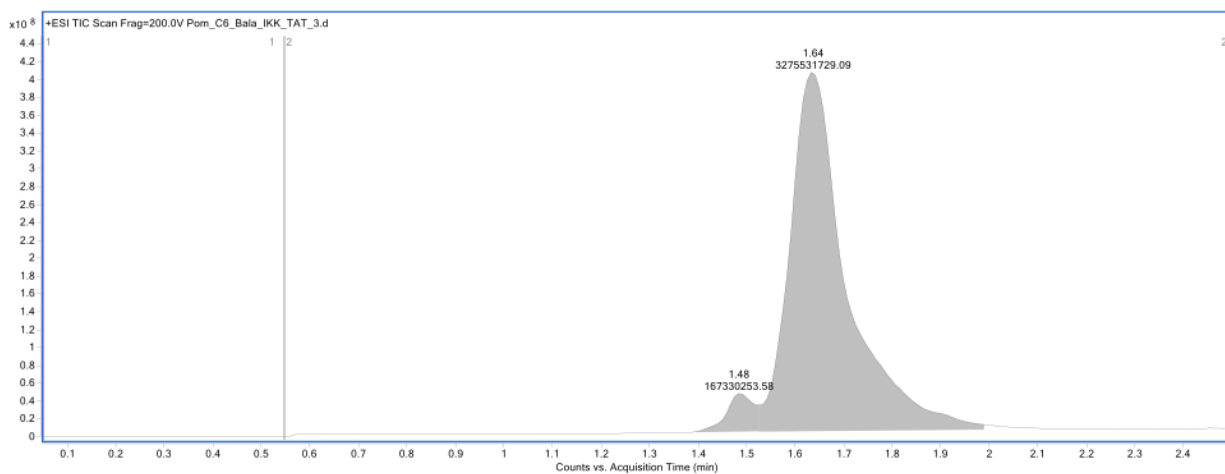
Characterization of NP-3. A). A chemical structure of the peptide with the FITC shown

in magenta. **B)** Analytical trace of the peptide monitored at 280 nm. The analytical

sample was run in a water with 0.1% TFA/ acetonitrile system. The sample was injected

with 0.1 % TFA/ acetonitrile. **C)** LC-MS using LC-MS qTOF. Samples were run in 50/50

0.1% TFA in water, and acetonitrile. Samples were injected onto a C8 column with a C4

guard. Identity was confirmed under negative mode ionization conditions. The expected

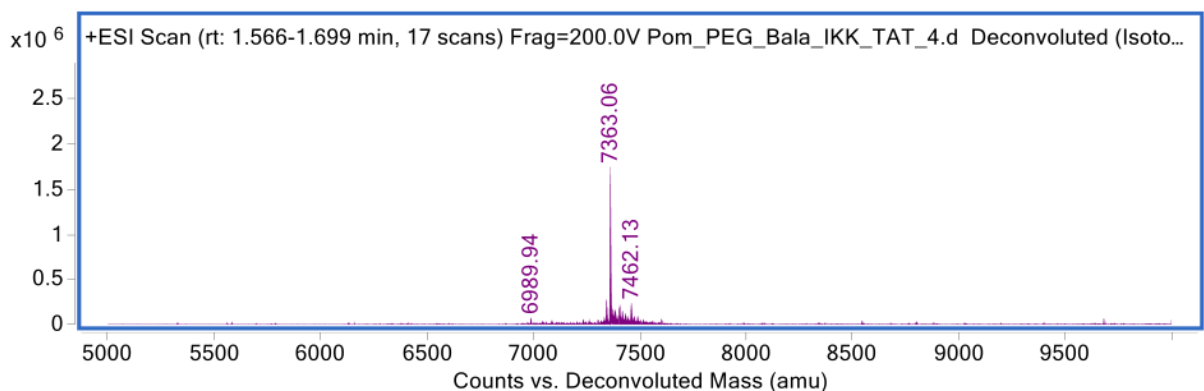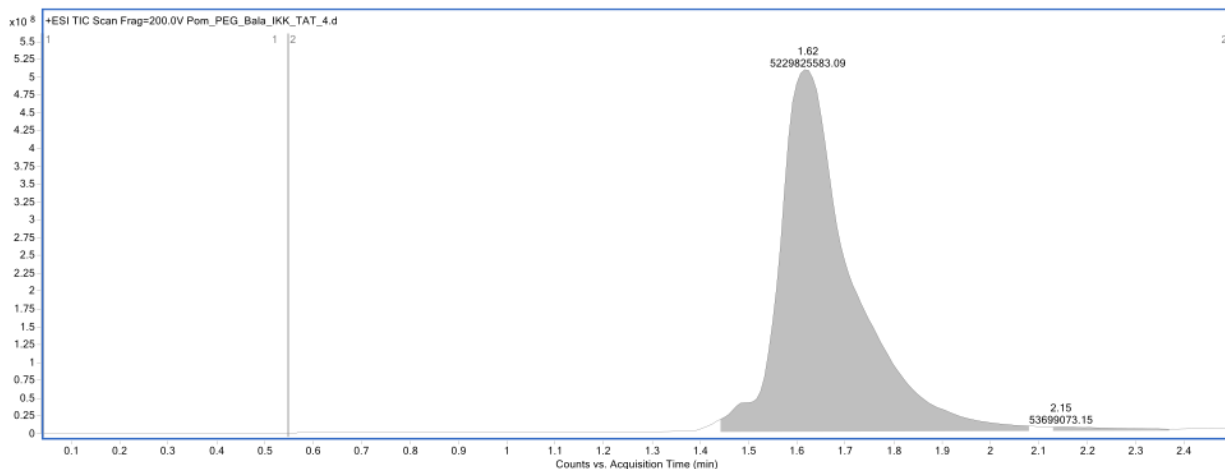m/z (full) is 3607.22 and the deconvoluted mass is 3606.97.

Characterization of NP-4. A). A chemical structure of the peptide with the FITC shown in magenta. **B)** Analytical trace of the peptide monitored at 280 nm. The analytical sample was run in a water with 0.1% TFA/ acetonitrile system. The sample was injected with 0.1 % TFA/ acetonitrile. **C)** LC-MS using LC-MS qTOF. Samples were run in 50/50 0.1% TFA in water, and acetonitrile. Samples were injected onto a C8 column with a C4 guard. Identity was confirmed under negative mode ionization conditions. The expected m/z (full) is 3607.22 and the deconvoluted mass is 3606.97.
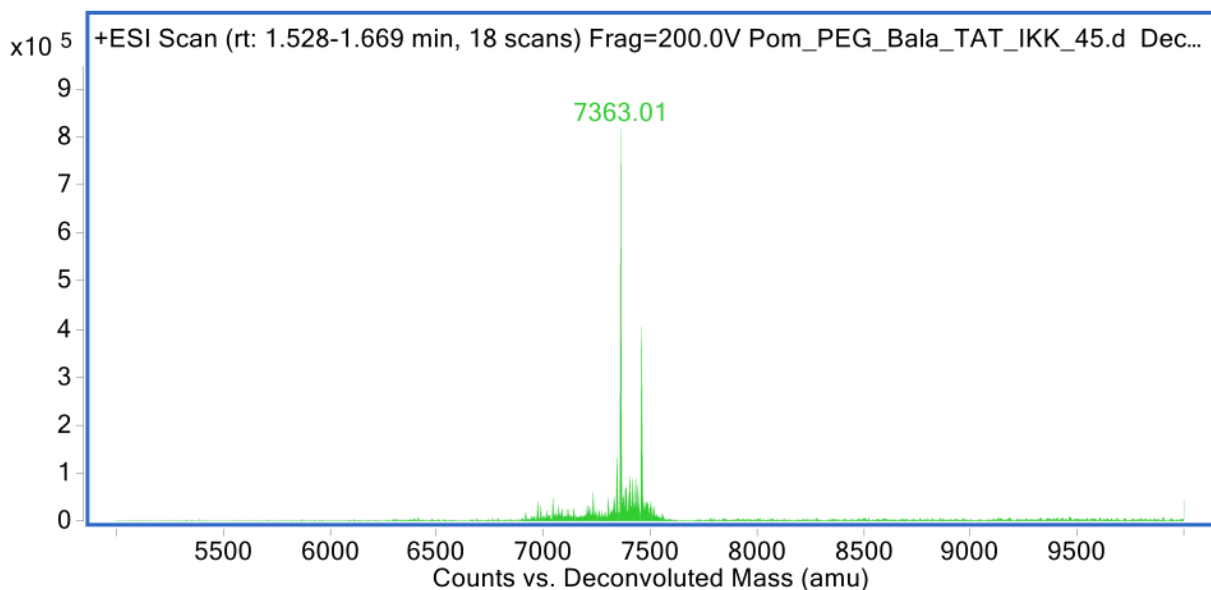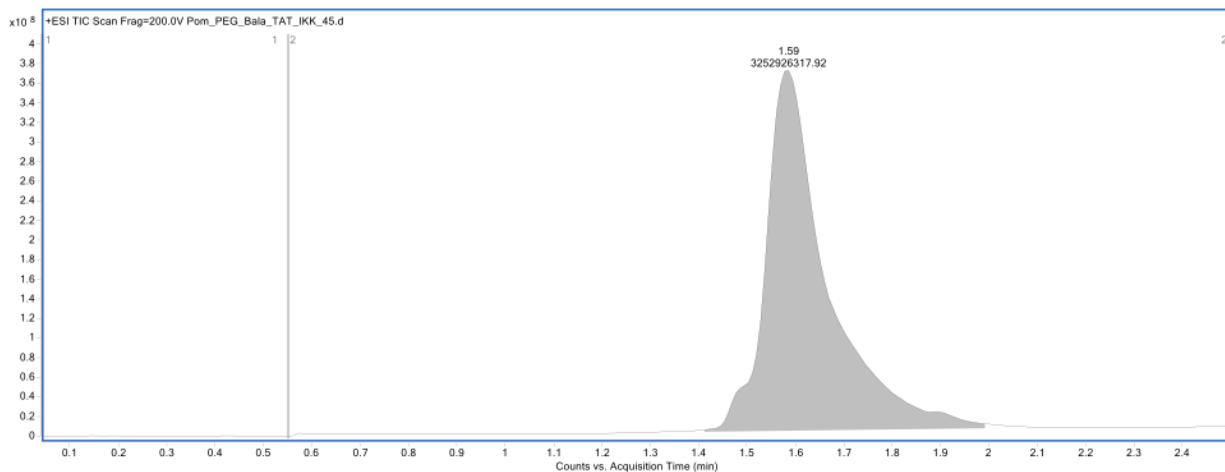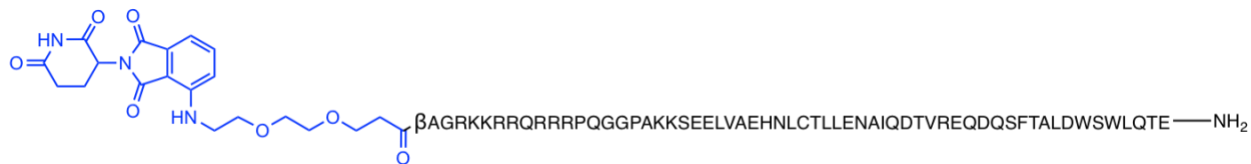
Characterization of NP-5. A). A chemical structure of the peptide with the FITC shown

in magenta. **B)** Analytical trace of the peptide monitored at 280 nm. The analytical

sample was run in a water with 0.1% TFA/ acetonitrile system. The sample was injected

with 0.1 % TFA/ acetonitrile. **C)** LC-MS using LC-MS qTOF. Samples were run in 50/50

0.1% TFA in water, and acetonitrile. Samples were injected onto a C8 column with a C4

guard. Identity was confirmed under negative mode ionization conditions. The expected

m/z (full) is 7331.20 and the deconvoluted mass is 7330.94.

Characterization of NP-6. A). A chemical structure of the peptide with the FITC shown

in magenta. **B)** Analytical trace of the peptide monitored at 280 nm. The analytical

sample was run in a water with 0.1% TFA/ acetonitrile system. The sample was injected

with 0.1 % TFA/ acetonitrile. **C)** LC-MS using LC-MS qTOF. Samples were run in 50/50

0.1% TFA in water, and acetonitrile. Samples were injected onto a C8 column with a C4

guard. Identity was confirmed under negative mode ionization conditions. The expected

m/z (full) is 7331.20 and the deconvoluted mass is 7330.98.

Characterization of NP-7. A). A chemical structure of the peptide with the FITC shown in magenta. **B)** Analytical trace of the peptide monitored at 280 nm. The analytical sample was run in a water with 0.1% TFA/ acetonitrile system. The sample was injected with 0.1 % TFA/ acetonitrile. **C)** LC-MS using LC-MS qTOF. Samples were run in 50/50 0.1% TFA in water, and acetonitrile. Samples were injected onto a C8 column with a C4 guard. Identity was confirmed under negative mode ionization conditions. The expected m/z (full) is 7363.19 and the deconvoluted mass is 7363.06.

Characterization of NP-8. A). A chemical structure of the peptide with the FITC shown

in magenta. **B)** Analytical trace of the peptide monitored at 280 nm. The analytical

sample was run in a water with 0.1% TFA/ acetonitrile system. The sample was injected

with 0.1 % TFA/ acetonitrile. **C)** LC-MS using LC-MS qTOF. Samples were run in 50/50

0.1% TFA in water, and acetonitrile. Samples were injected onto a C8 column with a C4 guard. Identity was confirmed under negative mode ionization conditions. The expected m/z (full) is 7363.19 and the deconvoluted mass is 7363.01.